Deciphering the functional role of the LIS1/NDEL1/14.3.3ε protein complex in the expansion of human cortical progenitors in an iPSC-derived organoid model

Dissertation

Zur Erlangung des Doktorgrades (Dr. rer. nat.) der Mathematisch-Naturwissenschaftlichen Fakultät der Rheinischen Friedrich-Wilhelms-Universität Bonn

Vorgelegt
von

Vira
Iefremova

aus Bila Tserkva, Ukraine

Bonn
2021

Anfertigung mit der Genehmigung der Mathematisch-Naturwissenschaftlichen

Fakultät der Rheinischen Friedrich-Wilhelms-Universität Bonn

The human brain has 100 billion neurons, each neuron connected to 10 thousand other neurons. Sitting on your shoulders is the most complicated object in the known universe.

Michio Kaku

Table of contents

1. Introduction

1.1. Physiological development of the human cerebral cortex

The human cerebral cortex is a highly specialised and distinct six-layered structure, supplying higher brain functions such as cognition. It develops through a cascade of extraordinarily complex processes. The first stage initiates around 18 days of gestation when the neural plate begins to form. Around day 33 of gestation, the next significant stage occurs — differentiation of the cerebral vesicles (Barkovich, 2005). Brain hemisphere development begins with the formation of a single-cell layer of columnar epithelium. Although the development of the cerebral cortex is remarkably complex, two key processes are crucial: cell proliferation and neuronal migration.

Cell proliferation is critical during early cortical development and begins in the ventricular zone (VZ) with the generation and propagation of progenitor cells that later migrate and populate the cortex. This process occurs in the germinal zones in the developing brain and expands the pool of precursor cells. These cells undergo a series of division events, predominantly symmetrical, which enables both daughter cells to re-enter the cell cycle as progenitors. Eventually, the ratio between symmetric and asymmetric cell division begins to shift in favour of increased asymmetric events, generating neuroblasts and glial progenitors.

Numerous studies of primates have produced compelling evidence that neocortex development is characterised by a significant increase in the size of the subventricular zone (SVZ). Furthermore, two distinct regions have been identified: an inner (ISVZ) and outer (OSVZ) subventricular zone (Smart et al., 2002; Zecevic et al., 2005; Fish et al., 2008). Moreover, experiments applying thymidine-labelling in primates suggest that progenitor cell proliferation in the OSVZ corresponds with significant neocortical neurogenesis (Rakic, 1974; Lukaszewicz et al., 2005), indicating that cells originating from the OSVZ have a significant role in generating neurons, which later form the cortical plate (Figure 1.1).
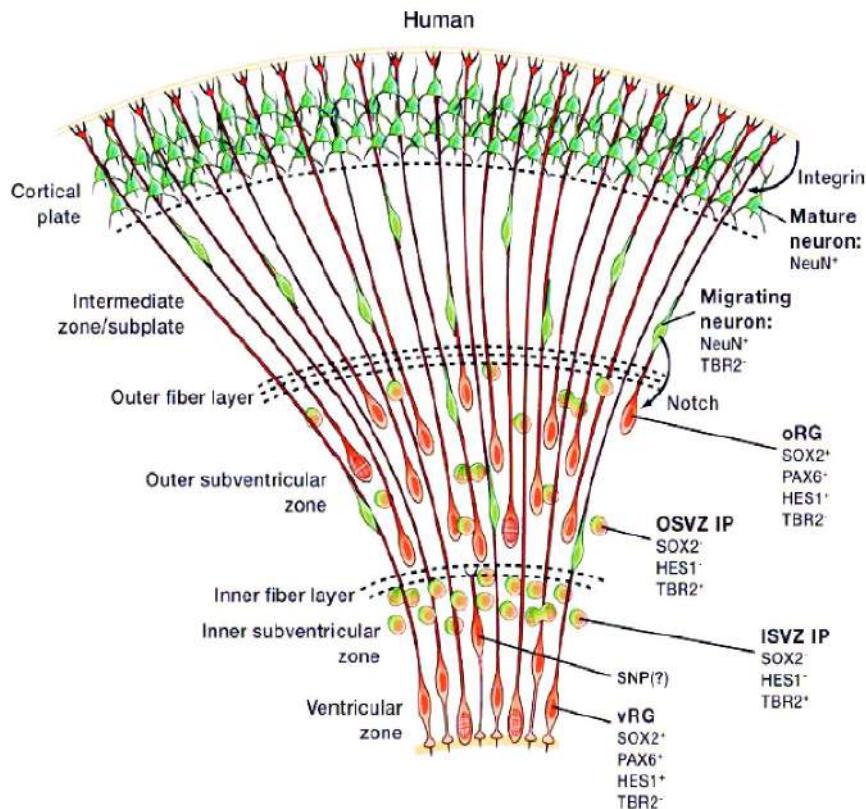
Figure 1.1. Schematic structure of the developing human cortex. Ventricular radial glial (vRG) cells represent the main source of intermediate progenitor (IP) cells. Increased size of the human outer subventricular zone (OSVZ) in developing cerebral cortex provides essential space and microenvironment for migration of neurons (red to green). These neurons are derived from intermediate progenitor (IP) cells and use RG fibres to migrate to the cortical plate (modified from Lui et al., 2011).

The stem cell niche (referred to in some studies as the neurogenic niche) provides an essential microenvironment for maintaining different neural progenitors. Furthermore, the niche — specifically its organisation, the density of neuronal progenitors, and their spatial orientation — is pivotal for conducting signalling pathways (e.g., Notch, Wnt) that guide the preliminary stages of neuronal differentiation (Stolp and Molnar, 2015). Both Notch and ß-catenin signalling pathways have been identified as having a substantial impact on cell proliferation within the VZ, through the cell junctions between neuronal progenitors (Shen et al., 2004). Furthermore, data obtained from the mouse model indicates that N-cadherin and ß-catenin are essential elements for forming these junctions. Therefore, a disruption in ß-catenin expression across the apical surface results in a decreased level of proliferation, potentially leading to cortical malformation (Junghaus et al., 2005).

Moreover, Hatakeyama et al. (2014) demonstrated that adherent junction disruption by electroporation, with a form of cadherin lacking an extracellular domain, leads not

only to the disorganisation of N-cadherin across the ventricular surface but also impairment in the Zona occludens-1 (Zo-1) pattern and increased neuron production within the VZ of developing brain. This study has highlighted the crucial role of the way proteins (Notch1 and one of its ligands Dll1), which physically interact with Zo-1, distributed around the ventricle. Furthermore, utilising the live-cell imaging technique has shown that active Notch signalling and subsequent proper interaction of Notch proteins with Zo-1 is essential for inhibiting premature differentiation of neuronal differentiation.

The RG-specific markers widely expressed by cells in the OSVZ have been extensively researched. Such studies identified many markers, including nestin (NES), vimentin (VIM), paired box 6 (PAX6), and glial fibrillary acidic protein (GFAP), as well as T-box brain protein 2 (TBR2), the cell marker for intermediate progenitors (IPs) (Zecevic et al., 2005; Bayatti et al., 2008; Mo and Zecevic, 2008).

Intermediate progenitors are reportedly a highly diverse group of progenitor cells (Hansen et al., 2010). These findings describe (Lui et al., 2011) three significant human-specific features in corticogenesis that cause progenitors to undergo an active expansion phase, resulting in an increased number of neocortical neurons. These features are as follows: (1) increased precursor cells due to the presence of non-ventricular, or outer RG cells (oRGs), (2) IPs derived from multiple cycles of asymmetric oRG division, and (3) increased proliferative capacity in the IPs enabling increased neuron generation (Figure1.2).
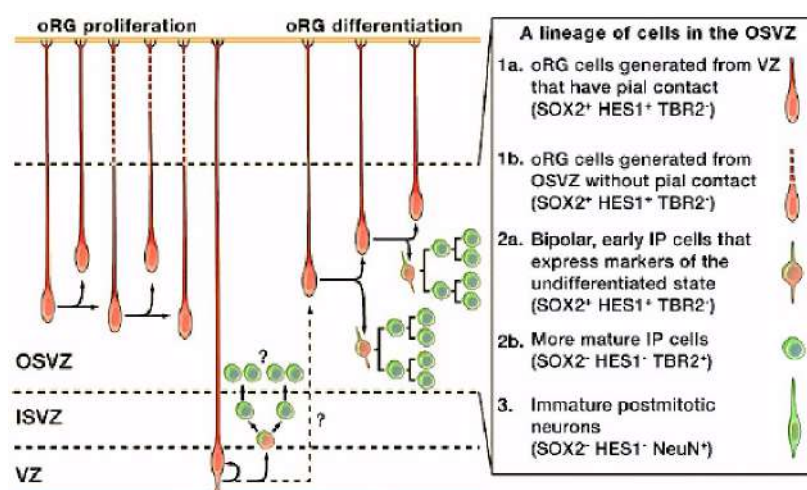
Figure 1.2. Schematic representation of the cell diversity within the OSVZ. The loss of Sox2 expression and active Notch signalling (HES1) with the subsequent activation of TBR2 expression illustrates the process of differentiation of oRG daughter cells. And as the result of highly coordinated processes of proliferation and differentiation, expanded OSVZ to an increased number of neurons (modified from Lui et al., 2011).

Both cell proliferation and neuronal migration require precise spatial and temporal control during cerebral cortex development. The first evidence of preplate (PP) formation is detectable at GW5. At this stage, PP consists of a layer of early-born neurons, and by GW7-8 will be subdivided into the marginal zone (MZ) and the deeper subplate (SP) in the developing cortical plate (CP) (Barkovich, 2012).

To generate a multi-layered cortex, late-born neurons pass early-born neurons while migrating in the CP (Molyneaux et al., 2007). Subsequently, the cerebral cortex is organised in an 'inside-out' manner, with early-born neurons located in the deep layers and late-born neurons ultimately residing in the superficial layers (Zecevic et al., 2011; Ayala et al., 2007; Stouffer et al., 2016). Shortly after the final stages of OSVZ formation (GW11), the active phase of neuronal migration begins, with its peak occurring in GW12-20 (Hansen et al., 2010; Stouffer et al., 2016).

In the developing cerebral cortex, there are two well-defined patterns of neuronal migration: radial and tangential migration. Radial migration is a prevalent form of neuronal movement during corticogenesis (Barkovich, 2014). One of the distinguishing features of this type of cell migration is that neurons, which originate in the proliferative zones of the developing brain, move along radially oriented glial fibres orthogonally to the surface of the brain. Prior to the onset of radial migration to the CP, cells undergo several changes. Initially, they switch to multipolar morphology (Tabata et al., 2003), influenced by diverse molecules promoting differentiation and locomotion along the basal process of RGCs towards the CP (Molyneaux et al., 2007; Stouffer et al., 2016; Nadarajah et al., 2001). Extracellular signals also contribute to the appropriate localisation of new-born neurons within the CP. The Reelin signalling pathway is best described among respective extracellular guidance. Cajal-Retzius neurons have been demonstrated to secrete reelin, which activates factors that drive migration in neurons (Stouffer et al., 2016; Jossin et al., 2011). Neurons characterised by radial migration to the CP region largely produce pyramidal projection neurons (Nadarajah et al., 2002). It is thought that this type of neurons represents approximately 75% of all neurons in the cortex. Through their axons, projection neurons connect to other areas of the cortex, as well as distant parts of the brain.

The second mode of movement is tangential migration. Neurons characterised by tangential migration originate from ganglionic eminences, move parallel to the brain's surface along axons or other neurons, differentiate into inhibitory GABA-ergic

neurons, and consequently integrate into local neuronal networks in the cerebral cortex (Marin et al., 2003; Marin, 2012).

In the developing human brain, neurogenesis is eventually followed by gliogenesis. Glia may comprise as much as 50-90% of the entire cell count in the human brain. From an evolutionary perspective, it is suggested that a significant number of glial cells are necessary for achieving brain complexity. Possible indications of this are an enlarged glial pool and increased long-range conduction across white matter tracts (Freeman et al., 2013). Based on their origin, morphology, and functions, glial cells may be divided into two groups: macroglia (astrocytes and oligodendrocytes) and microglia. Glial cells that belong to the first class originate from RGGs, and both form pre- as well as postnatally. Conversely, microglia differ by their place of origin. Studies have compellingly demonstrated that microglia evolve from yolk sac precursors (Ginhoux et al., 2016; Hoeffel et al., 2015; Ginhoux et al., 2010). Microglial progenitors subsequently migrate to the brain parenchyma and rapidly diverge from other tissue-resident macrophages, in their gene expression and specific role in modulating cellular immune response (Li et al., 2018).

1.2. Pathophysiological development of the human cerebral cortex

Due to the complexity of cerebral cortex development in humans, spatial and/or temporal disruption leads to anatomical and functional malformations with different degrees of severity. Approximately 2-5% of children worldwide have been diagnosed with intellectual disabilities of differing origins (Ropers, 2010; Sheridan et al., 2013). Causal factors in the malformation in cortical development (MCD) include neuronal migration disorders resulting from infectious, toxic, or vascular events, and genetic disorders resulting from single or multiple gene mutations (Romero et al., 2018; Jamuar et al., 2014).

1.2.1. Malformations in cortical development

As a rare congenital abnormality within the cerebral cortex, MCD has drawn much attention from neuroscientists as well as paediatricians. Patients affected by MCD suffer from epilepsy (frequently an intractable form of epilepsy) and different degrees of intellectual retardation or disability. Approximately 40% of children with an intractable form of epilepsy are also estimated to have MCD (Lee, 2017). The term 'malformations of cortical development' was introduced in 1996 (Barkovich et al.,

1996; Barkovich et al., 2012). The first general classification of MCD was implemented the same year and was largely based on the development stage in which the disruption occurred (Barkovich et al., 1996). Due to continued advances in genetic techniques and visualisation approaches, the original classification scheme has been revised several times. The most up-to-date version (Barkovich et al., 2012) is based on two key factors: the time point and the pathogenesis of the disruption. Considering these factors, MCDs are divided into three main groups: group I, MCD secondary to abnormal neuronal and glial proliferation or increased apoptosis; group II, MCD caused by abnormal neuronal migration; and group III, MCD resulting from abnormal postmigrational development.

Group I refers to MCD arising from interruptions in early-stage cortical development and comprises abnormalities in the proliferation of neuronal progenitors, as well as an imbalance between the proliferation and apoptosis. Group I is divided into three subgroups: group IA, microcephaly; group IB, megalencephaly; and group IC, cortical dysgenesis with abnormal cell proliferation. One of the main characteristics of primary microcephaly is decreased brain size, without any distinct size abnormality in any other body organs. Brain MRIs in patients diagnosed with primary microcephaly exhibit a comparably normal structure. However, the brain volume is less than two standard deviations below the average (Figure 1.3.A).

In rare cases of primary microcephaly, MRIs also reveal a reduction in gyral pattern complexity, cortical heterotopia, or cerebral hypoplasia (Pang et al., 2008). There are two widely accepted theories behind the development of this type of microcephaly: a decreased proliferation of neural progenitors and an acceleration of apoptosis (Lee, 2018). Numerous studies have identified several contributory genes. These gene mutations largely affect neurogenesis by interfering in several processes including cell cycle regulation, transcription in other genes, centrosome duplications, and DNA repair (Feng et al., 2004; Desir et al., 2008; Griffith et al., 2008; Thornton et al., 2009; Shen et al., 2010; Yu et al., 2010; Barkovich et al., 2012). Overall, such interference may result in proliferation abnormalities and consequently fewer neurons.
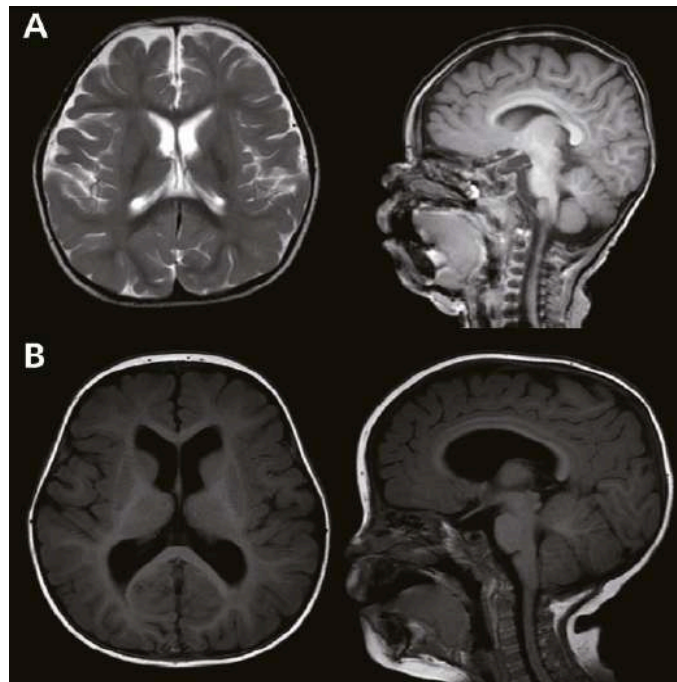
Figure. 1.3. Brain MRI of patients suffering from microcephaly (A) and megalencephaly (B). (A) MRI of the brain of an 18-month old male patient showing a significant decrease in total brain volume with the maintenance of the relatively normal overall structure. **(B)** MRI of the brain of a 3-year old male patient revealing the larger size of the head and a mild level of the ventriculomegaly without any other prominent structural abnormality (modified from Lee, 2017).

Megalencephaly describes a condition in which brain volume is two or more standard deviations above the average (Figure 1.3.B). This group of MCDs is not clearly defined, with approximately 6% of patients with polymicrogyria also demonstrating phenotypic characteristics of megalencephaly (Leventer et al., 2010).

However, extensive study of the pathways involved in regulating cell proliferation has revealed the pathogenesis of several MCD types. For instance, the mammalian target of rapamycin (mTOR pathway) has been demonstrated to have a significant role in abnormal cortical development in the tuberous sclerosis complex (TSC) (Crino et al., 2006). The protein products of the TSC1 and TSC2 genes (Hamartin and Tuberin, respectively) form the TSC complex. This complex plays an essential role in inhibiting the mTOR activity. The regulation of the TSC complex itself is subjected to extensive regulation. Receptor binding of various growth factors activates intracellular protein kinases such as mitogen-activated protein kinase or Akt that suppress the activity of the TSC complex by phosphorylation. The deviations in the mTOR activity could affect numerous expression patterns associated with mitochondria biogenesis and hypoxia-response and subsequently inhibits autophagy (Lipton, J. O. and Sahin, M., 2014). Imbalance in the mTOR signalling could lead to

various changes in the number of cellular processes, including cell growth and proliferation. The discovery of the mTOR pathway's contribution to TSC development has significant therapeutic implications: mTOR pathway inhibitors are now used in clinics as a potential treatment for subependymal giant cell astrocytoma (de Vries et al., 2010).

Group II MCDs (MCDs largely derived from the disruption of neuronal migration) comprise four subgroups: (1) periventricular heterotopia (the interruption of neuronal migration during the initiation stage); (2) generalised abnormalities in neuronal migration (a diverse group of lissencephalies with different grades of severity); (3) localised deviations in the migration process (subcortical heterotopia); and (4) MCD originating from abnormally terminated migration or structural defects in the pial membrane ('cobblestone malformations') (Barkovich et al., 2012).

Lissencephaly, referred to as 'smooth brain' (Figure 1.4.A), is among the most widely known MCDs. Although many causative genes have been identified, the exact pathophysiological mechanisms are poorly understood. It is characterised by an absence of sulci/gyri and a thickening of the cerebral cortex. Furthermore, it is associated with defects in neural proliferation, neurogenesis, and neuronal migration, resulting in severe developmental impairment.
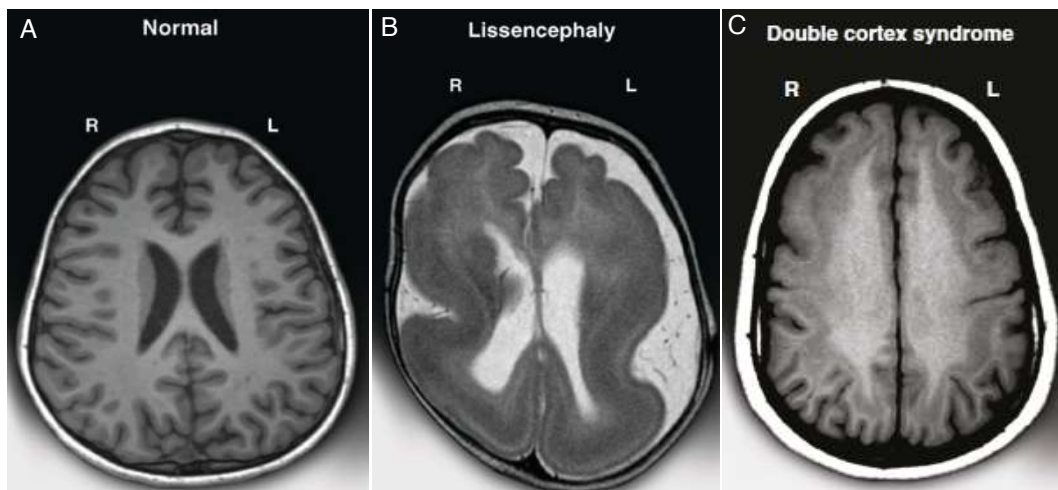
Figure 1.4. Representative brain MRIs of different subgroups of MCD caused by neuronal migration abnormalities. (A) Axial T1-weighted MRI scan exhibits normally folded cortex with distinct gyri and sulci. **(B)** Axial T2-weighted MRI scan shows the most severe simplification of the gyri structure of the cortex. This clinical case is an example of agyria (absence of gyrification), and it is more pronounced posteriorly. **(C)** Axial T1-weighted scan from a patient diagnosed with a mosaic case of double cortex syndrome involving the mutation of the DCX gene. The extra band of grey matter is located under the normal outer fraction of the cerebral cortex (modified from Poduri et al., 2013).

Mutations linked to the development of lissencephaly have been identified in six genes. Two of these are instrumental in the majority of lissencephaly cases: LIS1 (PAFAH1B1 — platelet-activating factor acetylhydrolase, isoform 1b, subunit 1) and DCX (doublecortin). Both have a role in microtubule assembly, structure, and transport. LIS1 is a cofactor of cytoplasmatic dynein (a minus end-directed microtubule motor) and regulates its function (McKenney et al., 2010). DCX binds to and stabilises microtubules. Like LIS1 and DCX, TUBA1A (tubulin α1a) is a microtubule-related protein. RELN (reelin) and VLDLR (very low-density lipoprotein receptor) are involved in signalling pathways, and ARX (aristaless-related homeobox) functions as a transcriptional regulator (Gleeson et al., 1998; Reiner et al., 1993; Poirier et al., 2007; Keays et al., 2007).

DCX has also been identified as having a crucial role in regulating typical neuronal migration from the brain VZ to the superficial cortical layers. A mutation in DCX results in migration that terminates approximately halfway to the cortex and the formation of a 'double cortex' (Figure 1.4.C) (Sicca et al., 2003; Gleeson et al., 2000).

1.2.2. Miller-Dieker syndrome

Miller-Dieker syndrome (MDS) represents the most severe form of lissencephaly (Figure 1.5). It is largely characterised by defective neuronal migration and an abnormally thick cortex lacking the typical sulci/gyri of the folded cortical surface. The majority of patients suffering from MDS have grade 1 lissencephaly (complete agyria). However, several reported cases have exhibited grade 2 lissencephaly (Dobyns et al., 1999).
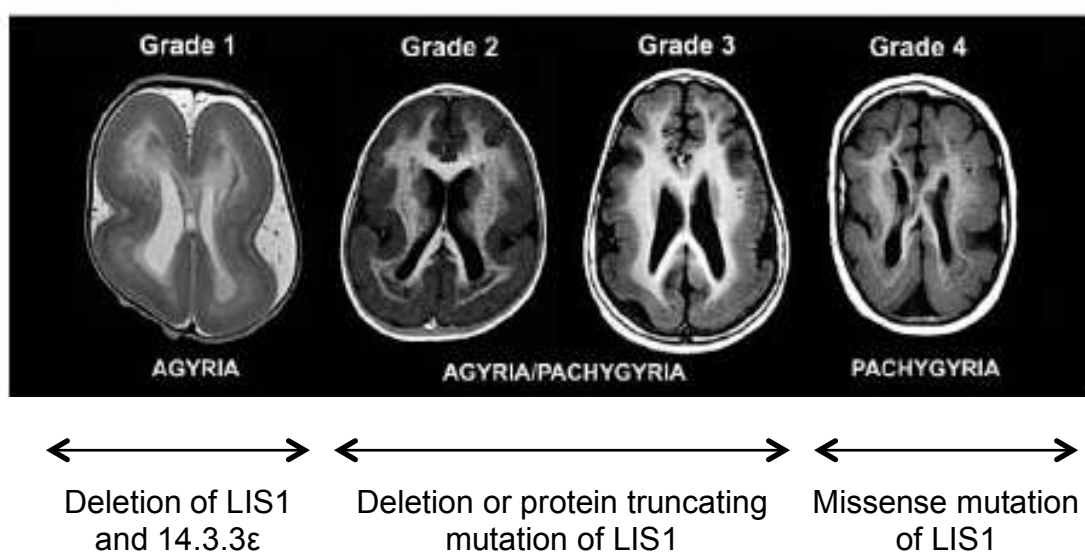
Figure 1.5. The spectrum of lissencephaly severity grades. Four grades of lissencephaly are shown, assigned grades 1 to 4 (from most to least severe) according to the Dobyns et al. classification, 1999. **(Grade 1)** Agyria is characterized by a complete absence of the gyri/sulci (MDS). **(Grade 2 and 3)** Agyria/pachygyria represented by severe simplification of the gyrification; however, the manifestation is not as prominent as in the case of pure agyria. (Grade 4) Pachygyria is a mild form of lissencephaly and reflects a more modest clinical phenotype with unusually thick convolutions of the cortex (modified from Poduri et al., 2013).

MDS has severe neurological consequences such as mental retardation and intractable epilepsy, as well as dysmorphic facial features. The syndrome is caused by heterozygous deletions in the short arm of chromosome 17 (17p13.3) and involves a loss of function in a subset of genes, including *LIS1* and *YWHAE* (coding for 14.3.3ε protein).

Approximately 80% of individuals diagnosed with MDS reportedly experience a *de novo* deletion of the *YWHAE* gene. The remaining 20% inherit a deletion from a parent carrying a balanced chromosome rearrangement (Dobyns and Das, 2014). Heterozygous *LIS1* mutations occur with equal frequency in males and females. The dosage has a critical role in haploinsufficiency development in *LIS1* (Reiner and Sapir, 2003). In 60% of cases, the development of MDS is considered to involve a disruption in splicing variants of the *LIS1* gene (Saillour et al., 2009). An estimated 90% of individuals with MDS carry a visible or submicroscopic deletion in chromosome 17p13.3 (Ledbetter et al., 1992). In addition, 1 in 50,000–100,000 patients have a ring chromosome disorder (Kim et al., 2014). Since ring chromosomes originate from the fusion of short and long arms within the chromosome, it is highly likely that deletions might occur during this process (Kim et al., 2014). One reported case of MDS described a patient who had 46 chromosomes with a ring structure replacing chromosome 17 (Sharief et al., 1991). However, advanced techniques in cell reprogramming may eventually lead to therapeutic opportunities for such individuals. Bershteyn et al. (2014) have demonstrated that reprogramming fibroblasts from patients with ring chromosomes duplicates the wild-type homologous chromosome, eliminating the ring chromosome. Significantly, these results suggest that it is possible to develop an approach to correct large-scale chromosomal aberrations (Kim et al., 2017).

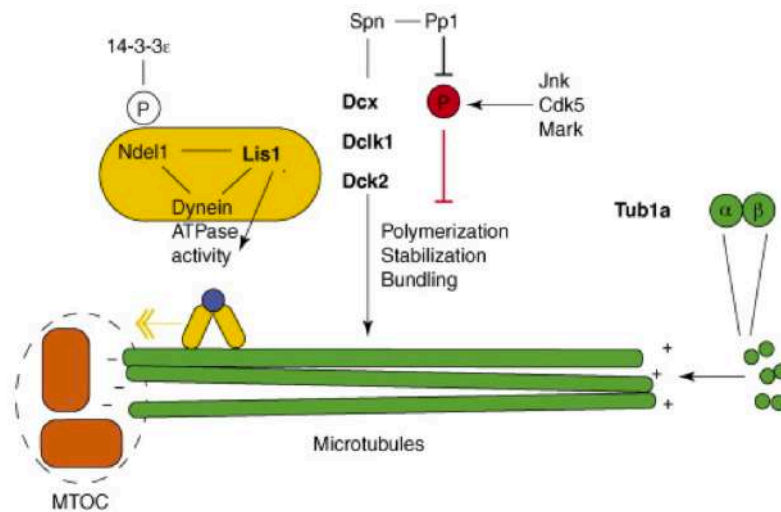### 1.2.3. Role of LIS1/NDEL1/14.3.3ε complex deficiency in developing MDS

LIS1 was the first gene identified as causative in this type of MCD. Specifically, it catalyses acetyl group removal at the SN-2 position of the platelet-activating

component (Hattori et al., 1994). LIS1 has been demonstrated to be a dose-dependent modifier of lissencephaly severity (Toyo-oka et al., 2003). Data obtained from models using LIS1- and NDEL1-deficient mice, has indicated that these protein levels impact the speed of neuronal migration and neurite length. Applying two-photon confocal time-lapse microscopy, Youn et al. (2009) demonstrated a proportional decrease in the speed of neuronal migration combined with neurite elongation due to reduced LIS1 levels in embryonic day 14.5 cortical slices. Moreover, a complete loss of LIS1 or NDEL1 inhibited nuclear movement in cortical slice cultures. Data obtained from studying LIS1 and NDEL1-deficient mice models demonstrated that the level of those proteins has an impact on both speed of neuronal migration and the length of neurites. By applying two-photon confocal time-lapse microscopy, Youn and colleagues were able to show the proportional decrease in speed of neuronal migration combined with elongation of neurites under reduction of the level of LIS1 protein from 50% to 35% in embryonic day 14.5 cortical slices. Interestingly, in contrast to the increased length of the leading process, the number of branching points was significantly reduced, resulting in a largely straight pattern of neuronal migration. Moreover, a comprehensive loss of LIS1 or NDEL1 inhibited cell movement in cortical slice cultures.

LIS1 binds proteins such as NDEL1 to form larger protein complexes with dynein (Figure 1.6) (Efimov and Morris, 2000). NDEL1 is a spindle-associated gene, and mutations have reportedly lead to severe microcephaly characterised by defects in RGGs on both quantitative and morphological levels (Niethammer et al., 2000; Feng and Walsh, 2004; Alkuraya et al., 2011; Guven, 2011).

Blocking NDEL1 activity affects centrosomal duplication, resulting in cell spindle disassembly (Tsai et al., 2007). A significant aspect of LIS1 activity is its association with the microtubule complex (Reiner and Sapir, 2003). Protein 14.3.3ε binds with proteins containing phosphoserine and mediates intracellular signal transduction. An interaction partner of LIS1, it stabilises the complex by protecting it from dephosphorylation. Disruption in the LIS1 gene has been known to alter microtubule dynamics, eventually producing defects in proliferation and neurogenesis (Yingling et al., 2008), and neuronal migration (Smith et al., 2000). Loss-of-function experiments in mutant mice have been instrumental in revealing the basic mechanisms of lissencephaly. Hirotsune et al. (1999) produced LIS1 homozygous knockout (KO) mice to investigate the role of LIS1 in brain development. The KO mice embryos died

shortly after implantation, suggesting that LIS1 is essential in the initial stages of brain development.

Figure 1.6. The current model for the role of Lis1 and Ndel1 in the process of neuronal migration. Lis1 and Ndel1 are components of the dynein motor complex (gold ovals). Cargo (represented as a blue circle) attached to this complex will move from the "+" to the "-" end of microtubules (anchored to the microtubule-organizing centre (MTOC) by using dynein-mediated ATP hydrolysis. Lis1 is able to directly regulate the ATPase activity of dynein (labelled as an arrow), and by doing so; it may regulate the speed of cargo movement as well. One of the key roles of 14.3.3ε is to protect the phosphorylation state of Ndel1; however, it may have other roles that are not yet fully understand. The Dcx protein, along with homologs Dclk1 and Dclk2, directly regulate microtubule polymerization and bundling, an effect that is negatively regulated by the c-Jun N-terminal kinase (JNK), Cdk5, and mitogen-activated protein (MAP)/microtubule affinity regulatory kinase (Mark) kinases (inhibitory phosphorylation is depicted in red) (modified from Kerjan & Gleeson, 2007).

Blocking NDEL1 activity affects centrosomal duplication, resulting in cell spindle disassembly (Tsai et al., 2007). A significant aspect of LIS1 activity is its association with the microtubule complex (Reiner and Sapir, 2003). Protein 14.3.3ε binds with proteins containing phosphoserine and mediates intracellular signal transduction. An interaction partner of LIS1, it stabilises the complex by protecting it from dephosphorylation. Disruption in the LIS1 gene has been known to alter microtubule dynamics, eventually producing defects in proliferation and neurogenesis (Yingling et al., 2008), and neuronal migration (Smith et al., 2000). Loss-of-function experiments in mutant mice have been instrumental in revealing the basic mechanisms of lissencephaly. Hirotsune et al. (1999) produced LIS1 homozygous knockout (KO) mice to investigate the role of LIS1 in brain development. The KO mice embryos died shortly after implantation, suggesting that LIS1 is essential in the initial stages of brain development.

Furthermore, a series of experiments on homo $^{(-/-)}$ - and heterozygous $^{(-/+)}$ mutant mice, demonstrated that a phenotype caused by decreased LIS levels is dosage-sensitive. Additionally, the heterozygous phenotype in mice was revealed to be milder than the phenotype observed in patients carrying heterozygous LIS1 mutations. Animal models examined possible interventions to normalise disrupted developmental patterns (Yamada et al., 2009; Toba et al., 2013).

1.3. Model systems to study the process of human cortical development

Research dedicated to physiological and pathophysiological corticogenesis is frequently hindered by limited access to primary human brain tissue. Therefore, current knowledge has largely been obtained using animal models and advanced genetic and neuroimaging techniques. Compared to the human brain, however, the mouse brain is not only smaller in size but also has a less diverse pool of proliferating cortical progenitors and neuronal subtypes (Figure 1.7).
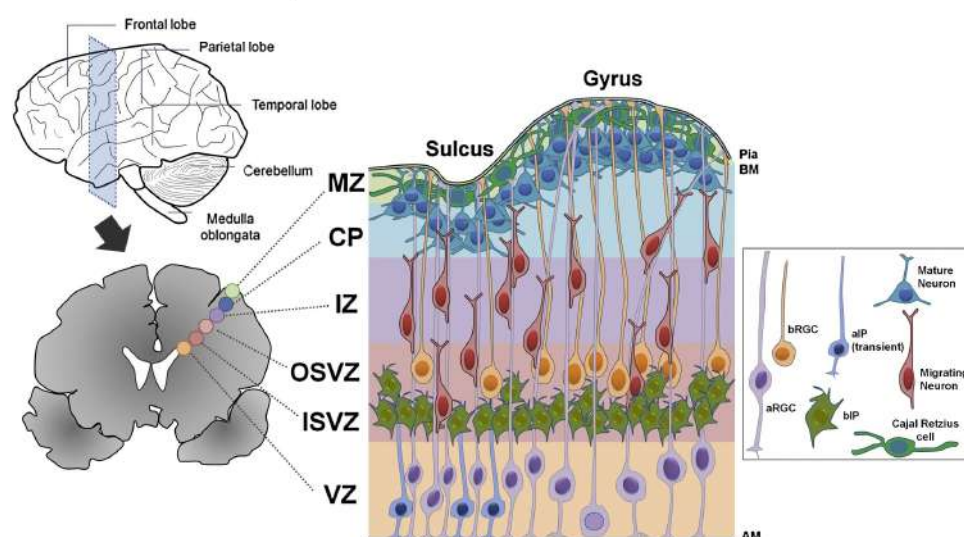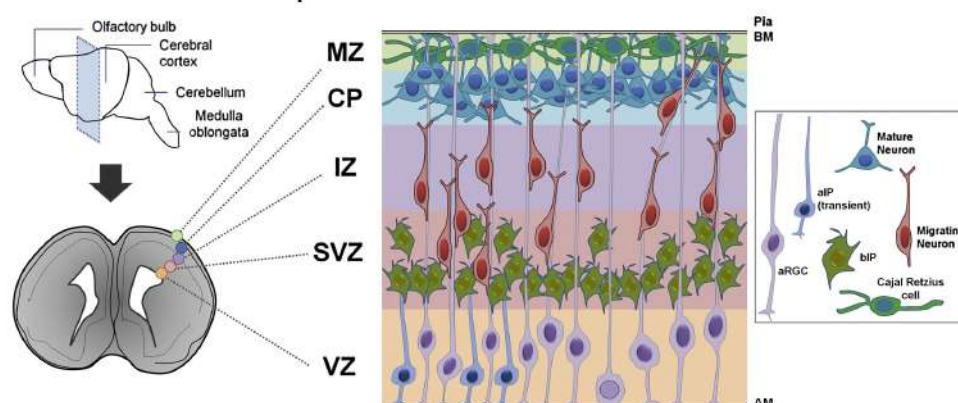
Figure 1.7. Schematic comparison of corticogenesis in the human gyrencephalic and mouse lissencephalic brains. The different color circles depict each developing cortical region (indicated on the right). The location and prototypical cell types present in each region are illustrated in the righthand panels. **(A)** Lateral view of an adult gyrencephalic brain (top left) and a slice of developing brain (coronal view, lower left). **(B)** Lateral view of an adult lissencephalic brain (top left) and a developing brain slice (coronal view, lower left). The division of the SVZ into iSVZ and oSVZ regions and the formation of sulci and gyri are the main organisational differences between human and mouse brains (adapted from Romero et al., 2018).

Furthermore, a much larger human cortex results in longer distances for neuronal migration through the six-layered cortical structure. Collectively, this has resulted in high demand for *in vitro* systems based on human cells, to overcome fundamental limitations in using animal models to study brain development. Moreover, evolutionary differences (humans are believed to have diverged from rodents approximately 75 million years ago) present challenges in using animal models to accurately recapitulate physiological and pathophysiological brain development (Sayed et al., 2016).

1.3.1. Induced pluripotent stem cells

In 2007, cells that closely resembled embryonic stem cells (ESCs) could be generated from skin fibroblasts by reprogramming them using a combination of four transcriptional factors (later termed 'Yamanaka factors') — Oct4, Sox2, Klf4, and c-Myc (Takahasi et al., 2007). These cells were named induced pluripotent stem cells (iPSCs), and they shared the key properties of hESCs (potency and ability to self-renewal) without requiring the use of human embryos for their derivation. Methods of generating iPSCs have revolutionised fundamental research and cell-based disease modelling. Hence, iPSCs have become a popular tool for overcoming limitations associated with animal models.

Currently, reprogramming several types of somatic cells (e.g., skin fibroblasts and blood cells) followed by differentiation into previously inaccessible cell types (including human neurons and cardiomyocytes) has become routine laboratory practice (Shi et al., 2017; Sayed and Wu, 2017). Accordingly, scientists have used patient-derived iPSCs to unveil previously unknown aspects of the disorder, as well as information regarding human-specific features of cerebral development.

Considerable progress in iPSC differentiation into neuronal progenitors, specifically into cortical neurons, has enabled distinct aspects of human corticogenesis to be modelled *in vitro (*Shi et al., 2012; Espuny-Camacho et al., 2013; Maroof et al.,

2013). The combined inhibition of two signalling pathways — the transforming growth factor-β (TGF-β)-pathway (which is crucial for maintaining pluripotency in ESCs) and the bone morphogenetic protein (BMP)-pathway — produces neuronal progenitors with a high level of expression in the PAX6 marker and forebrain identity (Chambers et al., 2009). Under neuronal differentiation in two-dimensional (2D) cultures, iPSC-derived progenitors may be dorsal (producing glutamatergic cortical projection neurons) or ventral (creating cortical interneurons). In addition, differentiation along the dorsal specification occurs in a specific order, with reelin-positive cells generated first, followed by deep- and upper-layer neurons (Espuny-Camacho et al., 2013). The iPSC-based 2D culture system has successfully modelled several neurological disorders, including neurodevelopmental and psychiatric conditions (reviewed in detail by Ardhanareeswaran et al., 2017).

1.3.2. iPSC-derived 3D cortical organoids

Although an iPSC-derived 2D culture (as in any other *in vitro* platform) has many advantages, there are also several limitations. Foremost, is a lack of histoarchitecture that presents in tissue- and organ-like contexts. In recent years, tremendous efforts have been made to overcome this limitation by establishing a three-dimensional (3D) model that more accurately reflects aspects of tissue organisation during human brain development. Numerous studies have demonstrated that under appropriate conditions, iPSCs form 3D structures, termed organoids (Eiraku et al., 2008; Mariani et al., 2012; Kadoshima et al., 2013; Lancaster et al., 2013; Sasai, 2013, Quian, 2015).

Organoids may be defined as *in vitro* structures, the formation of which is based on the ability of stem cells to self-organise and assemble in complex tissue structures. After undergoing differentiation, they resemble (at least in part) the histoarchitecture of *in vivo* organs (Di Lullo and Kriegstein, 2017). When these self-organised structures contain areas resembling several different regions of the brain, they are generally referred to as 'whole brain organoids' or 'cerebral organoids'. Such definitions reflect the broad regional identities of organoids. Conversely, if small molecules are used to prime the cultures and direct them into a specific brain region, they may be referred to as 'forebrain organoids' or 'midbrain organoids' (Kadoshima et al., 2013; Jo et al., 2016; Qian et al., 2016). Numerous studies have demonstrated that such culture systems facilitate investigation into fundamental aspects of

physiological human brain development, as well as phenotypical alterations associated with congenital cortical malformations, in a controlled manner (Camp et al., 2015; Kadoshima et al., 2013; Lancaster et al., 2013; Mariani et al., 2015; Qian et al., 2016). Cited 'method of the year' in 2017, organoids drew much attention and became an increasingly popular platform for studying human-specific features in different applications (Method of the Year 2017: Organoids; Nature Methods, 2018). Eiraku et al. (2008) were among the first to successfully use 3D cultures to study fundamental mechanisms underlying the initial stages of the developing nervous system. They introduced hPSC-derived 3D cultures that they termed SFEBq (serum-free floating culture of embryoid body-like aggregate with quick reaggregation). As a result of this study, they have obtained self-organised cultures that exhibit apical-basal polarity in forebrain cortical tissue with distinct ventricular- and subventricular-like zones and cortical plate-like regions containing different neuronal subtypes. The field of 3D brain organoids is among the most rapidly evolving cell-based approaches to modelling human brain development. As such, considerable progress has been made in the past five years. A key feature of 3D culture is its ability to not only generate human-specific cell types but also observe their pattern of cell division and/or migration over an extended period, in a tissue-like context. One of the clearest examples of it is the presence of the human-specific oRG progenitors (also known as basal radial glial cells) in the SVZ-like region of developing organoids (Fietz et al., 2010; Hansen et al., 2010; Lancaster et al., 2013; Qian et al., 2016). Hence, human cell types observed in iPSC-derived brain organoids have made this cell culture system optimal for studying human-specific aspects of brain development, particularly during the initial stages.

1.4. Aim of the study

Using human stem cell models, this study aims to investigate the role of the LIS1 gene in human cortical development and its contribution to Miller-Dieker syndrome (MDS). Animal models have been highly instrumental in identifying the role this gene plays during corticogenesis. When compared to the human brain, however, mice models reveal several limitations. The mouse brain naturally lissencephalic and comprises a less diverse pool of proliferating progenitors and neuronal subtypes. Consequently, data obtained from these models is not completely transferable to humans. Therefore, there is a requirement for models that more accurately reflect aspects of human cortical development and MDS in a tissue-like context. In this study, we will establish a standardised induced PSC-derived 3D cortical organoid model to interpret the role of the LIS1/NDEL1/14.3.3ε protein complex during human corticogenesis. To achieve this, we will reprogram fibroblasts from patients diagnosed with MDS and confirmed haploinsufficiency in chromosome 17p13.3, involving genes that code for LIS1 and 14.3.3ε proteins. We will differentiate these cells into cortical cultures and analyse proliferation and neurogenesis on morphological, biochemical, and molecular levels. The main goal of the current study is to provide an experimental model to investigate the functional role of the LIS1/NDEL1/14.3.3ε protein complex during human cortical progenitor expansion and, therefore, gain a deeper understanding of its involvement in the development of MDS pathology.

2. Materials

2.1. Technical equipment

Appliance	Name	Manufacturer	Registered office
Autoclave	D-150	Systec	Wettenberg, Germany
Balance	BL610	Sartorius	Göttingen, Germany
Balance	LA310S	Sartorius	Göttingen, Germany
Block heater	Thermomixer compact	Eppendorf	Hamburg, Germany
Centrifuge (cell culture)	Megafuge 1.0R	Sorvall	Hanau, Germany
Centrifuge(table top)	5415D	Eppendorf	Hamburg, Germany
Counting chamber	Fuchs-Rosenthal	Faust	Halle, Germany
Cryostat	Cryostat HM 560	Microm Laborgeräte	Walldorf, Germany
Digital camera	C 5050 Zoom	Olympus Optical	Hamburg, Germany
Embedding molds	Tissue-Tek Cryomold	Sakura Finetek	Iphen aan den Rijn, The Netherlands
Fluorescence lamp	HAL100	Carl Zeiss	Jena, Germany
Fluorescence microscope	Axioskop 2	Carl Zeiss	Jena, Germany
Freezer -80°C	HERAfreeze	Kendro	Hanau, Germany
Gel electrophoresis chamber	Agagel	Biometra	Göttingen, Germany
Imaging system	Chemidoc 2000	Bio-Rad	München, Germany
Imaging system	Geldoc EZ	Bio-Rad	München, Germany
Incubator	HERAcell	Kendro	Hanau, Germany
LED light source	Colibri 2	Carl Zeiss	Jena, Germany

Appliance	Name	Manufacturer	Registered office
Liquid nitrogen store	MVE 611	Chart Industries	Burnsville, USA
Microscope	Axiovert 200M	Carl Zeiss	Jena,Germany
Microscope	IX 81 Confocal	Olympus	Hamburg, Germany
Microscope	Axio Imager Z1	Carl Zeiss	Jena,Germany
Microscope	DMI6000 B	Leica Microsystems	Wetzlar, Germany
Microscope camera	Axiocam MRM	Carl Zeiss	Jena, Germany
Microscope laser	Laser Mells Griot	Griot Lasergroup	Carlsbad, Germany
Microscope slides	Superfrost plus	Menzel-Gläser	Braunschweig, Germany
Micro-spectrophotometer	Nanodrop ND-1000	Thermo Fisher Scientific	Wilmington, USA
Micropipettes	Labmate L10, L100, L1000	Labmate	Langenfeld, Germany
Multilabel reader	EnVision 2104	Perkin Elmer	Rodgau, Germany
Nucleofector	Nucleofector 2b	Lonza	Basel, Switzerland
PAGE/Blot equipment	Mini-Protean 3	Bio-Rad	München, Germany
PCR cycler	T3000 Termocycler	Biometra	Göttingen, Germany
pH-meter	CG840	Schott	Mainz, Germany
Pipette-boy	Accu-Jet	Brand	Wertheim, Germany
Power supply for electrophoresis	Standard Power Pack P25	Biometra	Göttingen, Germany
Real-time qPCR machine	Mastercycler realplex	Eppendorf	Hamburg, Germany
Refrigerators 4°C /-20°C	G 2013 Comfort	Liebherr	Lindau, Germany
Stereo microscope	STEMI 2000-C	Carl Zeiss	Göttingen, Germany

Appliance	Name	Manufacturer	Registered office
Secure horizontal flow hood	HERAsecure	Kendro	Hanau, Germany
Sterile laminar flow hood	HERAsafe	Kendro	Hanau, Germany
Shaker	Bühler Tilt Shaker WS 10	Johanna Otto	Hechingen, Germany
Table centrifuge	Centrifuge 5415R	Eppendorf	Hamburg, Germany
Thermocycler	T3 Thermocycler	Biometra	Göttingen, Germany
Ultracentrifuge	Sorvall	Discovery 90 SE	Hanau, Germany
Vacuum pump	Vacuubrand	Brand	Wertheim, Germany
Vortexer	Vortex Genie 2	Scientific Industries	New York, USA
Water bath	1008	GFL	Burgwedel, Germany
Water filter	Millipak 4	Millipore	Eschborn, Germany

2.2. Cell culture consumables

2.2.1. Cell culture plastic ware

Consumables	Manufacturer	Registered Office
6-well culture dishes	BD Falcon	Bedford, USA
12-well culture dishes	BD Falcon	Bedford, USA
24-well culture dishes	BD Falcon	Bedford, USA
96-well lipidure-coat plates	Ambsbio	Abingdon, U.K.
Cell Strainer 40 µm Nylon	BD Falcon	Bedford, USA
Cryovials 1 ml	Nunc	Wiesbaden, Germany
Cryovials 1.8 ml	Nunc	Wiesbaden, Germany
PCR strip tubes 0.2 ml	peqLab	Erlangen, Germany

Consumables	Manufacturer	Registered Office
Low-adhesion plates ⌀ 6 cm	Labomedic	Bonn, Germany
Low-adhesion plates ⌀ 10 cm	Labomedic	Bonn, Germany
Serological pipettes 1 ml	BD Falcon	Bedford, USA
Serological pipettes 2ml	Corning Life Sciences	Schiphol-Rijk, The Netherlands
Serological pipettes 5ml	Corning Life Sciences	Schiphol-Rijk, The Netherlands
Serological pipettes 10ml	Greiner Bio-One	Solingen, Germany
Serological pipettes 25ml	Corning Life Sciences	Schiphol-Rijk, The Netherlands
Syringes Omnifix Luer 50 ml	Braun	Melsungen, Germany
Syringe fier 0.2 µm	Pall	Dreieich, Germany
TC dishes ⌀ 3.5 cm	PAA	Pasching, Austria
TC dishes ⌀ 6 cm	PAA	Pasching, Austria
TC dishes ⌀ 10 cm	PAA	Pasching, Austria
Tubes 0.5 ml	Greiner Bio-One	Solingen, Germany
Tubes 1.5 ml	Greiner Bio-One	Solingen, Germany
Tubes 2 ml	Greiner Bio-One	Solingen, Germany
Tubes 15 ml	BD Falcon	Bedford, USA
Tubes 50 ml	BD Falcon	Bedford, USA

2.2.2. Chemicals and additives

Substance	Manufacturer	Registered office
Agar	Sigma-Aldrich	Deisenhofen, Germany
Agarose	PeqLab	Erlangen, Germany
Ampiciline	Sigma-Aldrich	Deisenhofen, Germany
BDNF	Cell guidance systems	Cambridge, UK

Substance	Manufacturer	Registered office
BSA solution (7.5%)	Sigma-Aldrich	Deisenhofen, Germany
B27 supplement mix	Invitrogen by Thermo Fisher	Carlsbad, USA
CaCl$_2$	Sigma Aldrich	Deisenhofen, Germany
CHIR99021	Cell guidance systems	Cambridge, UK
Chloroform	Carl Roth	Karlsruhe, Germany
DAPI	Axon Medchem	Groningen,The Netherlands
D-Glucose	Sigma-Aldrich	Deisenhofen, Germany
DMEM	Gibco by Life Technologies	Waltham, USA
DMEM/F12 (1:1)	Gibco by Life Technologies	Waltham, USA
DMSO	Sigma Aldrich	Deisenhofen, Germany
DNA ladder (100bp/1kbp)	PeqLab	Erlangen, Germany
DNase	Invitrogen by Thermo Fisher Scientific	Carlsbad, USA
dNTPs	PeqLab	Erlangen, Germany
Doxycycline	Sigma Aldrich	Deisenhofen, Germany
EDTA	Sigma Aldrich	Deisenhofen, Germany
Ethanol	Sigma Aldrich	Deisenhofen, Germany
Ethidium bromide	Sigma-Aldrich	Deisenhofen, Germany
FCS	Invitrogen by Thermo Fisher Scientific	Carlsbad, USA
GDNF	Cell guidance systems	Cambridge, UK
Gelantin	Sigma-Aldrich	Deisenhofen, Germany
Geltrex	Gibco by Life Technologies	Waltham, USA
Glucose	Sigma-Aldrich	Deisenhofen, Germany
Glutamax	Sigma-Aldrich	Deisenhofen, Germany
Glycerol	Sigma-Aldrich	Deisenhofen, Germany
Glycin	Sigma-Aldrich	Deisenhofen, Germany

Substance	Manufacturer	Registered office
H_2O_2	Sigma-Aldrich	Deisenhofen, Germany
HCl	Sigma Aldrich	Deisenhofen, Germany
Isopropanol	Sigma Aldrich	Deisenhofen, Germany
IWR-1	Enzo	Lörrach, Germany
KnockOut™Serum Replacement	Gibco by Life Technologies	Waltham, USA
Laminin	Thermo Fisher Scientific	Waltham, USA
LB-Medium powder	Carl Roth	Karlsruhe, Germany
L-glutamine (100x)	Gibco by Life Technologies	Karlsruhe, Germany
Luminol	Sigma Aldrich	Deisenhofen, Germany
2-Mercaptoethanol	Invitrogen by Thermo Fisher Scientific	Carlsbad, USA
Methanol ROTIPURAN	Carl Roth	Karlsruhe, Germany
Mowiol	Carl Roth	Karlsruhe, Germany
N2 supplement (100x)	Life Technologies	Karlsruhe, Germany
Neurobasal medium	Life Technologies	Karlsruhe, Germany
Non-essential amino acids (100x)	Life Technologies	Karlsruhe, Germany
DPBS	Life Technologies	Waltham, USA
PFA	Sigma Aldrich	Deisenhofen, Germany
Penicillin-Streptomycin	Gibco by Life Technologies	Karlsruhe, Germany
PluriPro	Cell guidance systems	Cambridge, UK
Poly-L-ornithine	Sigma-Aldrich	Deisenhofen, Germany
Puromycin	PAA	Pasching, Austria
Powdered milk	Carl Roth	Karlsruhe, Germany
Rho-Kinase-Inhibitor Y-27632	Cell guidance systems	Cambridge, UK
Puromycin	PAA	Pasching, Austria

Substance	Manufacturer	Registered office
SDS	Sigma Aldrich	Deisenhofen, Germany
Sodium pyruvate (100x)	Invitrogen by Thermo Fisher Scientific	Carlsbad, USA
Sucrose	Carl Roth	Karlsruhe, Germany
TriFast peqGOLD	PeqLab	Erlangen, Germany
Tris	Sigma Aldrich	Deisenhofen, Germany
Triton-X-100	Sigma Aldrich	Deisenhofen, Germany
Trypane Blue	Invitrogen by Thermo Fisher Scientific	Carlsbad, USA
Trypsin inhibitor (TI)	Gibco by Life Technologies	Waltham, USA
Trypsin-EDTA (10x)	Gibco by Life Technologies	Waltham, USA
XAV 939	Enzo	Lörrach, Germany

2.2.3. Cell culture media compaunds and its final concentration

Reagent	Concentration	Solvent	Manufacturer	Registered office
A83-01	500 nM	DMSO/ Ethanol	Miltenyi Biotec	B.Gladbach, Germany
B27	supplement mix, 1:100	supplement mix	Life Technologies	Karlsruhe, Germany
BDNF	20 ng/mL	PBS; 0,1% BSA	Cell guidance systems	Cambridge, UK
cAMP	150 ng/mL	H_2O	Sigma Aldrich	Deisenhofen, Germany
CHIR99021	1 µM	DMSO	Cell guidance systems	Cambridge, UK
Glucose	0,2 mg/mL	H_2O	Carl Roth	Karlsruhe, Germany

Reagent	Concentration	Solvent	Manufacturer	Registered office
Doxycycline	0,25 µg/mL	H_2O	Sigma Aldrich	Deisenhofen, Germany
GDNF	20 ng/mL	PBS; 0,1% BSA	Cell guidance systems	Cambridge, UK
Heparin	10µg/mL	PBS	Sigma Aldrich	Deisenhofen, Germany
Insulin	2,5µg/mL	H_2O	Sigma Aldrich	Deisenhofen, Germany
IWR-1	10µg/mL	DMSO	Enzo	Lörrach, Germany
LDN-193189	180 nM	DMSO	Miltenyi Biotec	B.Gladbach, Germany
N2	supplement mix, 1:200	supplement mix	Life Technologies	Karlsruhe, Germany
Puromycin	1 mg/mL	H_2O	PAA	Pasching, Austria
ROCK inhibitor Y-27632	5mM	H_2O	Cell guidance systems	Cambridge, UK
XAV939	10µg/mL	DMSO	Enzo	Lörrach, Germany

2.2.4. Cell culture media

All basal media were ordered from Life Technologies (Karlsruhe). All compounds were mixed and sterile-filtered (0.2 µm filter), stored at 4°C and used within 4 weeks.

iPSC medium	
99%	PluriPro
1x	Penicillin/Streptomycin

Neural stem cell (N2) medium	
98%	DMEM/F12
1x	N2 Supplement
1x	Penicillin/Streptomycin
1.5 mg/ml	D-Glucose

Neural induction medium for 2D adherent cultures	
96.5%	Neural stem cell (N2) medium
0.5x	N2 supplement
0.5x	B27 supplement
1x	A83-01
1x	LDN193189
1x	XAV939
1x	Non-essential amino acids
1x	Glutamax
1x	Penicillin/Streptomycin
1.5 mg/ml	D-Glucose

Neural induction medium for 3D forebrain organoids	
96.5%	DMEM/F12
0.5x	N2 Supplement
0.5x	B27 Supplement
1x	A83-01
1x	LDN193189
1x	XAV939
1x	Heparin

1x	Non-essential amino acids
1x	Glutamax
1x	Penicillin/Streptomycin
1.5 mg/ml	D-Glucose

Neural differentiation medium for 3D forebrain organoids	
98%	DMEM/F12
0.5x	N2 Supplement
0.5x	B27
1x	Insulin
1x	Penicillin/Streptomycin
1.5 mg/ml	D-Glucose

2.2.5. Cell lines

Skin fibroblasts from all donors were obtained from the Coriell Biorepository (Ctrl1, Ctrl2, and MDS1 fibroblasts were reprogrammed by non-integrative delivery of Oct4, Sox2, Klf4, and c-Myc using Sendai virus (SeV) vectors (Ban et al., 2011). MDS2 fibroblasts were reprogrammed using a retrovirus approach as previously described (Koch et al., 2011).

Cell line	Source
Ctrl 1	Catalogue ID GM00969, 2 year old female
Ctrl 2	Catalogue ID GM08680, 5 months old male
MDS 1	Catalogue ID GM06097, 1 year old female
MDS 2	Catalogue ID GM09208, 18th week male fetus

2.3. Molecular biology consumabales

2.3.1. Buffers

6x DNA loading buffer	
2 ml	EDTA (0.5M; pH 8.5)
6 g	Sucrose
0,2 ml	2% Bromphenol-blue-solution
0,2 ml	2% Xylene-cyanol-solution
0,2 g	Ficoll
3,8 ml	Aqua bidest.
The solution was mixed well, prepared in 1 ml aliquots and stored at 4°C	

PFA fixation solution (4%)	
40 g	PFA
1000 ml	H2O
The solution was heated until PFA dissolved completely, pH adjusted to 7.4 and sterile filtered.	

Immuno-blocking solution	
89.9%	PBS
10%	FCS
0.1% or 0.5%	Triton X100 (only for intracellular epitopes)

Moviol / DABCO	
12 ml	Tris solution (0.2 M; pH 8.5)
6 ml	H2O
6 g	Glycerol
2.6 g	Moviol
0.1 g	DABCO

50x Tris-acetate-EDTA-buffer (TAE)	
242 g	Tris
100 ml	EDTA solution (0.5M; pH 8.5)
57.1 ml	Water-free acetic acid (100%)
add	H2O to 1000ml

SDS-PAGE separation gel buffer	
99.6%	Tris solution (1.5M; pH 8.8)
0.4%	SDS

SDS-PAGE stacking gel buffer	
99.6%	Tris solution (1.5M; pH 6.8)
0.4%	SDS

SDS-PAGE buffer 10x	
30 g	Tris
144 g	Glycin
add H2O to 1000 ml (pH 8.0)	
For running buffer add 1% SDS to 1x SDS-PAGE buffer	
For blotting buffer add 20% Methanol to 1x SDS-PAGE bufffer	

Protein loading buffer	
75.75%	Tris solution (0.1 M; pH 6.8)
20%	Glycerol
4%	SDS
0.25%	Bromphenol blue

10x TBS	
80g	NaCl
2g	KCl
30g	TrisBase

| add H$_2$O to 1000 ml, pH 7.4 |
| For 1x TBST dilute 10x TBS 1:10 with H$_2$O and add 1% Tween-20 |

Lysis buffer	
2.5 ml	Tris HCl (1 M)
5 ml	NaCl (1.5 M)
2.5 ml	EDTA (0.5 M)
Triton^{TM} X-100	100 µl
Add to 50 ml aqua bidest.	

TE4-buffer	
1.58 g	Tris-HCl
0.29 g	EDTA
add H$_2$O to 1000 ml	
Adjust pH to 8 with solid NaOH	

2.3.2. Solutions

Enhanced chemiluminescence (ECL) solution	
4.5 ml	H$_2$O
0.5 ml	Tris HCl (1 M)
50 µl	Luminol
20 µl	p-coumaric acid
1.5 µl	H$_2$O$_2$ (30%)

PCR master mix (10 ml)	
1 ml	10x reaction buffer
600 µl	MgCl$_2$ (50 mM)
40 µl each	dNTPs
8.24 ml	Ampuwa H$_2$O

qPCR master mix (5 ml)	
2000 µl	GoTaq® Flix buffer
1000 µl	MgCl$_2$ (25 mM)
20 µl each	dNTPs
7.5 µl	1000x SYBR-green
1 µl	Fluorescin
400 µl	DMSO
1511.5 µl	Ampuwa H$_2$O

2.3.3. Ezymes

Enzyme name	Manufacturer	Registered office
Alkaline Phosphatase, Shrimp	Roche Diagnostics	Penzberg, Germany
DnaseI (molecular biology)	Invitrogen	Karlsruhe, Germany
GoTaq G2 Flexi DNA polymerase	Promega	Mannheim, Germany
Phusion High Fidelity DNA Polymerase	New England Biolabs	Frankfurt, Germany
T4 DNA Ligase	New England Biolabs	Frankfurt, Germany
Taq DNA Polymerase, recombinant	Invitrogen	Karlsruhe, Germany

2.3.4. Restriction endonucleases

Enzyme name	Restriction site	Manufacturer	Registered office
NotI	5'…GC^GGCCGC…3' 3'…CGCCGG^CG…5'	New England Biolabs	Frankfurt, Germany
MluI	5'...A^CGCGT...3' 3'...TGCGC^A...5'	New England Biolabs	Frankfurt, Germany
PstI	5'... GC^GGTAGC...3' 3'... CCTGCGC^A ...5'	New England Biolabs	Frankfurt, Germany
SalI	5'... TGC^AACGT...3' 3'... ACTTGG^CG...5'	New England Biolabs	Frankfurt, Germany

2.3.5. Plasmids

Plasmid name	Source or parent DNA sequence
PB-TetON-AAVS1-LIS1	AAV-CAGGS-EGFP
PB-TetON-AAVS1-YWHAE	AAV-CAGGS-EGFP
pRRLSIN.cPPT.PGK-GFP.WPRE	Addgene Plasmid #12252 (Fuerer et al., 2010)
pSuperTOPflash	Adgene Plasmid #24308

2.3.6. Bacterial solutions

LB agar	
20 g	LB-Medium powder (Roth)
15 g	Agar
H2O was added to 1 l, the mixture was autoclaved and stored at 4 °C	

LB medium	
40 g	LB-Medium powder (Roth)
H2O was added to 2 l, the mixture was autoclaved and stored at 4 °C	

2.3.7. Kits

Name	Producer	Office
DNeasy Blood Tissue Kit	Qiagen	Hilden, Germany
iScript cDNA Synthesis Kit	Bio-Rad	München, Germany
peqGOLD Gel Extraction Kit	Peqlab Biotechnologie	Erlangen, Germany
peqGOLD Plasmid Miniprep Kit I	Peqlab Biotechnologie	Erlangen, Germany
Pierce BCA Protein Assay Kit	Thermo Fisher	Rockford, USA
PureYield Plasmid Maxiprep System	Promega	Mannheim, Germany
RNeasy Kit	Qiagen	Hilden, Germany

2.3.8. Primers

Cloning primer Name	Primer sequence (5'-3')
Lis1_FWD	GAATTCATGGTGCTGTCCCAGAGA
Lis1_REV	GCGGCCGCTCAACGGCA
Ywhaε_FWD	ATGGATGATCGAGAGGATCT
Ywhaε_REV	TCACTGATTTTCGTCTTCCA
Wnt-GFP_FWD	GGCCCGAAGGAATAGAAG
Wnt-GFP_REV	AACGGGCCACAACTCCTC

RT-PCR primer name	Primer sequence (5'-3')
Emx1_FWD	AGACGCAGGTGAAGGTGTGG
Emx1_REV	CAGGCAGGCAGGCTCTCC
FoxA2_FWD	CCACCACCAACCCCACAAAATG
FoxA2_REV	TGCAACACCGTCTCCCCAAAGT
FoxG1_FWD	CCCTCCCATTTCTGTACGTTT
FoxG1_REV	CTGGCGGCTCTTAGAGAT
GAPDH_FWD	ACGACCCCTTCATTGACCTCAACT
GAPDH_REV	ATATTTCTCGTGGTTCACACCCAT
HoxA2_FWD	TTCAGCAAAATGCCCTCTCT
HoxA2_REV	TAGGCCAGCTCCACAGTTCT
HoxB2_FWD	TTTAGCCGTTCGCTTAGAGG
HoxB2_REV	CGGATAGCTGGAGACAGGAG
HoxB4_FWD	ACACCCGCTAACAAATGAGG
HoxB4_FWD	GCACGAAAGATGAGGGAGAG
HoxB6_FWD	GAACTGAGGAGCGGACTCAC
HoxB6_REV	CTGGGATCAGGGAGTCTTCA

RT-PCR primer name	Primer sequence (5'-3')
Nkx2.1_FWD	CGCATCCAATCTCAAGGAAT
Nkx2.1_REV	TGTGCCCAGAGTGAAGTTTG
Otx2_FWD	TGCAGGGGTTCTTCTGTGAT
Otx2_REV	AGGGTCAGAGCAATTGACCA
Pax5_FWD	AGGATGCCGCTGATGGAGTAC
Pax5_REV	TGGAGGAGTGAATCAGCTTGG
Lis1_FWD	TCTCCCCATTGAGTGTGTCA
Lis1_REV	CACGCTCCATTAAACCCTGT
Ywhaε_FWD	ATGGATGTGGAGCTGACAGT
Ywhaε_REV	CCAGTGTTAGCTGCTGGAAT
SeV_FWD	GGATCACTAGGTGATATCGAGC
SeV_REV	ACCAGACAAGAGTTTAAGAGATATGTATC
18S_FWD	TTCCTTGGACCGGCGCAAG
18S_REV	GCCGCATCGCCGGTCGG

2.3.9. Antibodies

Primary antibody	Dilution	Source
Acetylated α-tubulin rb	1:500	NEB
AFP ms	1.200	NEB
Akt (pan) (C67E7)	1:2000	Cell Signaling
Arl13b ms	1:50	DSHB
ß-actin ms	1:5000	Millipore
β-Catenin (6B3) ms	1:1000	Cell Signaling
ß-III-tubulin ms	1:2000	Sigma-Aldrich
Ctip2 rat	1:500	Abcam
Dach1 rb	1:100	ProteinTech
Foxg1 rb	1:300	TebuBio
Emx1 rb	1:500	Sigma-Aldrich

Primary antibody	Dilution	Source
Pax6 rb	1:500	DSHB
phoshpo-Akt (S473)	1:1000	Cell Signaling
phospho-β-Catenin (S552) rat	1:1000	Cell Signaling
phoshpo-GSK-3ß ms	1:1000	Cell Signaling
PLZF ms	1:50	Merck
Reelin ms	1:300	MoBiTec
N-Cadherin ms	1:500	BD
Otx2 gt	1:500	R&D Systems
Tbr1 rb	1:500	Abcam
Tbr2 rb	1:500	Abcam
Tra1-60 ms	1:300	Merck
Tra1-81 ms	1:300	Merck
Tpx2 rb	1:500	Novus Biologicals
Satb2 ms	1:500	Abcam
SMA rb	1:400	Abcam
SSEA4 rb	1:500	Abcam
Sox2 ms	1:300	R&D Systems
Zo1 rb	1:100	DSHB

Secondary antibody	Dilution	Source
Alexa488 gt-anti-ms	1:1000	Life technologies
Alexa488 gt-anti-rb	1:1000	Life technologies
Alexa555gt-anti-ms	1:1000	Life technologies
Alexa555gt-anti-rb	1:1000	Life technologies
HRP-gt-anti-ms	1:1000	GE Healthcare Life Sciences
HRP-gt-anti-rb	1:1000	Thermo Scientific

ms = mouse; rb = rabbit; gt = goat

2.4. Software

Name	Application	Producer
ApE – A plasmid Editor v2.0.47	Cloning strategies	M. Wayne Davis
AxioVision 40 4.5.0.0	Fluorescence microscopy	Carl Zeiss
ClustalW v1.83	Sequence alignment	EMBL-EBI
Excel 2008	Data analysis	Microsoft
Image J 1.42q	Quantifications	NIH
Imagelab 5.0 build 18	Western blot documentation	Bio Rad
GenomeStudio 2011	SNP analysis	Illumina
Microsoft Office 2008	Figures and text processing	Microsoft
Photoshop CS3	Figures processing	Adobe
Primer3 v0.4.0	Primer design	Rozen and Skaletsky (2000)
Prism 6	Data analysis and statistics	GraphPad
Quantity One 4.6.8	Electrophoresis gel documentation	Bio Rad
Word 2008	Writing documents	Microsoft

3. Methods

3.1. Generation, maintenance, and quality control of iPSCs cultures

Skin biopsies from a 1-year-old female donor (MDS1.1, Coriell Institute, catalogue ID GM06097) with Miller-Dieker syndrome (MDS) as well as skin biopsies from a 2-year-old female donor (Ctrl1, Coriell Institute, catalogue ID GM00969) and a 5-month-old male donor (Ctrl2, Coriell Institute, catalogue ID GM08680) were reprogrammed by non-integrative delivery of Oct4, Sox2, Klf4 and c-Myc using Sendai virus vectors supplied by ID Pharma Co.Ltd (formerly DNAVEC Corporation) (Ban et al., 2011). Skin biopsies from a male fetus (MDS2, 18FW, Coriell Institute, catalog ID GM09208) with MDS were reprogrammed using a retrovirus approach as previously described (Koch et al., Nature 2011). IPSC lines were maintained on Geltrex (GT, Gibco)-coated cell culture plates in PluriPro (PP) medium (Cell guidance systems) with daily medium change. IPSCs were dissociated to single cells by TrypLE Express (Gibco) treatment when cultures reached 100% confluency and split in a 1:2 – 1:4 ratio. Following dissociation to single cells, the medium was supplemented with 5µM ROCK inhibitor Y-27632 (Cell guidance systems) to promote single cell survival. All human iPSC lines were regularly checked and confirmed negative for mycoplasma. Generated iPSCs were fully characterized for a normal karyotype, and, in the case of patient-derived iPSCs, disease-specific microdeletion along chromosome 17 was confirmed by single nucleotide polymorphism (SNP). All iPSCs cell lines were validated for pluripotency and multi germ-layer differentiation using immunocytochemical staining.

3.1.1. SNP analysis of iPSCs

Genomic DNA was prepared using the DNeasy Blood & Tissue Kit (Qiagen). Whole-genome single nucleotide polymorphism (SNP) genotyping was performed at the Institute of Human Genetics at the University of Bonn. Genomic DNA at a concentration of 50ng/ml was used for whole-genome amplification. Afterwards, the amplified DNA was fragmented and hybridized to sequence-specific oligomers bound to beads on an Illumina Human610-Quad chip or a HumanCytoSNP-12 chip. Data were analyzed using Illumina BeadStudio.

3.1.2. Germ layer differentiation of iPSCs

In order to induce spontaneous differentiation into cell types of all three germ layers, iPSCs were dissociated into single cells using TrypLE Express and plated in an ultra-low-binding 96-well plate (9000 cells/well; Amsbio, lipidurecoat plate A-U96) in PP-medium supplemented with 50 µM ROCK inhibitor to induce embryoid body (EB) formation. After 2 days, EBs were plated onto GT-coated dishes in DMEM containing 10% fetal calf serum (FCS), 1% pyruvate and 1% non-essential amino acids (NEAA, Gibco). Cells were cultured for 4 weeks before being subjected to immunocytochemical analysis.

3.2. Generation of iPSC-derived cortical rosettes

Differentiation of iPSC-derived cortical rosettes was performed as described with slight adaptations (Shi et al., 2012). In brief, iPSCs were cultured in PluriPro medium (Cell Guidance Systems). Once the cell culture reached 95% confluence, neural induction was initiated by changing the culture medium to neural induction media containing DMEM/F12 (N2 supplement; 1:50), Neurobasal (B27 supplement; 1:50) mixed at a 1:1 ratio and cAMP (300 ng/ml, Sigma-Aldrich), LDN-193189 (0.5 µM, Miltenyi), A83-01 (0.21 µg, Miltenyi) and XAV939 (2 µM, Enzo). Cells were maintained in this medium for 8–11 days, collected by dissociation with TrypL Express (Invitrogen) and replated in neural differentiation media containing DMEM/F12 (N2 supplement; 1:50), Neurobasal (B27 supplement; 1:50) mixed at a 1:1 ratio and cAMP (300 ng/ml, Sigma Aldrich) on GT-coated plastic dishes. For analyzing neurogenesis, rosettes were passaged every 5 days in a 1:3 ratio. Quantification of ßIII-tubulin positive cells was performed at day 2 of each passage. For blocking of N-cadherin function, cells were plated at 140.000/cm2 on GT coated plastic dishes in neural differentiation media containing 20 µ g/ml N-cadherin blocking Antibody (Sigma, C3865), 25 µg/ml BDNF and 12.5 µg/ml GDNF (both Cell Guidance Systems). N-cadherin activation was performed by plating cells at $140.000/cm^2$ on plastic dishes coated with GT and 5 µg/ml N-cadherin protein (1388-NC, R&D Systems). Half of the media was changed on a daily basis. Quantification of ßIII-tubulin positive cells was performed on day 6. Analysis of neurogenesis was performed together with Fabio Marsoner.

3.3. Generation of standardized iPSC-derived forebrain-type organoids

On day 0 of organoid culture, iPSCs were dissociated into single cells by TrypLE Express treatment. For control and patient-derived iPSCs 6000 or 9000 cells/ml were plated in each well of an ultra-low-binding 96-well plate (Amsbio, lipidure-coat plate A-U96) in PP medium and 50µM ROCK inhibitor Y-27632, respectively. EBs were fed every other day for up to 5 days with PP-medium and then transferred to low-adhesion 6-cm plates (Labomedic) in neural induction medium containing DMEM/F12 (GIBCO) supplemented with N-2 supplement (GIBCO) and glucose (0.4mg/mL) mixed in a 1:1 ratio with Neurobasal (GIBCO) supplemented with B-27 supplement (GIBCO). Neural inducing medium was supplemented with Heparin (10 µg/ml, Sigma), 1% NEEAE, 1% GlutaMax TM, LDN-193189 (180nM, Milteneyi Biotec), A83-01 (500nM, STEMGENT) and XAV (10 µg/ml, Enzo). Following 5-6 days, the medium was switched to neural differentiation media containing DMEM/F12 supplemented with N-2 supplement and glucose (0.4mg/mL) mixed in a 1:1 ratio with Neurobasal supplemented with B-27 supplement. Organoids were embedded within the next 5 days as described previously in GT (GIBCO) (Lancaster & Knoblich, *2014*) and further cultured on a cell culture shaker with a medium chance every 2-4 days.

3.4. Generation of Lis1 and 14.3.3ε rescue lines

For the generation of PB-TetON-AAVS1-LIS1 or PB-TetON-AAVS1-YWHAE vector, homologous regions from the human AAVS1 locus were PCR-amplified from AAV-CAGGS-EGFP (addgene, cat. No.: 22212) using the following primer pairs: left homology region (HR-L), forward: GATATCTGCTTTCTCTGACCAGC; reverse, GATATCGCCCCACTGTGGGGTGG; right homology region (R-HR), forward: ACGCGTACTAGGGACAGGATTGG; reverse: ACGCGTAGAGCAGAGCCAGGAAC. The resulting PCR products were subcloned into the pCR-Blunt-II-TOPO Vector (Invitrogen) and the correct sequence was confirmed by Sanger sequencing resulting in pCR-Blunt-HR-L and pCR-Blunt-HR-R, respectively. pCR-Blunt-HR-L was digested with EcoRV and HR-L and cloned into the PBCAG-TIP-rtTA3-TRE-Tight-PolyA vector (gift by James D. Glover; (Glover et al., 2013) resulting in PBTetON-HR-L. pCR-Blunt-HR-R was digested with MluI and HR-R and cloned into the PB-TetON-HR-L vector resulting in PB-TetON-AAVS1. Successful cloning of HR-L/HR-R was confirmed by restriction digest and Sanger sequencing. LIS1 and YWHAE were PCR-amplified from cDNA obtained from commercially available human fetal brain tissue (single donor, female, 19 weeks of gestation). The resulting PCR products

were digested with HpaI for cloning into the PBTetON-AAVS1 resulting in PB-TetON-AAVS1-LIS1 and PB-TetON-AAVS1-YWHAE, respectively. Successful integration was determined by restriction digest and Sanger sequencing. The gRNA_AAVS1-T2, the hCas9_D10A and either the PB-TetON-AAVS1-LIS1 or the PB-TetON-AAVS1-YWHAE were transfected into MDS-derived iPSCs using the NucleofectorTM II system according to company protocols (Amaxa). In brief, 1 to 2 million cells were transfected with 0.5 µg DNA per plasmid. Following nucleofection, cells were plated on GT-coated cell culture plates in PP-medium supplemented with 5 µM ROCK inhibitor. Puromycin selection (0.25 µg/mL) was initiated 48 h following transfection. Generation, characterization and further experiments with Lis1 and 14.3.3ε rescue lines were performed together with George Manikakis.

3.5. Generation of Wnt-GFP reporter lines and quantification of the corrected total cell fluorescence

For examining the level of activation of Wnt signalling pathway control- (Ctrl2.1) and patient (MDS1.2) derived iPSCs were transduced with a lentiviral vector expressing GFP under activation of Wnt signalling (pRRLSIN.cPPT.PGK-GFP.WPRE, Addgene plasmid #12252, Feuer et al.). Puromycin (1 µg/ml, Sigma-Aldrich) selection was initiated 48h following transduction. IPSC lines with Wnt-GFP reporter were used to generate forebrain cortical organoids along with the standard protocol that was applied to all the other iPSC lines in the frame of this study. On day 20 of the forebrain cortical differentiation, 3D organoids were fixed, cryosectioned, and analyzed. The level of activation of the Wnt signalling pathway was analyzed based on the calculation of the corrected total cell fluorescence (CTCF) of the GFP signal along the ventricular-like area within cortical loops from Ctrl2.1 and MDS1.2 iPSC lines with Wnt-GFP reporter-derived organoids. For the CTCF quantification was used images of unstained cortical loop-like structures from the respective organoids. Images were acquired with an Apotome (Zeiss) using an AxioCamMRn (images were generated by combining 10 Z stacks with 1µm step stack each and with the acquisition time of 640 ms), processed using Axiovision Rel. 4.8 Software (Zeiss) and analyzed in ImageJ software using the formula: CTCF = integrated density – (area of selected cell multiplied with the mean fluorescence of background readings) along the protocol described by Burgess and colleagues in the number of papers (McCloy R. et al., 2014; Burges, A., 2012; Burgess A. et al., 2010).

3.6. Generation of Wnt reporter lines with luciferase activity and luciferase assay

For conducting luciferase assay control- (Ctrl1.2) and patient (MDS1.2) derived iPSCs were transduced with a lentiviral vector expressing luciferase under the control of the Wnt responsive TCF promoter element (pSuperTOPflash; Adgene Plasmid #24308). Puromycin (1 µg/ml, Sigma-Aldrich) selection was initiated 48h following transduction. Following selection, iPSC-reporter lines were differentiated into cortical rosettes. For luciferase assay, cortical cells were seeded on GT coated or GT and N-cadherin protein (5 µg/ml) coated 96 well plates at 100.000/per well. Cells were either cultured with neural differentiation media only or with neural differentiation media containing N-cadherin blocking antibody (20 µg/ml). After 24 h, cells were subjected to luciferase assay (Promega, following the supplier's instructions). The readout was performed at the Envision Multilabel reader (Perkin Elmer). The protein concentration of cell lysates was determined using the BCA protein assay kit (ThermoFischer, #23225). Luciferase signals were normalized to protein concentration. Generation of Wnt reporter lines expressing luciferase and luciferase assay itself were performed by Ammar Jabali and Kevin Weynans.

3.7. RT-PCR analysis

Triplicate total mRNA samples were isolated using TRIzol (Life Technologies) or an mRNA extraction kit (Quiagen) following the supplier's instructions. 1 µg total mRNA was used for reverse transcription with the iScript cDNA synthesis kit (BioRad) following the manufacturer's protocol. Semiquantitative PCR reactions were run in at least triplicates using Taq Polymerase (Invitrogen). PCR conditions and cycle numbers were adjusted to each primer pair for specific DNA amplification on cDNA obtained from commercially available human fetal (single donor, female, 19 weeks of gestation) or adult (single donor, female, 66 years old) brain tissue. For quantitative RT-PCR (q-RT-PCR), PCR products were assessed by dissociation curve and gel electrophoresis. Data were normalized to GAPDH or 18S rRNA levels.

3.8. Western immunoblotting

Cells were washed with cold PBS, scraped off into PBS, and collected via centrifugation. Cell pellets were lysed in RIPA buffer (50 mM Tris-HCl, pH 7.4, 150 mM NaCl, 1% TritonX-100, 1% sodium deoxycholate, 0.1% SDS) containing complete protease inhibitor cocktail (Roche, 04693159001) and PhosSTOP

phosphatase inhibitor (Roche, 04906837001) for 1 h on ice. Subsequently, cell debris was precipitated by centrifugation at 16,000 rcf for 15 min. The protein concentration of cleared cell lysates was determined using the BCA protein assay kit (ThermoFischer, #23225). For immunoblotting, 20 µg of protein were boiled in 6x SDS sample buffer for 2min at 95°C. Lysates were resolved on 8% or 12% gels and transferred onto 0.2 µm PVDF membranes by semi-dry blotting. PVDF membranes were blocked in 5% milk/TBS-T for 1 h at room temperature and subsequently incubated overnight with primary antibody at 4°C. Phospho-antibodies were diluted 1:1000 in 5% BSA/TBS-T, non-phospho-antibodies 1:1000 in 5% milk/TBS-T. The next day, blots were washed three times in TBS-T, incubated with corresponding HRP-conjugated secondary antibody diluted in TBS-T for 1h at room temperature. Eventually, blots were washed three more times in TBS-T and then visualized using the BioRad ChemiDoc XRS+ molecular imager. Western immunoblotting analysis was performed by Ruwen Wilkens.

3.9. Quantitative analysis of iPSC-derived forebrain organoids

Quantitative analysis of iPSC-derived forebrain organoids include measurements of the overall size of organoids, cortical loop parameters, assessment of the level of cell death, quantification of Tbr2+ intermediate progenitors, acetylated α-tubulin (ac-tubulin) strand density, plane of mitotic cell division and quantification of the apical membrane alignment.

The overall size of organoids was measured under a calibrated 4X bright field microscope. The total organoid area in $µm^2$ was determined by using ImageJ. For quantification of loop parameters, neural tube structures were nuclei stained by DAPI. Images were acquired with an Apotome (Zeiss) using an AxioCamMRn, processed using Axiovision Rel. 4.8 Software (Zeiss) and analyzed in ImageJ software. For quantification of the loop diameter, three measurements for each ventricular structure were performed, forming a right angle fan area pointing to the nearest pial surface at 0, 45, and 90 degrees, and the mean was calculated thereof. The length for the apical and basal membrane was measured in ImageJ software. The loop tissue area was defined as the ratio of the total loop area to the ventricle area (both assessed using ImageJ). Cell death was quantified in neural tube structures by counting activated caspase-3+ nuclei over total nuclei stained by DAPI. Tbr2 was quantified in neural tube structures by counting Tbr2+ stained nuclei over nuclei stained by DAPI. Ac-Tubulin strand density measurements were performed by

drawing a plot profile line at the 33rd percentile (apical side) and 66th percentile (basal side) of the loops and subsequently determining the numbers of ac-Tubulin strands crossing the plot profile line using ImageJ. Mitotic planes were quantified in neural tube structures by analyzing ≥2 20µm thick tenner serial sections stained for p-vimentin (to identify dividing cells) and Tpx2 (a spindle assembly factor used to visualize the plane of dividing cells). The orientation of the mitotic spindle of vRGCs was investigated in at least four different loops per organoid in relation to the prospective ventricular surface. For quantification of the apical membrane alignment four measurements (at 90°, 180°, 270°, and 360° to the loop centre) for each ventricular structure were performed, and the mean value was calculated. Loop parameters, Ac-Tubulin strand density and quantification of the apical membrane alignment were performed by Olivia Krefft. Quantification of the plane of mitotic cell division was performed together with George Manikakis.

3.10. Statistical analysis

Quantitative data was generated at least in biological triplicates. No statistical methods were used to predetermine sample sizes, but our sample sizes are similar to those generally employed in the field. All data were collected and processed randomly. Data distribution was assumed to be normal, but this was not formally tested. Means and s.d. were computed. All results presented as bar graphs show mean + s.d. Student's t-test using Prism 6 software, one-way ANOVA test using Prism 6 software or two-proportion z-test two-proportion z-test, or Kruskal-Wallis test followed by Bonferroni-corrected pairwise comparisons using a Mann-Whitney U test was performed to determine whether a significant difference exists between groups.

4. Results

4.1. Establishing standardized lissencephaly patient-specific iPSC-derived cortical culture systems

The field of cellular reprogramming has revolutionized the cell-based *in vitro* models of physiological and pathological development of the human brain. Due to the rapid development of advanced techniques, virtually any somatic cell may be efficiently reprogrammed and subsequently differentiated into a desired cellular phenotype. Numerous studies have successfully demonstrated the *in vitro* differentiation of iPSCs into telencephalic progenitors and, subsequently, cortical neurons (Shi et al., 2012; Espuny-Camacho et al., 2013; Maroof et al., 2013), indicating that human corticogenesis may be partially recapitulated *in vitro*. Much attention has been given to investigations of neurodegenerative diseases, both early- and late-onset. However, studies of developmental cortical malformations remain to be fully addressed in cell-based *in vitro* models of human development.

4.1.1. Generation and validation of induced pluripotent stem cells

Fibroblast lines derived from patients suffering from MDS (GM09208, GM06097) as well as age-matched healthy controls were obtained from the Coriell Institute for Medical Research, USA, and ISCN (International Standard of Cytogenetic Nomenclature) data is available (Coriell database, see the materials section). Three iPSCs lines (Ctrl1, Ctrl2, and MDS1) were generated by introducing the non-integrative reprogramming factors Oct4, Sox2, Klf4, and C-myc, using Sendai virus technology (a negative sense, single-stranded RNA virus from the Paramyxoviridae family). A fourth line (MDS2) was reprogrammed using a retroviral approach, as previously described (Koch et al., 201). The iPSCs were analysed for a regular karyotype and, if applicable, disease-specific microdeletion in chromosome 17. The analysis was conducted using single nucleotide polymorphism (SNP) (Figure 4.1. G) and validated for both pluripotency (Figure 4.1. A-C) and multiple germ-layer differentiation using immunocytochemical staining (Figure 4.1. D-F). SNP analysis of the iPSCs revealed a typical karyotype and specific microdeletion along chromosome 17 in iPSCs derived from MDS patients.
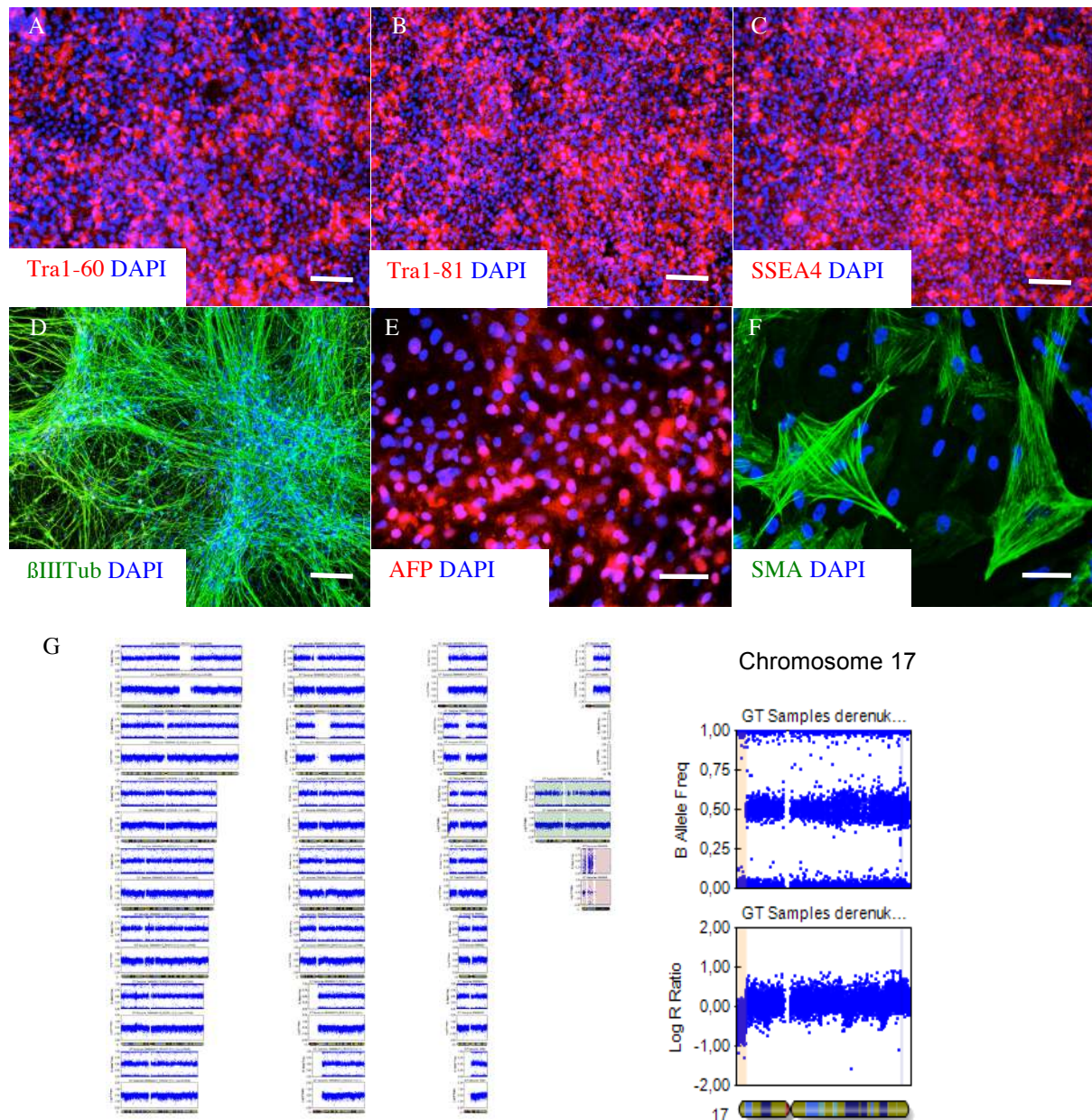
Figure 4.1. Basic characterisation and validation of control- and MDS-derived iPSCs.
(**A-C**) Immunocytochemical analyses of iPSCs demonstrate an elevated level of expression in several pluripotency-associated markers: Tra1-60 (**A**), Tra-1-81 (**B**), and SSEA4 (**C**). Representative images of iPSC clone MDS2.2 are depicted. Scale bars are set at 25 µm. (**D-F**) Following four weeks of *in vitro* differentiation, immunocytochemical analyses detected derivatives of all three germ layers, notably ßIII-tubulin+ (**D**, ßIII-Tub, ectoderm), alpha-1-fetoprotein+ (**E**, AFP, endoderm), and smooth muscle actin+ cells (**F**, SMA, mesoderm). Representative images of iPSC clone MDS2.2 are given. Scale bars are set at 25 µm (D) and 50 µm (E-F). (**G**) SNP analysis confirms heterozygous deletion along the short arm of chromosome 17 (17.3.3p) in MDS-derived iPSCs. The right panel illustrates the enlargement of chromosome 17. SNP refers to single nucleotide polymorphism.

4.1.2. Generation and validation of LIS1 and 14.3.3ε MDS-derived rescue lines

Much of the current data regarding the roles of LIS1 and Ywhaε in the pathological phenotype observed in MDS was obtained from KO mouse studies. The data

45

suggests that, on a molecular level, LIS1 gene disruption results in altered microtubule dynamics, leading to defects in cortical progenitor proliferation (Yingling et al., 2008) and neuronal migration (Smith et al., 2000). However, KO mice characteristically exhibit relatively mild deviations in the cortical organisation, which may be explained by the fact that their cortices are naturally lissencephalic compared to humans. Considering these factors, it is evident that the human-specific roles of LIS1 and YWHAE must be addressed. MDS caused by a deletion along the short arm of chromosome 17 (the exact length of the deleted region varies from patient to patient) cannot be completely repaired due to its size, as is possible in case of a point mutation. We applied the CRISPR/Cas9 gene-editing technique to perform LIS1 and 14.3.3ε rescue experiments, due to its improved integration and advanced gene expression. Conversely, lentiviral, doxycycline-inducible systems have been known to result in a somewhat random integration into the host genome. Moreover, they may produce a non-standard number of integrated genes, introducing bias due to selective pressure on cells with fever integration events. To overcome these issues, we used is a doxycycline-inducible and targets the AAVS1-locus, known as a 'safe harbour locus' (Sadelain, Papapetrou, & Bushman, 2012). Integration into the AAVS-1 locus of the genome provides control over the location and number of transgene copies (Cong et al., 2013; Gilbert et al., 2013). Stable iPSC lines were generated via guide RNA co-transfection, the modified Cas9, CRISPR-Lis1, and CRISPR-Ywhaε, using Amaxa nucleofection technology. The stable integration of CRISPR- LIS1 and CRISPR-Ywhaε, resulting in restored expression, was confirmed at the mRNA level. Accordingly, iPSC lines were harvested from MDS-LIS1 and MDS-14.3.3ε cultured for four days with or without doxycycline. The controls were mRNA from the corresponding starting cell line and healthy unedited iPSC lines. The mRNA was transcribed into cDNA and used to assess the level of expression in LIS1 and Ywhaε via qRT-PCR. The rescue strategy using CRISPR/Cas9 demonstrated a significant difference following the induction of the integrated genes, to transcriptional levels approximating healthy control lines (Figure 4.2. C-D). Once the stable doxycycline-inducible lines had been generated, they were used to create 2D and 3D cortical progenitor cultures enabling investigation into the contribution of LIS1 and YWHAE in the disease phenotype. The MDS-LIS1 and MDS-14.3.3ε rescue lines were generated and validated in collaboration with George Manikakis.
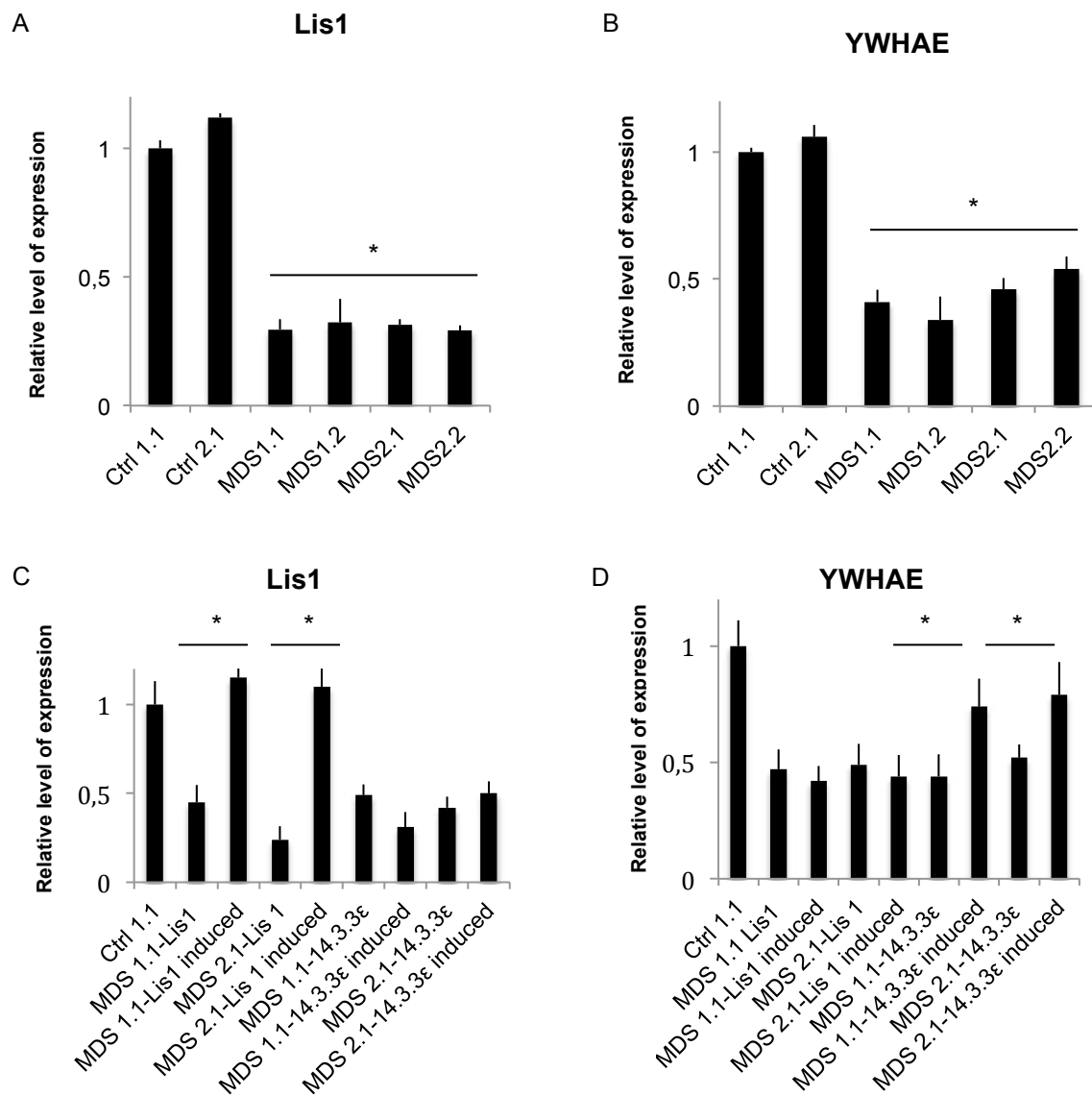
Figure 4.2. Validation of the level of Lis1 and Ywhaε expression in control-, MDS-derived, and genetically rescued iPSC lines. The qRT-PCR analysis demonstrates reduced expression levels of LIS1 (**A**) and YWHAE (**B**) in MDS-iPSC-derived cultures. Error bars, ±SD. *p<0.001. Validation of LIS1 (**C**) and YWHAE (**D**) relative expression levels in LIS1- and 14.3.3ε -rescue cell lines following 4 days of doxycycline induction of transgene. Error bars, ±SD. *p<0.001. (MDS-LIS1 and MDS-14.3.3ε rescue lines were generated and validated in collaboration with George Manikakis, figure modefied from Iefremova et al., 2017).

4.1.3. Generation and validation of iPSC-derived cortical progenitors and neurons

Extensive progress in the *in vitro* differentiation of iPSCs into telencephalic progenitors, and subsequently cortical neurons (Shi et al., 2012; Espuny-Camacho et al., 2013; Maroof et al., 2013), compellingly demonstrates that the complex process of human corticogenesis may be recapitulated *in vitro*, to a certain extent. Depending on the study aim, iPSC-derived neuronal progenitors may be differentiated into dorsal

progenitors, producing glutamatergic cortical projection neurons, or directed towards ventral progenitors that differentiate into cortical interneurons. In this study, patient and control iPSCs were differentiated into cortical rosettes according to the Shi protocol (Shi et al., 2012) with minor adaptations (described in the methods section). Applying this protocol to iPSCs lines, we generated homogeneous two-dimensional (2D) dorsal neuronal progenitor cultures expressing the typical neural precursor markers and early neuroepithelium markers (Figure 4.3. A-B, D-E).
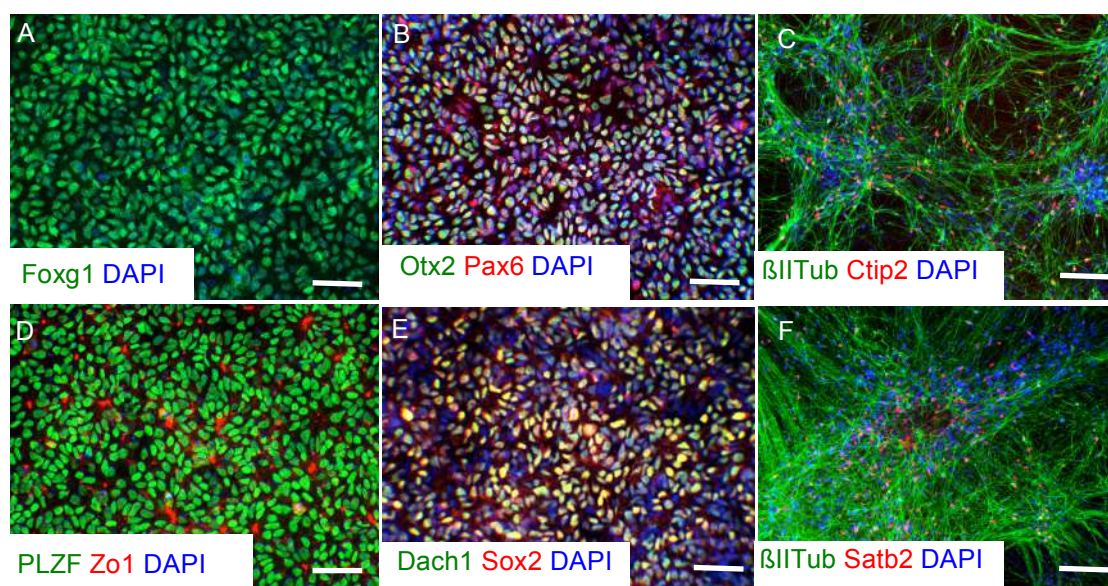
Figure 4.3. Generation of 2D iPSC-derived forebrain cortical cultures. Cortical progenitors express Sox2, Pax6, Dach1 and PLZF and exhibit polarized, apical expression of the tight junction protein Zo1 (**B, D, E**). The forebrain identity of the progenitors confirmed by Foxg1 (**A**) and Otx2 expression (**B**). Further differentiation of iPSC-derived neuronal progenitors yielded ßIII-tubulin positive neurons with several cortical phenotypes (Ctip2, Satb2; **C, F**).

Forebrain identity was confirmed by the expression of Foxg1 and Otx2 (Figure 4.3. A and B). Further differentiation in iPSC-derived cortical progenitors provided cortical neuronal cultures that strongly exhibited ßIII-tubulin and markers for different cortical neuronal layers such as Ctip2 and Satb2 (Figure 4.3. C and F).

4.1.4. Generation and validation of iPSC-derived forebrain-type organoids

While 2D cortical cultures have several advantages (e.g., a high degree of cell homogeneity, reproducibility, and efficiency), they lack essential aspects of tissue-like cytoarchitecture (such as self-organisation and the ability to form highly-stratified structures) required for studying human brain development.

Figure 4.4. Characterization of forebrain-type organoids.
(**A**) Schematic overview of the organoid protocol and representative images. Scale bar, 500 mm. (**B–F**) Immunocytochemical characterization of organoids at day 20 ± 2. Organoids organize in multiple neuroepithelial loops (**B**). Neuroepithelial cells express Sox2 (**C**), Pax6 (**D**), and Emx1 (**E**). Active proliferation of the neuronal progenitors around the ventricle marked by p-Vim expression (**F**) Scale bars, 50 μm. (**J**) RT-PCR analysis for region-specific transcription factors at day 20. FB, fetal brain control; AB, adult brain

49

Studies that have addressed these challenges using 3D culture systems (Kadoshima et al., 2013; Lancaster et al., 2013; Sasai, 2013) have previously demonstrated that under appropriate conditions, organoid cultures represent essential aspects of human brain development (e.g., curving morphology, intracortical polarity and the laminar arrangement of layer-specific cortical neurons) more accurately than adherent 2D cultures.

Additionally, cerebral/cortical organoids are characterised by the presence of human-specific progenitor zones (VZs), notably inner- and outer-subventricular zones (iSVZs and oSVZs) organised in an apical-basal order. Therefore, the organoid culture system may serve as a useful platform to help overcome the limitations of two-dimensional cultures. To address several questions regarding corticogenesis, we generated forebrain-type 3D organoids that permit greater insight into the cyto- and histo-architecture of developing cortical structures, including cell-autonomous/non-cell-autonomous processes in corticogenesis under healthy and MDS conditions, as well as observed collective cell behaviour over an extended period (Figure 4.4.).

4.2. MDS-derived organoids exhibit disease-associated alterations

Much of the available knowledge regarding regular and pathophysiological corticogenesis is largely derived from neuroimaging techniques, advances in genetics, and the investigation of animal models. However, these models have several limitations, as discussed in the introduction. Once we established a standardised and reproducible protocol for generating iPSC-derived forebrain cortical organoids, we applied it to determine the underlying mechanism of MDS.

4.2.1. Reduced size in MDS-derived forebrain-type organoids coincides with the *in vivo* data

We generated iPSC-derived cortical forebrain organoids from the skin biopsies of two patients with MDS and two gender- and age-matched healthy controls (two clones from each iPSC cell line). The MDS-derived organoids were organised into neuroepithelium loops, similar to the control 3D cultures. However, they appeared to be smaller in overall size than the control organoids (Figure 4.5. A and B).
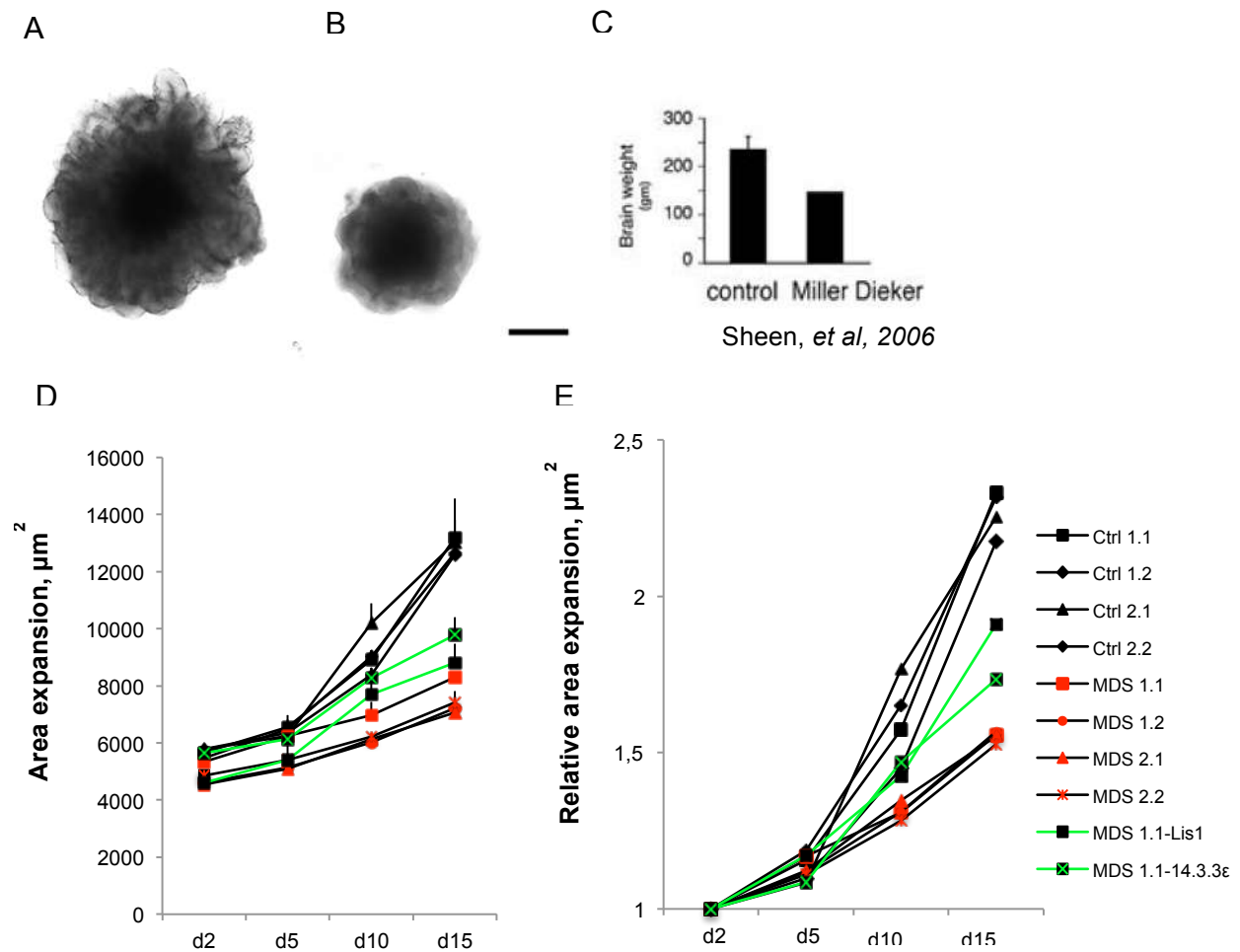
Figure 4.5. Reduced size and expansion rates of MDS patient-derived forebrain-type organoids. Representative bright-field images of a control- **(A)** and MDS-derived organoids **(B)** at day 15. Scale bar, 500 µm. (**C**) *In vivo* data from the comparative analysis of the brain size in healthy individuals and MDS patients confirms our *in vitro* findings. Expansion rates (absolute (**D**) and relative (**E**)) of control- (n=3, N=30 for each clone), MDS- (n=3, N=30 for each clone), MDS-LIS1- (n=3, N=30), and MDS-14.3.3ε- (n=3, N=30) derived organoids. Depicted is the organoid area in mm^2 at days 2, 5, 10, and 15. Error bars, **±**SD.

Additionally, patient-derived 3D organoids exhibited a significant decrease in expansion rate over time. This phenotypic feature was particularly prominent during the initial stages of differentiation (days 2–15) (Figure 4.5. A-B, D-E). To quantify the expansion rate, the expansion area at days 5, 10, and 15 was normalised to the day 2 expansion measurement for each organoid batch (one biological replicate with ten technical replicates). Quantitative analysis demonstrated a relative areal expansion of 1.17–2.31 (Ctrl.1.1) in control organoids over 15 days. Conversely, patient-derived organoids displayed a significantly reduced areal expansion over the same course of differentiation, reaching 1.52 on day 15 (MDS 1.1). Moreover, reinstallation of LIS1 and 14.3.3ε levels in CRISPR/Cas9 edited lines resulted in a partial rescue of MDS-

associated deficits, reaching 1.91 and 1.73 respectively on day 15.

Observing remarkable differences in overall organoid structure, we conducted a more detailed examination of neuroepithelium loop structures, each of which represents a VZ-like region in the developing brain. We therefore introduced a multiparametric quantitative assessment measuring six cortical loop parameters: loop tissue area, total loop area and loop diameter, the ventricle-like area, and the apical and basal membranes (Figure 4.6. A). Olivia Krefft performed the loop parameter analysis. Interestingly, a detailed assessment of loop histoarchitecture revealed a significant reduction in patient-derived organoids in all six parameters when compared to controlled-derived organoids (Figure 4.6. B-G). Furthermore, a re-expression of LIS1 and 14.3.3ε to wild-type levels was observed, followed by a partial rescue towards healthy control rates (Figure 4.6. B-G).

The phenotypical differences in the MDS-derived organoids, in overall size as well as the organisation of neuroepithelium loops, are in line with clinical data obtained from autopsy examinations of MDS patients' brains exhibiting a significant reduction in total brain size (Figure 4.5. C; Sheen et al., 2006).

A
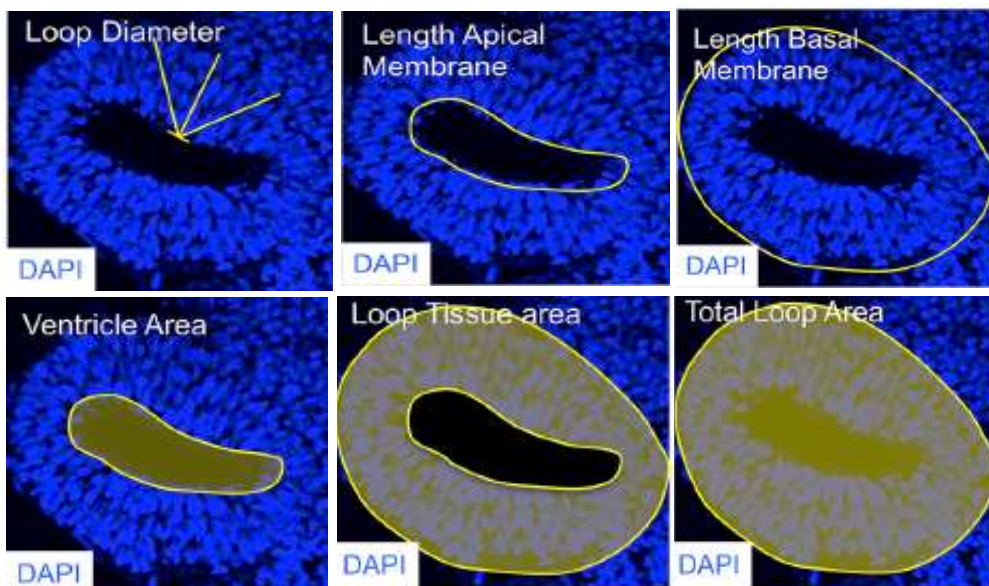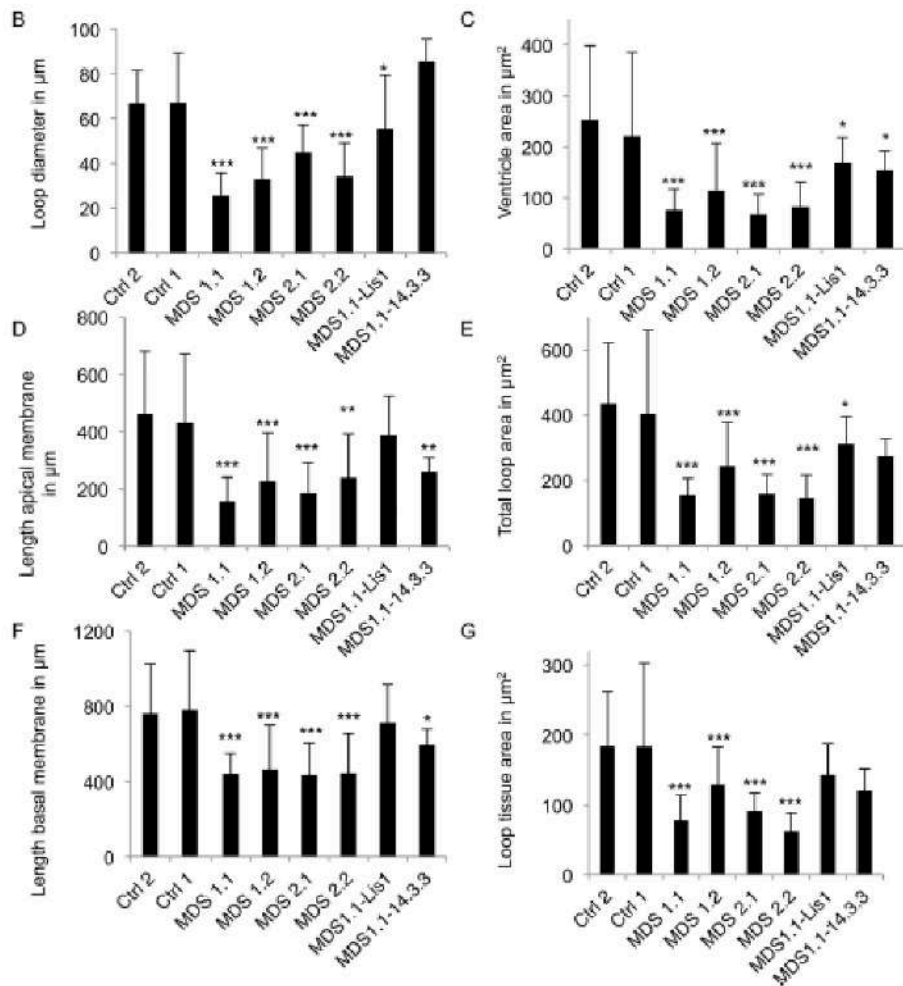
Figure 4.6. Quantitative characterization of neuroepithelium loops. (A) Schematic representation of how six different parameters were quantified. **(B-G)** Quantitatification of multiple parameters in cortical-like structures of control- (Ctrl2 n=3, N=42; Ctrl1 n=3, N=24), patient- (MDS1.1 n=3, N=29; MDS1.2 n=3, N=27; MDS2.1 n=3, N=29; MDS2.2 n=3, N=10) and CRISPR/Cas9 rescue (MDS-LIS1 n=3, N=14; MDS-14.3.3ε n=3, N=12) derived organoids at day 20 of neuronal differentiation. Loop diameter **(B)**, ventricle-like area **(C)**, length of apical membrane **(D)**, total loop area **(E)**, length of basal membrane **(F)** and loop tissue area **(G)**. Error bars ± SD. *p < 0.05, **p < 0.01, ***p < 0.001. (Quantification depicted in the figure was performed by Olivia Krefft, bar graph modified from Iefremova et al., 2017).

4.2.1.1. Analysis of apoptotic cell death in neuroepithelial progenitors revealed no significant increase in the rate in MDS-derived organoids

Observing a significant decrease in overall size among organoids derived from MDS patient iPSCs (in accordance with observations from *in vivo* studies of MDS patient brains), we suggest two possible sources. Firstly, an increase in apoptotic cell death may cause a decrease in organoid size. Secondly, premature neurogenesis may be an underlying cause of smaller patient-derived organoids. To address the first hypothesis, we performed a quantitative analysis of activated Caspase 3, a conventional marker of apoptosis, over 28 days (days 10, 15, 20, and 28, Figure 4.7.). From the analysis results, we observed that cell death in VZ-like regions was a

rare event at all time points.
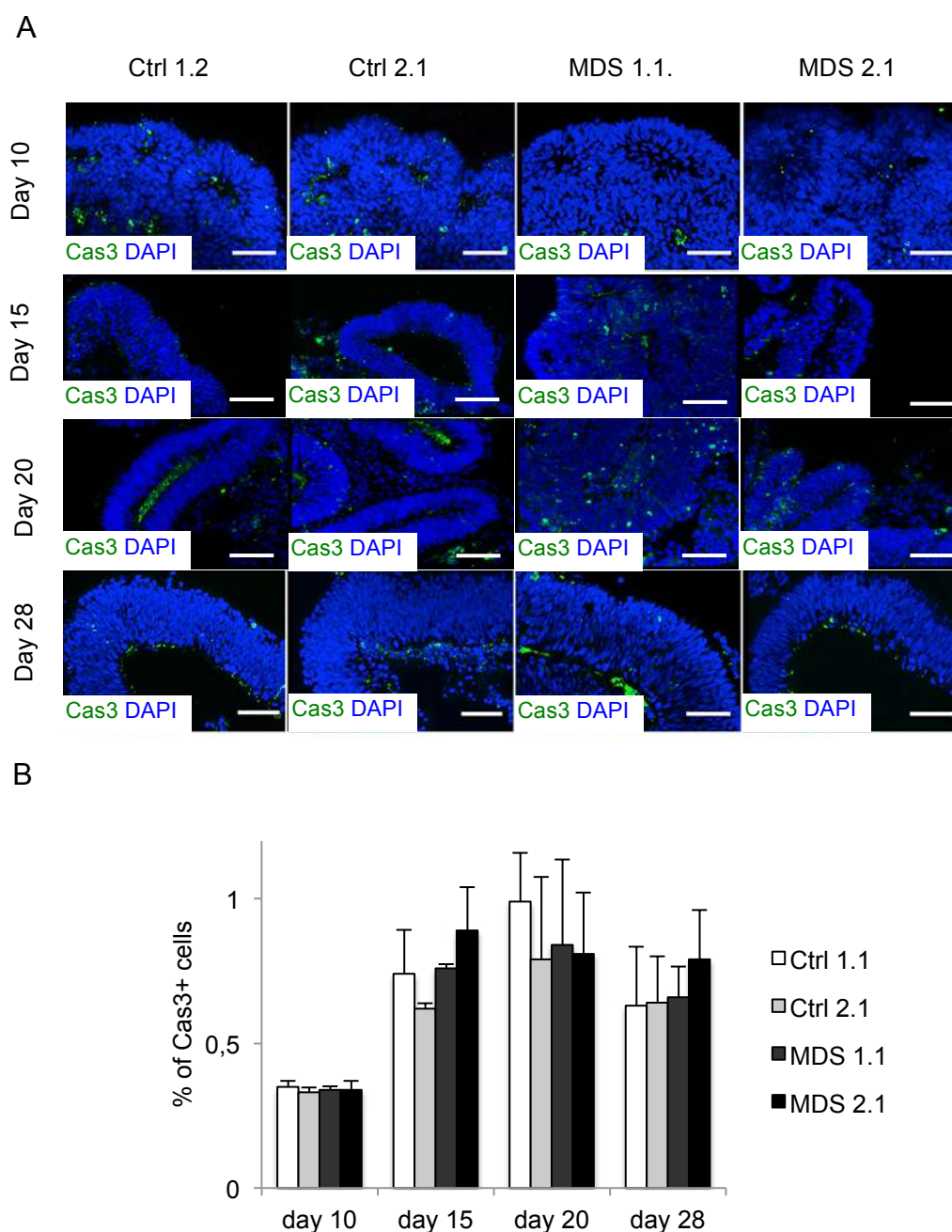
Figure 4.7. No increase in apoptotic cell death in patient-derived organoids compared to organoids from healthy controls. (A) Immunocytochemical analysis of activated (cleaved) caspase3 in neuroepithelial loops of control- and MDS-derived organoids. Shown are representative images of day 10, day 15, day 20, and day 28. Scale bars, 50μm. **(B)** Quantification of cleaved caspase3-positive cells in neuroepithelial loops of control and MDS-derived organoids at day 10, 15, 20, and 28 (for each time point N>1000 cells from n≥5 loops per condition). Error bars, ±SD. As a result of the performed analysis, no significant difference in the number of cleaved caspase3-positive cells over time from day 10 to day 28 could be observed between the groups.

Furthermore, no significant increase in cell death was observed when patient-derived organoids were compared to healthy controls: day 10, Ctrl 1.2: 0.35±0.02% (n=1140),

Ctrl 2.1: 0.33±0.02% (n=1180), MDS 1.1: 0.34±0.01% (n=1175), MDS 2.1: 0.34±0.03% (n=1160); day 15, Ctrl 1.2: 0.74±0.15% (n=1496), Ctrl 2.1: 0.62±0.01% (n=1112), MDS 1.1: 0.76±0.01% (1052), MDS 2.1: 0.89±0.14% (n=1118); day 20, Ctrl 1.2: 0.99±0.17% (n=1401), Ctrl 2.1: 0.79±0.29% (n=1104), MDS 1.1: 0.84±0.29% (n=1054), MDS 2.1: 0.81±0.21% (n=1068); day 28, Ctrl 1.2: 0.63±0.20% (n=1357), Ctrl 2.1: 0.64±0.16% (n=1196), MDS 1.1: 0.66±0.10% (n=1494), MDS 2.1: 0.79±0.17% (n=1353). In some cases depicted in figure 4.7 (e. g., Ctrl 1.2 at day 20 and MDS 1.1 at day 28), there is an unspecific signal that resides outside of the neuroepithelium, and it was not considered during the quantification of Caspase 3 positive cells.

4.2.1.2. Increased numbers of intermediate progenitors as a sign of premature neurogenesis in MDS-derived organoids

Quantitative analysis of neuronal progenitors undergoing apoptotic death revealed no significant differences between the control and MDS-derived organoid cultures. Therefore, the first hypothesis — increased apoptotic rate results in decreased organoid size in patient-derived cultures — was dismissed.

To address the second hypothesis — premature neurogenesis produces smaller MDS cultures — we quantified the number of Tbr2 positive cells (Tbr2 is the marker for intermediate progenitors in the developing human brain) (Figure 4.8.). Interestingly, the results revealed a strong increase in the number of Tbr2+ IPs in patient-derived organoid cultures when compared to the control: day 21, Ctrl2.1 = < 1%, MDS1.1 = 11.35% ± 0.15%, MDS2.2 = 12.2% ± 1.98%; day 28, Ctrl2.1 = 2.64% ± 0.60%, MDS1.1 = 20.79% ± 1.22%, MDS2.2 = 20.65% ± 0.95%. Moreover, the re-expression of LIS1 and 14.3.3ε levels in MDS cultures resulted in a significant decrease in the number of Tbr2-positive IPs at day 28 of differentiation: MDS-LIS1 = 11.7% ± 1.28%, MDS-14.3.3ε = 5.36% ± 0.98%.

In conjunction, the data suggests that premature neurogenesis, rather than increased apoptotic activity, is a potential cause of significant size reduction in MDS-derived 3D organoid cultures.
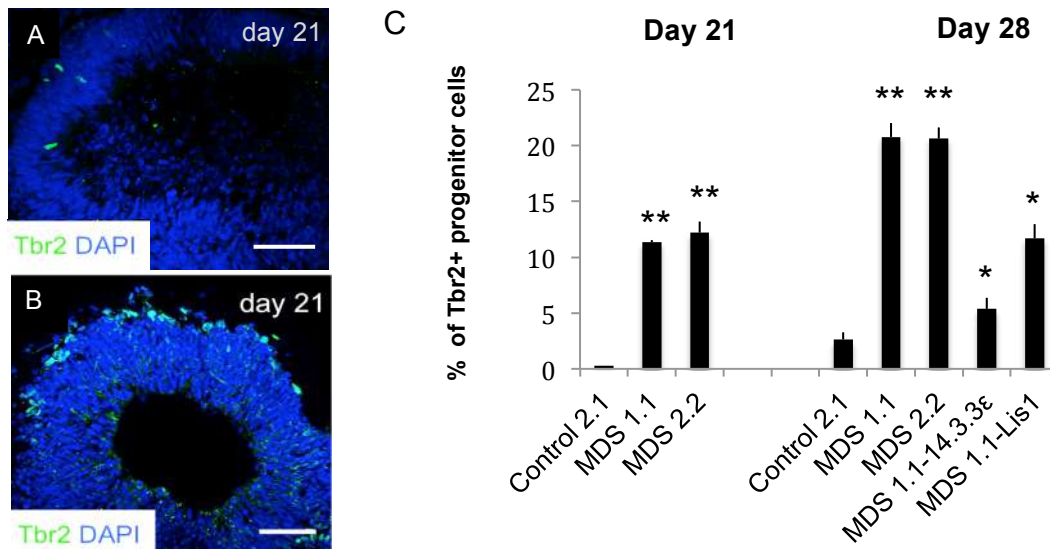
Figure 4.8. Premature neurogenesis in MDS patient-derived cultures.
(A) Representative images of control- (A) and MDS-derived (B) organoids stained with Tbr2 at day 21. Scale bars, 50 µm. **(C)** Quantification of Tbr2+ intermediate progenitors (IP) in control- and MDS-derived organoids (at day 21: N>2,000 cells from a total of n=6 loops per condition, day 28: N>1,200 cells from a total of n=6 loops per condition). Error bars, ±SD. *p < 0.05, **p < 0.01. Quantification of Tbr2 expression at day 28 in control-, MDS-, MDS-LIS1- and MDS-14.3.3ε organoids (N>1200 cells from a total of n=6 loops per condition). Error bars, SD. *p < 0.05, **p < 0.01. (Modified from Iefremova et al., 2017).

4.2.1.3. Altered microtubule networks in MDS-derived cultures

Based on the investigation of apoptotic cell death-rate in neuroepithelial loop-like structures (i.e., no significant increase in active Caspase3 in MDS cultures) and a significant increase in the number of Tbr2 positive IPs, we suggested that rather than apoptosis, an impairment in an underlying process may cause a decrease in the size of patient-derived iPSC structures. One process that may be highly susceptible in MDS cultures is the stability of plus-end microtubules in developing cortical-like structures. A key factor believed to contribute to microtubule instability is a disruption in the LIS1/NDEL1/14.3.3ε complex. Numerous experiments using KO mouse models have demonstrated that an impairment in the functional activity and overall stability of this protein complex results in the reduction and weakening of astral microtubules in the developmental SVZ, as well as numerous alterations to the entire microtubule network. Subsequently, processes that require precise microtubule control, such as mitotic spindle formation and exact orientation in the cell division plane, are considerably impaired in vRGCs. It is unclear whether an increased amount of oblique spindle orientation is crucial in long-term brain development in mice (Yingling et al., 2008); moreover, there is no substantial data yet obtained from hiPSC-derived systems to address this aspect in the human stem cell-based system.

We, therefore, analysed microtubule network organisation (microtubules were stained using acetylated α-tubulin, Figure 4.9. A-D) by measuring ac-Tubulin strand density at the apical (ventricular zone) and basal (marginal zone) aspects of the cortical loops. Using ImageJ, we drew a plot profile line at the 33rd (apical side) and 66th (basal side) percentiles of the loops and determined the numbers of ac-Tubulin strands crossing the plot profile line.

This investigation revealed severe alterations of vRGCs microtubule networks in MDS cultures. In healthy control-derived cultures, we observed the extension of microtubules from the apical to the basal sides of cortical loop-like structures. MDS-derived vRGCs microtubules, however, showed a reduction in the number of extensions able to cross the entire neuroepithelium loop towards the basal membrane, and approximately 50% of them were largely accumulated in the centre of the structures. In addition, morphologically wise, they appeared to be impaired and truncated.
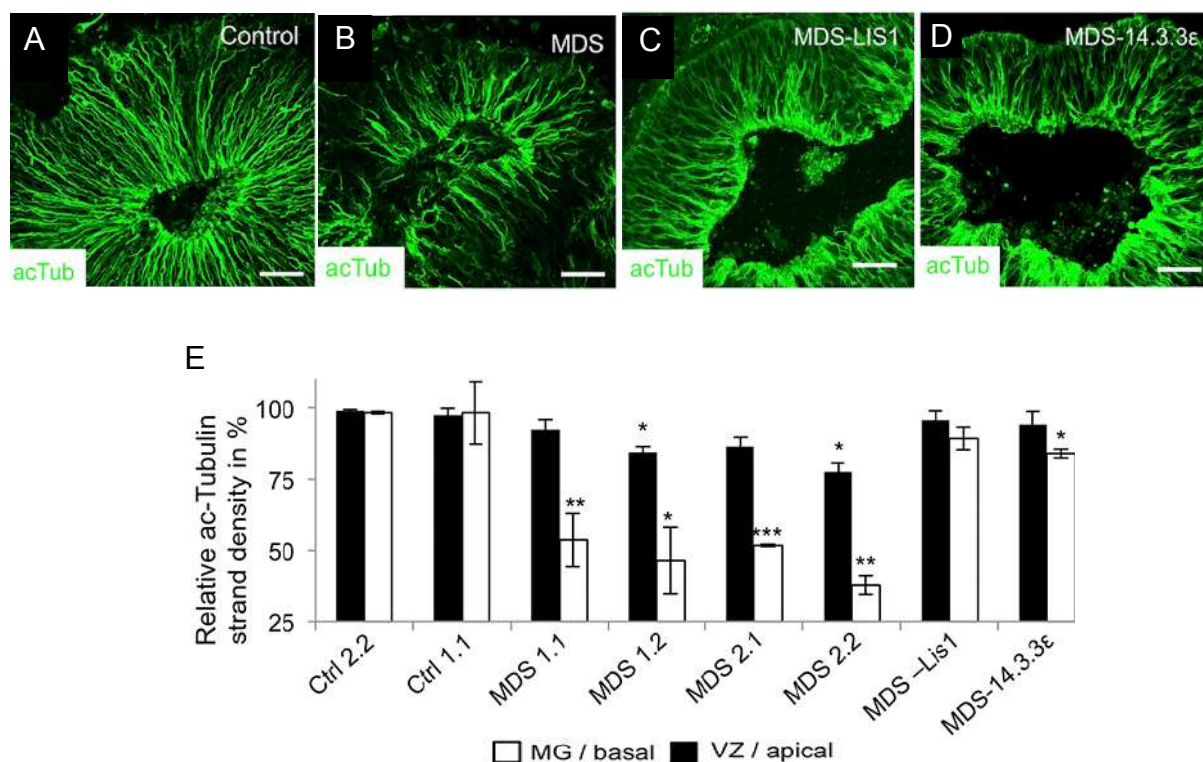
Figure 4.9. Analysis of altered microtubuli networks in MDS-derived cortical organoids. Immunostaining for acetylated alpha-tubulin (acTub) in control- (**A**), MDS- (**B**), MDS-LIS (**C**) and MDS-14.3.3ε (**D**) derived organoids. Scale bars, 50 μm. (**E**) Quantification of the ac-tubulin strand density at the apical (VZ) and the basal (MG) side in control (Ctrl2.2 n=3, N=5; Ctrl2.1 n=3, N=8), patient (MDS1.1 n=3, N=13; MDS1.2 n=3, N=5; MDS2.1 n=3, N=5; MDS2.2 n=3, N=10), and rescue organoids (MDS-LIS1 n=3, N=9; MDS-14.3.3ε n=3, N=10) Error bars, ±SD. *p < 0.05; **p < 0.01, ***p < 0.001. (Quantification depicted in the E section of the figure was performed by Olivia Krefft, bar graph modified from Iefremova et al., 2017).

Our hypothesis that the LIS1/NDEL1/14.3.3ε complex has a significant role as a stabilisation factor in the microtubule network is supported by the fact that in the case of the MDS-LIS1 and MDS-14.3.3ε rescue organoids, although LIS1 and 14.3.3ε were restored to nearly wild-type levels, microtubule networks still appeared to be altered. However, as it can be seen in Figure 4.9 C and D, cultures with rescued levels of LIS1 and 14.3.3ε respectively exhibited a more complete expansion of acetylated α-tubulin positive extensions towards the basal surface through the entire neuroepithelium loops. Olivia Krefft analysed the altered microtubule networks.

4.2.1.4. Switch from symmetric to asymmetric patterns of cell division in radial glia cells in the ventricular zone of MDS-derived organoids

Following the analysis of microtubule network stability, in which severe impairment in MDS-derived cultures was revealed, we considered whether this would result in an increased oblique plane in mitotic spindle in vRGGs, as demonstrated in the mouse models, or if a related human-specific trend could be observed in our 3D model of cortical development. To obtain greater insight into the pattern of cell division in vRGGs, we performed immunocytochemical staining using Tpx2 (a typical marker for mitotic spindle assembly, Figure 4.10. C-E) to label the spindle in cells actively undergoing division along the ventricular-like surface within the cortical organoids (Figure 4.10. B).

This method of assessing mitotic spindle orientation in apical RGCs is widely accepted and has been applied in the renowned organoid study conducted by Madeline Lancaster et al. (2013). A schematic representation of vertical, horizontal, and oblique cleavage planes is depicted in Figure 4.10. A). In this study, we investigated mitotic spindle orientation relative to the prospective ventricular surface in at least four different loops per organoid (Figure 4.10.).

Interestingly, the quantitative analysis demonstrated a clear shift in MDS-derived cultures from symmetric to asymmetric modes of cell division. Moreover, this occurred without a significant increase progenitors with an oblique mitotic spindle orientation: Ctrl1.1, vertical 57.14%, horizontal 31.87%, and oblique 11.0%, N = 91; MDS1.1, vertical 34.29%, horizontal 51.43%, and oblique 14.23%, N = 105.
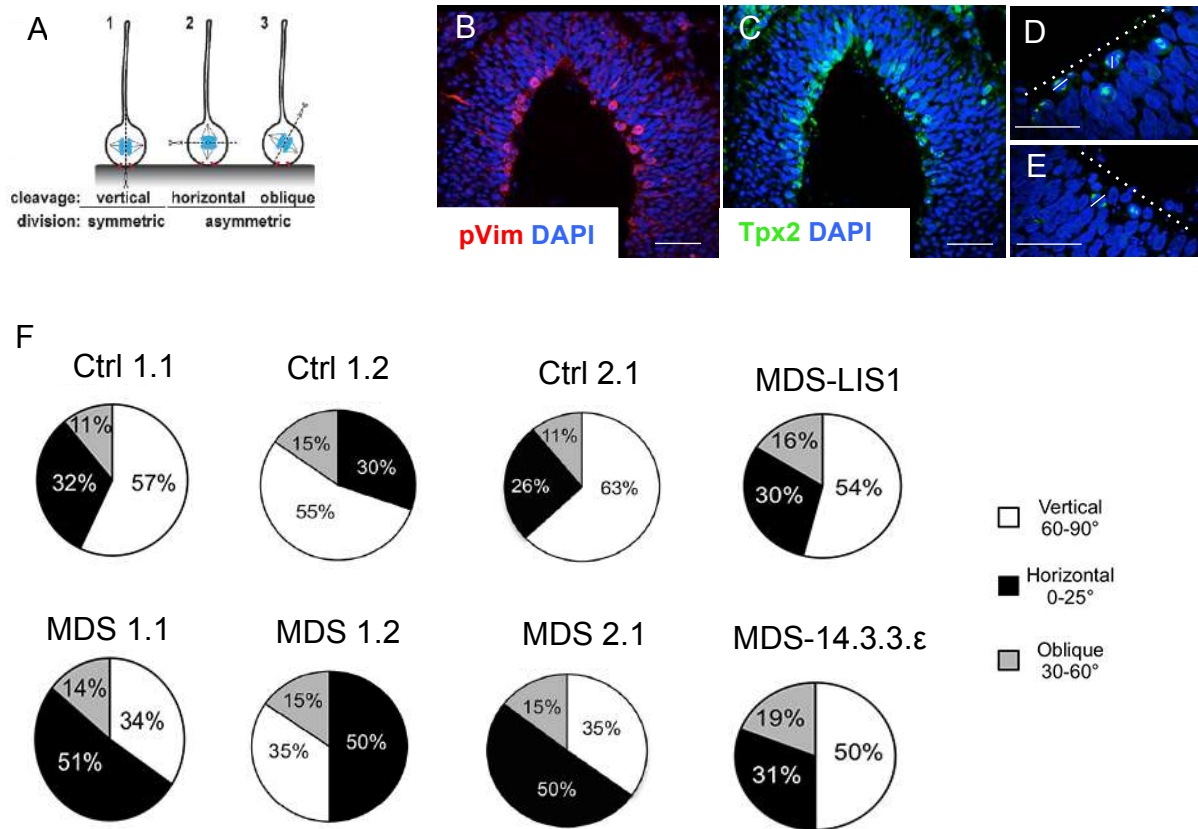
Figure 4.10. Switch from symmetric to asymmetric patterns of cell division in radial glia cells in the ventricular zone of MDS-derived organoids. (A) Schematic representation of vertical, horizontal, and oblique cleavage plane. **(B)** Most of the actively proliferative neuronal progenitors are observed around the ventricle and marked by p-Vim expression, and mitotic spindles are stained by Tpx2 **(C).** Scale bars, 25 µm. (**D-E**) Representative images of horizontal, oblique **(D)**, and vertical **(E)** division planes in mitotic vRGCs. Scale bars, 50 µm. (**F**) Quantification of the division planes of vRGCs in control (n=3, N=91), MDS (n=3, N=105), MDS-LIS1 (n=3, N=63), and MDS-14.3.3ε (n=3, N=118) organoids at day 20. (Quantification was performed together with George Manikakis).

Furthermore, in patient-derived cultures, a partial reinstallation of LIS1 and 14.3.3ε levels recovered the shift in mitotic cleavage planes: MDS-LIS1, vertical 54.84%, horizontal 29.84%, and oblique, 15.32%, N = 63; MDS-14.3.3ε, vertical 50.0%, horizontal 31.51%, and oblique 19.49%, N = 118. The mitotic spindle planes were analysed in collaboration with George Manikakis.

These results suggest that a clear shift in the mode of cell division and consequently a somewhat premature transition from symmetric to asymmetric mitotic events in vRGCs. Moreover, a significant increase in fate-restricted Tbr2+ IPs at the expense of the actively proliferating stem cell pool may be the primary mechanism underlying the reduced size and expansion rates of MDS-derived cortical organoids.

4.2.2. Disruption of the niche organisation resulted in the impairment of N-cadherin/ß-catenin signalling in MDS-derived organoids

From the mitotic spindle analysis of vRGGs, we conclude that there is a clear shift in spindle orientation from vertical to horizontal in hiPSC-derived cortical cultures, as opposed to a simple increase in the oblique pattern of cell division observed in mouse models. We argue that this shift, in conjunction with microtubule network instability, results in increased asymmetric cell division in MDS-derived cultures. Moreover, additional signalling pathways with a significant role in the described phenotype within the SVZ-like region may contribute to an observed weakening in astral microtubules with a cell-autonomous defect. There is evidence that cell-cell interaction within the developing neuronal progenitor niche, particularly adherent junctions, may be crucial in controlling the proliferation of the vRGGs (Marthiens et al., 2010; Stocker and Chenn, 2009). Additionally, data obtained from studies of transgenic mouse models revealed that an impairment in the functional activity of the LIS1/NDEL1/14.3.3ε complex disrupts cell-cell interaction within the SVZ and causes a deviation in the expression of apical adhesion molecules (Pawlisz et al., 2008; Pramparo et al., 2011). Considering these factors, we suggest that disorganisation in the apical surface structure in neuroepithelium loops, observed in our MDS-derived cultures, may be the cause. Extensive analysis of niche organisation (including tissue organisation, formation, cilium orientation, expression pattern, and the alignment of adherent molecules) revealed significantly impaired MDS-derived organoids in all the investigated parameters (Figure 4.11.).

Beginning with tissue organisation, control cultures showed a well-organised and densely-packed VZ-like region. In contrast, MDS cultures exhibited less tightly-packed neuronal progenitors that were not strictly organised and consistently oriented in the ventricle cell layers (Figure 4.11. A and B).
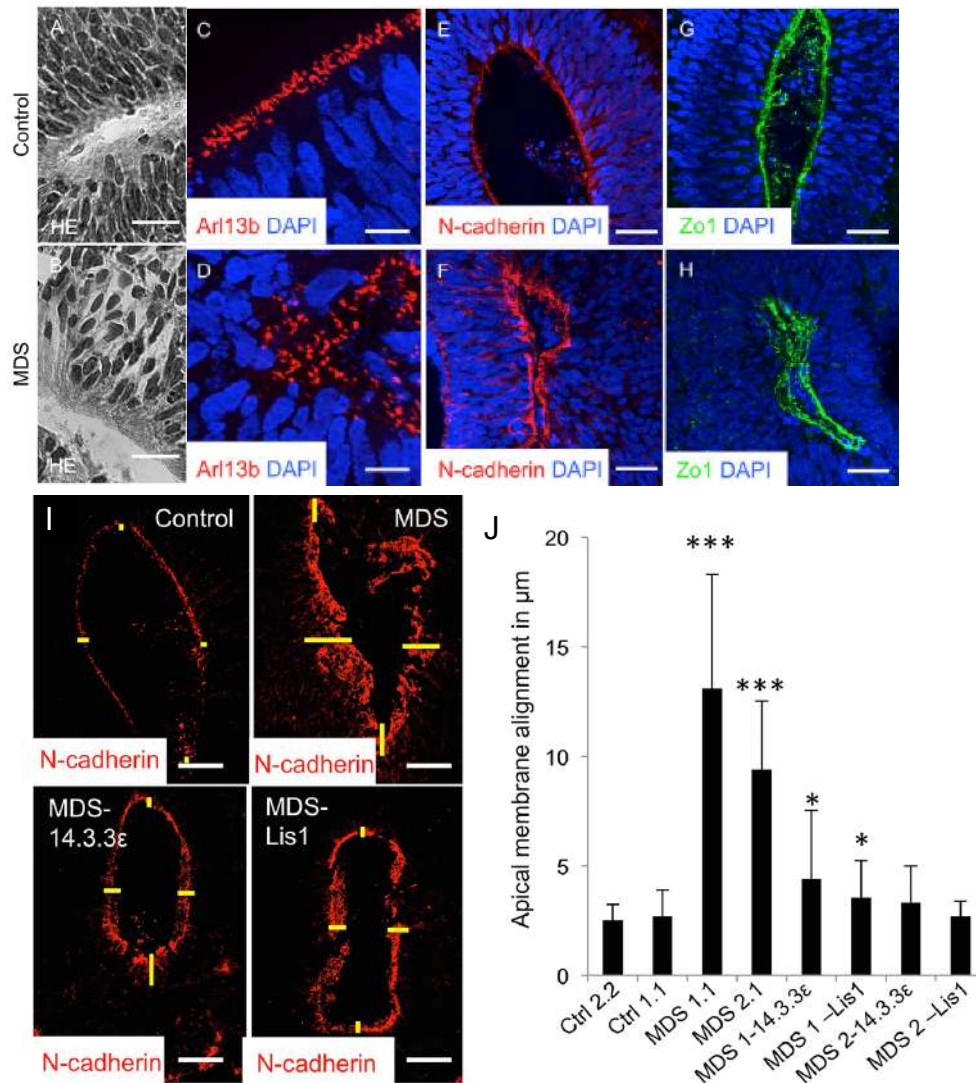
Figure 4.11. A significant disruption of the VZ niche organisation of MDS-derived organoids. (**A and B**) H&E staining of the VZ-like area in control- (**A**) and in MDS- (**B**) derived organoids. Scale bars, 30 μm. (**C–H**) Immunostainings for Arl13b, N-cadherin and Zo1 in control- (**C, E and G**) and MDS- (**D, F and H**) derived organoids. Scale bars, in (**C**) and (**D**) 10 μm, and in (**E**), (**F**), (**G**) and (H) 50 μm. (**I**) Immunostaining for N-cadherin in control, MDS, MDS-LIS1 rescue, and MDS-14.3.3ε rescue organoids. Scale bar, 50 μm. (**J**) Quantification of the apical membrane alignment in control (Ctrl2.2 n=3, N=16; Ctrl1.1 n=3, N=6), MDS (MDS1.1 n=3, N=23; MDS2.1 n=3, N=15), MDS-LIS1 rescue (MDS1-LIS1 n=3, N=18; MDS2-LIS1 n=3, N=16), and MDS-14.3.3ε rescue (MDS1-14.3.3ε n=3, N=14; MDS2-14.3.3ε n=3, N=15) organoids. A schematic illustration of the area of measurement (yellow lines at 90^0, 180^0, 270^0, and 360^0) is shown in (**I**). Error bars, ±SD. *p < 0.05; **p < 0.01, ***p < 0.001. (H&E stainings were performed together with George Manikakis, immunostainings of Arl13b were perdormed by Dr Julia Ladewig, quantification of N-cadherin distribution along the apical membrane was performed by Olivia Krefft, bar modified from Iefremova et al., 2017).

In addition, we observed irregular apical lining in the cilia along the ventricular surface in MDS-derived organoids after performing immunostaining of the cilia-specific marker - Arl13b (Figure 4.11. D). Arl13b, a small GTPase of the Arf/Arl family, reportedly controls the microtubule-associated, ciliary axoneme structure that

appears to be essential for the proper establishment of a radial glial scaffold, which in turn is crucial for the generation and migration of the early-born neurons in the cortex (Higginbotham et al., 2013). Moreover, there were severe deviations in the organisation of certain cell adhesion molecules (N-cadherin and Zo1) of the VZ-like niche. Compared to the control cultures characterised by a fine adherent belt, MDS cultures exhibited an accumulation of N-cadherin and Zo1 proteins along the apical membrane. In our MDS-LIS1 and MDS-14.3.3ε rescue organoids, in which we restored LIS1 and 14.3.3ε level, niche disorganisation was less severe than in MDS-derived organoids, and the expression of adhesion molecules (e.g., N-cadherin) was closer to that in the control cultures (Figure 4.11. I and J). Changes in the organisation of the VZ-like region in our organoid culture are in line with data from MDS patient autopsies reporting severe disorganisation in tissue structure in the ventricular region of the brain (Shen et al., 2006). Immunocytochemical analysis of the Arl13b marker was performed by Dr Julia Ladewig. H&E organoid staining was conducted together with George Manikakis. Olivia Krefft performed the quantitative analysis of the niche disruption.

4.3. Activation of canonical Wnt signalling pathway promotes rescue changes in phenotypical alterations in MDS-derived organoids

As previously discussed, a clear, non-random shift in mitotic cell division may occur due to disrupted microtubule networks as well as signalling within the VZ-like niche. Furthermore, data obtained from mouse studies revealed that active Wnt/ß-catenin signalling controls vRGCs proliferation (Chenn and Walsh, 2002; Zechner et al., 2003). Moreover, studies conducted by Zhang et al. (2010, 2013) suggested that N-cadherin had a role in controlling Wnt activity by regulating AKT phosphorylation. This may subsequently trigger the phosphorylation of the ß-catenin at a particular position (Ser552, p-Ser552-ß-catenin), consequently securing ß-catenin activation and stabilisation (Figure 4.12. B). Therefore, our subsequent approach was to determine whether ß-catenin is phosphorylated at Ser552 in actively dividing vRGGs, in our 3D cortical cultures. After performing immunocytochemical analysis of the control cultures, we observed that over 70% of the dividing p-Vimentin-positive progenitors were also positive for p-Ser552-ß-catenin: Ctrl1.1, 71.5% ± 8.78%, n = 10; Ctrl2.2, 87.87% ± 12.27%, n = 15) (Figure 4.12. B-D). In contrast, MDS-derived organoids demonstrated a significantly decreased amount of double-positive cells for

p-Vimentin and p-Ser552-ßcatenin: MDS1.1, 34.79% ± 9.41%, n = 9; MDS1.2, 39.84% ± 9.76%, n = 15; and MDS2, 30.21% ± 11.33%, n = 9) (Figure 4.12. B-D). Data from the rescue organoid cultures revealed more widespread of double-positive cells for p-Vimentin and p-Ser552-ß-catenin in the vRGGs: MDS-LIS1, 68.62% ± 8.15%, n = 11; MDS-14.3.3ε, 71.93% ± 7.41%, n = 11) (Figure 4.12. D). The data suggests that vRGCs in MDS-derived organoids demonstrate an impaired activation of ß-catenin that may originate from the disrupted N-cadherin/ß-catenin signalling.
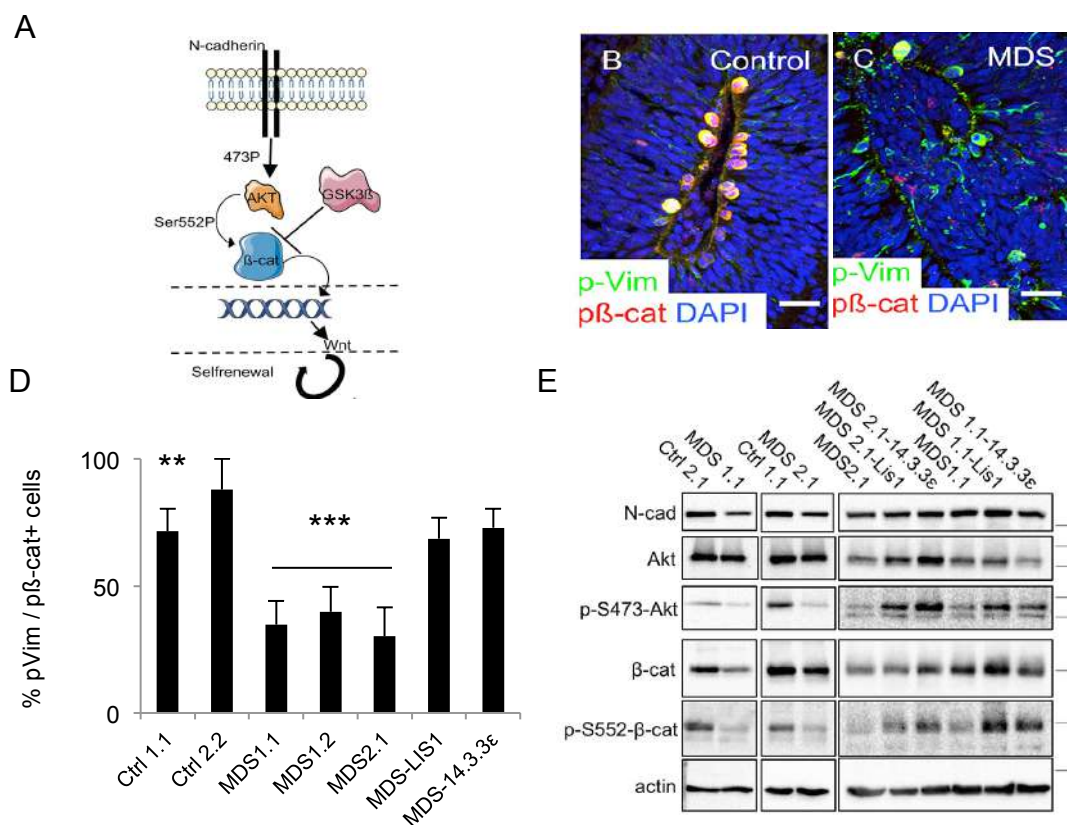
Figure 4.12. Impairment of the N-cadherin/ß-catenin signalling pathway in MDS-derived cortical cultures. (A) Schematic overview of how N-cadherin is connected to the Wnt signalling pathway. **(B and C)** P-vimentin (p-Vim) and p-Ser552-ß-catenin (pß-cat) immunostaining in control- **(B)** and MDS- **(C)** derived organoids. Scale bars, 25 μm. **(D)** Quantification of double-positive for p-vimentin/p-Ser552-ß-catenin vRGCs in relation to the total amount of p-Vimentin positive vRGCs in control (Ctrl1.1 n=3, N=10; Ctrl2.2 n=3, N=15), MDS (MDS1.1 n=3, N=9; MDS1.2 n=3, N=15; MDS2.1 n=3, N=9), MDS-LIS1 n=3, N=11, and MDS-14.3.3ε N=3, N=11 cortical loops. **(E)** Detection of N-cadherin, AKT, phosphorylated AKT (pS473-AKT), ß-catenin, and phosphorylated ß-catenin (p-S552-ß-cat) in control, patient, and rescue cells by immunoblotting. Error bars, ±SD. **p < 0.01, ****p < 0.0001. (Immunostaining and quantification of p-Ser552-ß-catenin positive cells were completed by Dr Julia Ladewig, Immunoblotting was conducted by Ruven Wilkens, figure modified from Iefremova et al., 2017).

To address the precise function connecting N-cadherin and ß-catenin, we manipulated activity in the Wnt signalling pathway in MDS and control cultures. We

switched to 2D cultures of cortical progenitors due to their increased homogeneity and reproducibility (for this series of experiments, were utilised neuronal progenitors 15 days since the beginning of the neuronal induction via dual SMAD inhibition). By performing immunoblot analysis of neuronal progenitors derived from cortical rosettes, we demonstrated that MDS-derived progenitors exhibit reduced levels of proteins involved in intracellular cascades connecting VZ-like niche and ß-catenin signalling (i.e., reduced levels of N-cadherin, phosphorylated AKT at Ser473, ß-catenin phosphorylated at Ser552, and total ß-catenin) (Figure 4.12. E).

LIS1 and 14.3.3ε may have contributed to the observed alterations since their reinstallation in rescue cultures resulted in protein expression and phosphorylation levels closer to those found in the wild-type (Figure 4.12. E).

To further investigate the Wnt signalling pathway and the potential influence of N-cadherin on its activity, we generated Wnt reporter cell lines expressing the pSuper8XTOPFlash luciferase reporter. For conducting this luciferase assay, both control- (Ctrl1.2) and patient- (MDS1.2) derived iPSCs were transduced with a lentiviral vector expressing luciferase under the control of the Wnt responsive TCF promoter element. Wnt signalling activity induces Wnt target genes that contain TCF binding element. As a result, cells expressing luciferase proteins under the TCF promoter element will be used to detect the stimulus-dependent activity of the Wnt signalling pathway. This analysis of luciferase activity revealed that MDS-derived cortical progenitors showed decreased levels of Wnt reporter activity in comparison to the control-derived cultures (Figure 4.13. A).

Moreover, when we blocked N-cadherin activity by applying blocking antibodies to the cortical progenitors, this produced a significant decrease in Wnt reporter activity. Additionally, N-cadherin activation by exposing cortical cultures to recombinant N-cadherin protein-induced activation in the Wnt reporter supports our proposed link between N-cadherin activity and Wnt signalling (Figure 4.13. A).
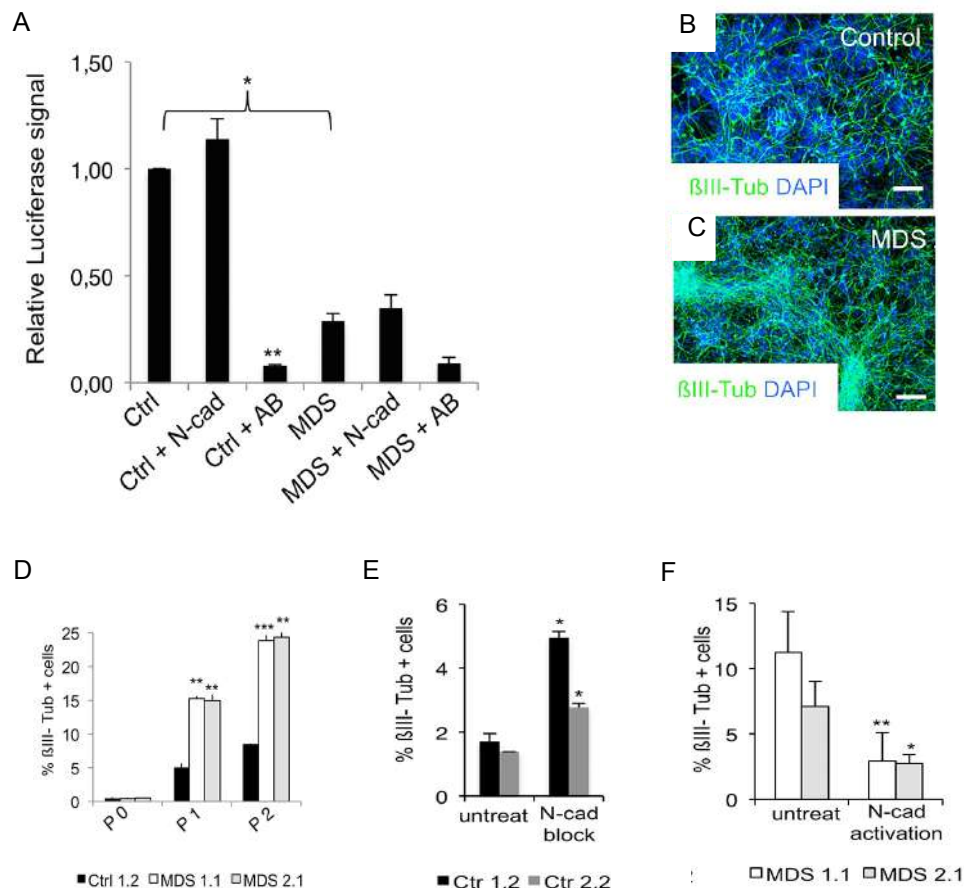
Figure 4.13. Disruption of the N-cadherin/ß-catenin signalling axis in MDS-derived cortical cultures. **(A)** Quantification of the relative luciferase signal in the pSuper8XTOPFlash Wnt reporter lines (Ctrl and MDS, standard culture conditions; +N-cad, exposure to recombinant N-cadherin protein; +AB, exposure to N-cadherin blocking antibody). Error bars, ±SD. *$p < 0.05$, **$p < 0.01$. **(B and C)** Immunocytochemical staining for ßIII-tubulin in control- **(B)** and MDS- **(C)** derived cortical cultures maintained for three passages (15 days). Scale bars, 100 μm. **(D)** Quantification of ßIII-tubulin-positive cells overtime/passages (fixed at day 2 of every passage) in control and MDS-derived cortical cultures. Error bars, ±SD. **$p < 0.01$, ***$p < 0.001$. **(E and F)** Quantification of ßIII-tubulin-positive cells in control-derived cortical cultures either untreated or treated with the N-cadherin blocking antibody for 6 days **(E)**. Quantification of ßIII-tubulin-positive cells in MDS-derived cortical cultures either untreated or exposed to recombinant N-cadherin protein for 6 days. **(F)**. Error bars, ±SD. *$p < 0.05$, **$p < 0.01$. (Ammar Jabali and Kevin Weynans performed the luciferase activity assay, experiments of blocking and activating N-cadherin activity were performed in collaboration with Fabio Marsoner, figure modified from Iefremova et al., 2017).

To obtain further insight into the link between N-cadherin activation and the Wnt signalling pathway, we investigated the potential effect of N-cadherin levels on proliferation and differentiation in our cortical cultures. This was performed using 2D cultures cortical in the absence of factors for dual SMAD inhibition and assessing the neuronal differentiation by immunocytochemistry every five days in the course of fifteen days in total, starting with the withdraw of those inhibitors. As a result, the

MDS cultures exhibited a significant increase in the number of neurons in the culture. These findings indicate that a reduction in the level of Wnt signalling also results in premature neurogenesis in 2D cortical progenitor cultures (Figure 4.13 B-D). Moreover, blocking N-cadherin activity by exposing control-derived cortical cultures to N-cadherin blocking antibodies, significantly increased the number of neurons (Figure 4.12. E), while activating N-cadherin in MDS-derived cortical progenitors rescued early neurogenesis (Figure 4.13. F). The immunostainings and quantification of p-Ser552-ß-catenin positive cells were completed by Dr Julia Ladewig. Immunoblotting was conducted by Ruven Wilkens. Ammar Jabali and Kevin Weynans performed the luciferase activity assay. Experiments of blocking and activating N-cadherin activity were performed in collaboration with Fabio Marsoner.

In conjunction, these results indicated a direct link between active N-cadherin signalling and the Wnt pathway. We, therefore, evaluated the possibility of pharmacologically manipulating ß-catenin via GSK3ß inhibition, and more significantly, whether this would influence the variations observed in MDS-derived cultures. Hence, we applied CHIR99021, a widely used GSK3ß inhibitor, to our cortical cultures. To evaluate the level of activation of the Wnt signalling pathway, we calculated the corrected total cell fluorescence (CTCF) of the GFP signal along the ventricular-like area within cortical loops from Ctrl2.1 and MDS1.2 iPSC lines with Wnt-GFP reporter-derived organoids. For the CTCF quantification was used images of unstained cortical loop-like structures from the respective organoids (described in details in method section 3.5) applied the formula: CTCF = integrated density – (area of selected cell multiplied with the mean fluorescence of background readings) along the protocol described by Burgess and colleagues in the number of papers (McCloy R. et al., 2014; Burges, A., 2012; Burgess A. et al., 2010).

First, control and MDS organoids derived from iPSC lines with the Wnt-GFP reporter were exposed to CHIR99021 to confirm that GSK3ß inhibition would lead to an increased Wnt signalling activation in patient-derived cultures (Figure 4.14. A). Significantly, CHIR treatment of 3D cortical organoids resulted in a significantly increased level of Wnt activity in the ventricular-like zones. Without CHIR99021 treatment, MDS1.1 was 47,333.45±1,177.36, and after exposure of the 3D organoids to the GSK3ß inhibitor 141,168.1±7,726.8. Conversely, CHIR99021 treatment of the control cultures produced an insignificant increase in corrected cell fluorescence GFP: Ctrl 2.1 was 393,351.5±35,159.01 with treatment and 286,457.65±45,917.98

without treatment (Figure 4.14. B).
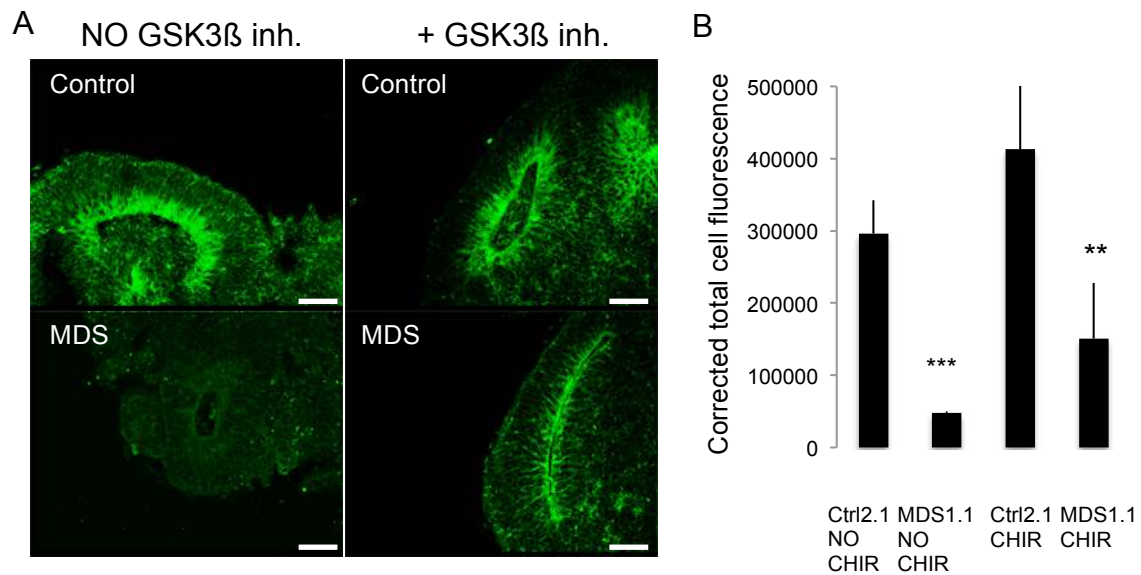
Figure 4.14. Exposure to the GSK3ß inhibitor resulted in an increased level of activation of the Wnt signalling pathway in MDS-derived organoids. (A) Representative pictures of unstained cortical loops from control- and MDS-derived organoids. Level of activation of the Wnt signalling pathway around the ventricles depicted as a green fluorescence signal (Wnt-GFP reporter). Scale bars, 25 µm. **(B)** Quantification of the corrected total cell fluorescence. CHIR treatment of cortical organoids led to a significant increase of Wnt signalling activity in MDS-derived cultures without strongly affecting control cultures (Ctrl2.1. no CHIR n=3, N=30; Ctrl2.1. +CHIR n=3, N=30; MDS1.1. no CHIR n=3, N=30; MDS1.1 +CHIR n=3, N=30). Error bars, ±SD. **p < 0.01, ***p < 0.001.

These findings, in conjunction with the luciferase assay results, provided additional confirmation of our working hypothesis that there is a decreased level of Wnt signalling activity in MDS-derived cultures (both in 2D and 3D), as well as a direct connection between the activation of N-cadherin and Wnt.

To further investigate the effects of MDS-derived culture exposure to CHIR, we performed a more detailed analysis of the overall organoid organisation and quantified all six loop parameters. These assessments revealed that treatment with the GSK3ß inhibitor resulted in a more efficient and homogeneous generation of cortical loops (Figure 4.15. A-D).
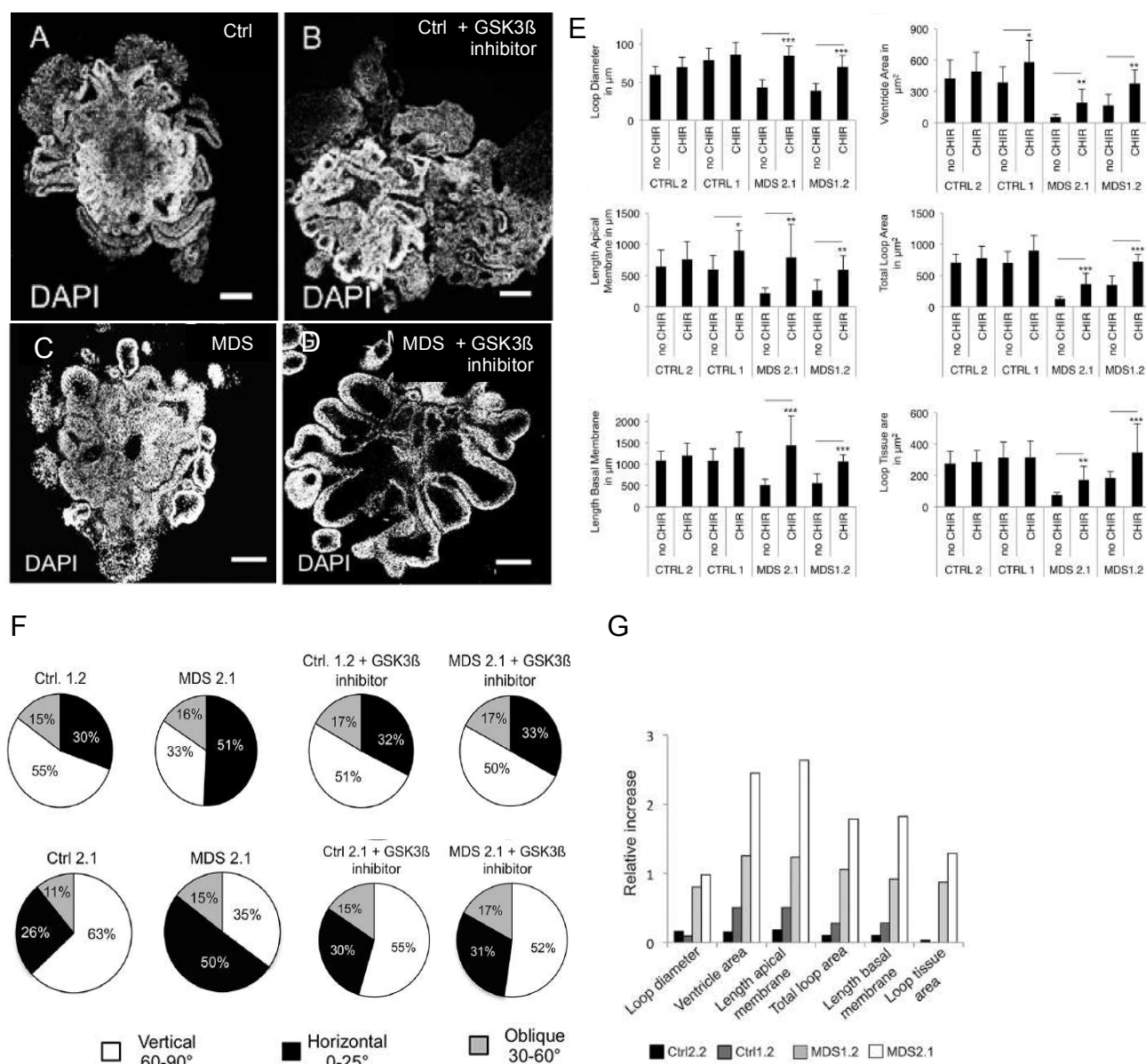
Figure 4.15. Activation of the canonical Wnt signalling pathway promotes rescuing changes of the phenotypical alterations of MDS-derived organoids. (A-D) Representative images of control (A-B)- and MDS (C-D)-derived organoids under standard culture conditions (**A and C**) and following exposure to the GSK3ß inhibitor CHIR99021 for 10 days (**B and D**), depicted are nuclei stained by DAPI. Scale bars, 200 µm. **(E)** Quantification of the loop diameter (**D**), length of apical membrane, length of basal membrane, ventricle area, total loop area and total tissue area in control- and patient-derived organoids in the absence (Ctrl2 n=3, N=10; Ctrl1 n=3, N=9; MDS2.1 n=3, N=8; MDS1.2 n=3, N=8) and the presence of the GSK3ß inhibitor (Ctrl2 n=3, N=8; Ctrl1 n=3, N=9; MDS2.1 n=3, N=8; MDS1.2 n=3, N=10). Error bars ±SD. *p < 0.05, **p <0.01, ***p < 0.001. **(F)** Quantification of vertical, horizontal, and oblique division planes of dividing vRGCs in control and patient-derived organoids in the absence and presence of the GSK3ß inhibitor at day 20. Ctrl 1.2 (n=3, N=127), MDS2.1 (n=3, N=115), Ctrl 1.2 + CHIR (n=3, N=78), and MDS 2.1 + CHIR (n=3, N=88). **(G)** Relative change of multiple parameters assessed in cortical neuroepithelial loops of control and patient organoids. Shown is the relative increase in the presence of the GSK3ß inhibitor compared to the non-treated control. (Quantification of the cortical loop parameters was performed by Olivia Krefft, figure modified from Iefremova et al., 2017).

68

Interestingly, not only were the morphological parameters of the cortical loops (loop diameter, length of apical and basal membranes, ventricle area, total loop area and total tissue area) affected (Figure 4.15. E), the vRGGs mitotic planes also shifted from horizontal back to vertical: MDS1.2 without treatment (vertical 35.09%, horizontal 50.88%, and oblique 15.79%) and MDS1.2+GSK3ß inhibitor (vertical, 51.85%, horizontal 32.10%, and oblique 16.05%).

Moreover, as in the case of the Wnt-GFP corrected fluorescence, the CHIR rescue effect was specific to MDS-derived organoids, since there was also no indication of significant change in mitotic spindle orientation: Ctrl1.2 without treatment (vertical 59.06%, horizontal 28.34%, and oblique 12.60%) and Ctrl 1.2+GSK3ß inhibitor (vertical 51.90%, horizontal 31.65%, and oblique 16.45%). Olivia Krefft performed the quantitative analysis of the cortical loop parameters (i.e., loop diameter, apical membrane length, basal membrane length, ventricle area, loop area, and loop tissue area).

5. Discussion

5.1. Suitability of 3D organoids for studying human-specific aspects of cortical development and deciphering MDS-associated changes

This study introduces the standardised and highly reproducible approach of using forebrain-type organoids to model the early stages of human cortical development, both under physiological and pathophysiological conditions associated with severe malformations in corticogenesis, such as MDS. We developed our protocol (Iefremova et al., 2017) based on two key studies (Kadoshima et al., 2013; Lancaster et al., 2013). Our approach applied dual SMAD inhibition (the combined action of two inhibitors of SMAD signalling, A83-01 and LDN-193189, to induce rapid and efficient differentiation of PSCs to neuronal progenitors) in combination with modulators of Wnt signalling pathways to prevent the posteriosation of neuronal cultures.

Applying a doxycycline-inducible CRISPR/Cas9 gene-editing approach to the hiPSCs derived from MDS patients, we successfully generated LIS1 and 14.3.3ε rescue cell lines enabling us to address the specific roles for each of these proteins. Adding doxycycline into the cell culture medium significantly elevated LIS1 and YWHAE expression to levels comparable to unedited patient-derived cell lines.

The VZ-like regions in both control- and patient-derived organoids exhibited unified expression of Sox2 (typical transcription factor expressed by neuronal progenitors), as well as numerous forebrain-specific transcription factors such as Foxg1, Emx1, Otx2, and Pax6. Conversely, as expected, there was no detection of the expression of typical mid- and hindbrain markers. However, despite the lack of difference in expression levels in markers specifying region and cell lineage, a remarkable difference in organoids size was observed. Furthermore, restoration in LIS1 and 14.3.3ε expression levels in rescue cell lines produced a partial recovery in organoid expansion. Apart from assessing the overall size and expansion rates, we performed a more detailed analysis of the neuroepithelial loops representing the ventricular zone niche in the developing brain. We defined six distinct loop parameters to comprehensively characterise cortical loop structure: basal and apical membrane length, total loop area, loop tissue area, loop diameter, and ventricle-like area. By completing this analysis, we observed a significant decrease in all the parameters in patient-derived organoids. Interestingly, as in the case of overall size and expansion rates, the re-expression of LIS1 and 14.3.3ε also resulted in a partial rescue effect.

The described phenotype is in line with clinical data obtained from autopsies MDS patients' brains exhibiting a significant decrease in size (Sheen et al., 2006).

We propose that a decrease in the size of MDS-derived organoids results from a clear shift from a symmetric pattern of vRGCs division to an asymmetric one rather than the activation of apoptotic processes in neuronal progenitors. Based on previous reports that the functionality of the LIS1/NDEL1/14.3.3ε protein complex is essential for the stability of the microtubule network, we investigated whether we could also observe this disease-associated change in our 3D model. As a result, we found a striking impairment in the organisation of the vRGCs microtubule network, accompanied by an altered distribution of adhesion molecules along the ventricle-like area. We hypothesised that the abovementioned phenotypic changes would subsequently cause a non-cell-autonomous disturbance in the N-cadherin/ß-catenin signalling axis. A strong indication in support of our hypothesis is the fact that we were able to rescue the pathway disturbance by reinstating active ß-catenin signalling, which subsequently rescued the mode of cell division in vRGCs, as well as the overall size differences.

Conclusively, this work highlights the immense potential of an organoid cell culture system for modelling human brain development in a tissue-like context, mimicking certain aspects of the process of cortical development. Furthermore, we have provided the first piece of evidence of a hitherto undescribed mechanism explaining how a deficiency in the LIS1/NDEL1/14.3.3ε protein complex results in the disruption of signalling cues and cell-fate determination within the ventricular niche of the developing brain.

5.2. LIS1/NDEL1/14.3.3ε protein complex and its essential role in the expansion of human cortical progenitors

Predominantly, previous studies have focused on the Lis1 protein individually rather than the function of additional components in the complex or the complex overall. The Lis1 protein has received attention due to its key role in developing LIS1-associated lissencephaly. Previous extensive studies have demonstrated that LIS1-associated lissencephaly is typically characterised by defects in neuronal migration. Therefore, such disorders were widely considered to be caused solely by migration defects (Moon and Wynshaw-Boris, 2013). Nevertheless, several reports indicate the likelihood that the LIS1/NDEL1/14.3.3ε complex has an essential role in proliferating

activity in radial glia cells (RGCs) (Tsai et al., 2005; Yingling et al., 2008; Bi et al., 2009). Most studies investigating the role of Lis1 and 14.3.3ε proteins in corticogenesis (under normal and pathological conditions) were conducted using mice models. Data obtained from animal models is undoubtedly valuable. However, in comparison to humans affected by a loss-of-function in LIS1, mutant mice largely exhibit only mild cortical disorganisation. This may be explained by the fact that the mouse brain is lissencephalic in its nature. Contrary to the human brain, the mouse brain is not only smaller in size but also characterised by significantly less diversity in subtypes of proliferating cortical progenitors and postmitotic neurons. Therefore, we conclude that human-derived cell-based models are essential for pinpointing the effects of Lis1 and 14.3.3ε proteins in humans. To investigate potential relationships between components of the LIS1/NDEL1/14.3.3ε complex and human corticogenesis, we applied 2D monolayer cultures of NSCs and 3D forebrain cortical organoids to hiPSCs in healthy controls and MDS patients. MDS was chosen as a suitable condition for studying the potential impacts of the LIS1/NDEL1/14.3.3ε complex in progenitor expansion during human corticogenesis. This is because the causative heterozygous deletion along chromosome 17 (17p13.3) involves encoding genes for two components of the LIS1/NDEL1/14.3.3ε complex: LIS1 and YWHAE (encodes 14.3.3ε protein).

While the role of LIS1/NDEL1/14.3.3ε in neuronal migration is widely acknowledged and well-documented, the contribution of this multiprotein complex in the proliferation of human neuronal progenitors remains to be clearly defined. This study highlights the essential role of the LIS1/NDEL1/14.3.3ε complex in expansion rates among neuronal progenitors and provides compelling evidence of a hitherto unknown mechanism explaining how a deficit in the multiprotein complex disrupts signalling cues in the ventricular zone of the developing brain and causes a shift in cell fate determination.

As previously described, by applying our 3D cortical organoid model, we demonstrated that patient-derived organoids were significantly smaller in size and exhibited decreased complexity in all measured loop parameters. Furthermore, clinical data has revealed that most patients suffering from MDS have a borderline reduced brain size or are defined as clearly microcephalic (Allanson et al., 1998). We hypothesised two possible scenarios leading to a decrease in overall brain size. The first hypothesis considered the possibility that a smaller brain size originated from

increased apoptosis during the active proliferation of neuronal progenitors. Alternatively, microcephaly may arise from changes in the pattern of division in neuroepithelium cells within the ventricular niche of the developing brain.

First, we investigated the possibility of a decreased brain size caused by increased apoptosis by performing a quantitative analysis of cleaved (active) caspase-3 at several time points (days 10, 15, 20, and 28). The analysis demonstrated that apoptotic cell death was relatively rare within the cortical loops-like structure at all investigated time points. Moreover, a comparison between the control and patient-derived groups of organoids revealed no significant difference in the numbers of apoptotic neuronal progenitors.

Data obtained from experiments using animal models indicates that the LIS1/NDEL1/14.3.3ε complex has an essential role in regulating cell division by controlling the precise orientation of the mitotic spindle in dividing neuroepithelium cells (Pawlisz et al., 2008; Yingling et al., 2008; Moon et al., 2014). Furthermore, since we detected no sign of increased apoptotic cell death, we addressed an alternative mechanism that may lead to reduced brain size in MDS patients. We propose that an impairment in the LIS1/NDEL1/14.3.3ε complex leads to a reduction in cortical microtubule numbers, a weakening of existing astral microtubules, and a destabilisation at the '+' end of the microtubules, subsequently resulting in alterations throughout the microtubule network. In animal models, this cascade of processes results in a loss of precision in mitotic spindle orientation in neuronal progenitors and produces a randomised change in the spindle orientation during mitosis (Yingling et al., 2008). Applying our 3D model, we also observed acute alterations in the organisation of the vRGCs microtubule network in patient-derived organoids. We demonstrated that in control-derived organoids, vRGCs microtubule networks (highlighted by ICH staining of acetylated a-tubulin) extend throughout the entire VZ-like region from its apical to basal membranes. In MDS-derived organoids, however, microtubules appeared to be somewhat truncated and failed to reach the basal end. Additionally, data obtained from LIS1 and 14.3.3ε rescue organoids revealed significantly extended microtubule networks towards the basal membrane, despite still appearing to be morphologically impaired.

We subsequently considered whether 3D organoids would reveal an increase in oblique orientation in cell spindles during mitosis, as reported by Yingling et al. (2008). Remarkably, contrary to data from rodent models, hiPSC-derived organoids

demonstrated a clear shift from largely symmetric to asymmetric cell division in MDS-derived cortical cultures (the mitotic spindle in cells undergoing division was labelled with Tpx2 and its orientation related to the VZ-like surface). Moreover, the number of cells with an oblique cleavage plane was not significantly changed. Intriguingly, we also observed an increase in the total number of Tbr2 positive IPs at two different time points: day 21 and 28 of organoid differentiation. These findings are in line with the pronounced shift towards asymmetric cell division, leading to an increased rate of early neurogenesis. Restoration in LIS1 and 14.3.3ε levels partially rescued the shift in cell division towards that in the healthy controls (MDS-LIS1, vertical 54.84%, horizontal 29.84%, and oblique 15.32%; MDS-14.3.3ε, vertical 50.0%, horizontal 31.51%, and oblique 19.49%). In addition, the number of Tbr2-positive IPs was significantly reduced.

Our observations suggest that the reported decrease in brain size among MDS patients results from the shift towards asymmetric cell division, leading to an increased rate of IPs generation at the expense of the neuronal stem cell pool.

A prominent shift in the mitotic spindle orientation from vertical (resulting in symmetric cell division) to horizontal (resulting in asymmetric cell division), without a significant increase in the oblique cleavage planes in the dividing cells, suggests the possible involvement of the signalling pathways rather than solely a disruption in the microtubule networks. Adherent junctions reportedly exert a certain amount of control over self-renewal processes in vRGCs (Stocker and Chenn, 2009; Marthiens et al., 2010). In addition, data obtained from mouse models has demonstrated that a deficiency in the LIS1/NDEL1/14.3.3ε complex leads to disruptions in cell-cell interactions and abnormal distribution of adhesion molecules along the apical surface (Pawlisz et al., 2008; Pramparo et al., 2011).

Considering the data previously obtained from animal models, we explored apical surface organisation in the VZ-like region. As a result of our investigation, we observed that the organisation of the ventricular niche was significantly altered in patient-derived cultures. Contrary to the vRGCs in control organoids, being densely packed and well organised, the vRGCs in MDS-derived organoids were less tightly packed with a somewhat random positioning in the ventricle. Moreover, we observed significant disorganisation in the distribution of cell adhesion molecules within the stem cell niche. The control organoid cultures demonstrated a clearly defined belt of adherent junctions along the apical membrane. Conversely, MDS-derived cultures

exhibited several disruptions in the distribution of cell-cell contact adherent molecules along the apical side. In LIS1 and 14.3.3ε rescue organoids, cell organisation within the stem cell niche, in addition to the distribution of cell adhesion molecules, was restored to a level more akin to control conditions (Figure 4.11. I and J).

The dramatic changes in the organisation of the VZ-like niche are consistent with clinical data retrieved from histological analysis of MDS patients' brains, which also exhibited severe disorganisation in the VZ surface (Sheen et al., 2006).

Based on our findings regarding the acute disorganisation of the VZ niche and a non-random change in the mode of the cell division, we propose that such significant alterations may be closely linked to the signalling pathway within the stem cell niche. In line with this observation, research (e.g., Chenn and Walsh, 2002; Zechner et al., 2003) suggests that active Wnt/ß-catenin signalling exerts control over vRGCs proliferation. Moreover, adhesion molecule N-cadherin may be involved in controlling Wnt activity by regulating the phosphorylation state of AKT, with the subsequent phosphorylation of ß-catenin at serine 552 (p-Ser552-ß-catenin), promoting its activation and stabilisation (Zhang et al., 2010, 2013). To confirm whether our model would also reflect this aspect, we examined the phosphorylation state of ß-catenin at Ser552 in vRGCs undergoing mitosis (labelled by p-vimentin). Indeed, we discovered that control cultures contain a high number of vRGCs that are double-positive for p-Ser552-ß-catenin and p-vimentin. Whereas the amount of such double-positive neuroepithelium cells within patient-derived organoids was significantly reduced. Re-expression of LIS1 and 14.3.3ε in rescue lines led to a significant increase in the number of p-Ser522-ß-catenin- and p-vimentin-positive dividing progenitors along the apical membrane (Figure 4.11. E).

In conjunction, the data suggests that vRGCs in patient-derived cultures exhibit a dysregulated process of ß-catenin activation, which may originate from an impairment in the N-cadherin/ß-catenin signalling axis. To evaluate our hypothesis and determine whether there is a functional link between N-cadherin and ß-catenin, we manipulated N-cadherin and investigated any changes in activity in the Wnt signalling pathway. At this stage of the study, 2D monolayer cultures, comprising a highly homogeneous population of vRGCs, were considered to be more beneficial than 3D organoids. Applying the 2D culture approach, we observed that MDS-derived cortical cultures demonstrated a decreased level of expression in the protein involved in a signalling pathway that connects signalling cues within the niche and ß-

catenin signalling (including N-cadherin, phosphorylated AKT at Ser 473, ß-catenin phosphorylated at Ser 552 and total ß-catenin). These changes may be reversed in the direction of healthy control rates, suggesting an existing link between the activation of Wnt signalling and the ß-catenin component of the common signalling axis.

To further investigate Wnt signalling and the effect of N-cadherin on its activity, we generated Wnt reporter cell lines carrying the pSuper8XTOPFlash luciferase reporter. By performing a luciferase assay, we observed that patient-derived neural progenitor cultures exhibited significantly reduced levels of Wnt activity in comparison with wild-type cultures. Moreover, and in line with a postulated hypothesis, the N-cadherin function may directly affect Wnt reporter activity. To determine whether this was the case, we blocked N-cadherin activity using an N-cadherin blocking antibody that produces a decline in Wnt reporter activity. To substantiate our suggested mode of interaction between N-cadherin and Wnt signalling activity, we considered whether direct N-cadherin manipulation would influence the proliferation-differentiation balance in cortical progenitor cultures. This was examined using cortical progenitors cultured in the absence of any growth factors with further differentiation into cortical neurons. Notably, in the 2D monolayer system, patient-derived cultures demonstrated a significantly elevated neuronal differentiation rate in comparison to the wild-type cultures, indicating that reduced levels of Wnt activity result in premature neurogenesis. This is in line with the data showing an increased number of Tbr2-positive IPs in MDS-derived cortical organoids. Furthermore, by blocking N-cadherin in control-derived progenitors, we induced rapid neuronal differentiation in these cultures. Conversely, activating the N-cadherin function in patient-derived cultures reversed early neurogenesis. This data verifies the existence of a direct link between functionally active N-cadherin and Wnt signalling pathways. Moreover, these findings highlight the significance of this pathway, and its impairment, in the balance between processes of cell proliferation and differentiation.

To summarise the above findings, we postulate that impairments in the microtubule networks of vRGCs result in the disorganisation of the VZ stem cell niche. This subsequently leads to a non-cell-autonomous imbalance in the N-cadherin/ß-catenin/Wnt signalling axis. Overall, the data suggests that a deficiency in the LIS1/NDEL1/14.3.3ε complex results in the severe disruption of signalling within the VZ-like niche and controls cell-fate determination.

5.3. Rescue strategies to overcome the impairments caused by a deficiency in the LIS1/NDEL1/14.3.3ε complex

In this study, two distinct approaches were introduced to rescue the key phenotypic changes observed in MDS patient-derived cultures. The first rescue strategy involved the re-expression of LIS1 and 14.3.3ε to levels closely resembling those in the wild-type control using a doxycycline-inducible CRISPR/Cas9 gene-editing technique. Supplementing the cell culture medium with doxycycline increased LIS1 or YWHAE expression to levels comparable to unedited cell lines. We subsequently observed a significant recovery in the main phenotypic changes associated with MDS: overall size and expansion rates of the organoid cultures, the switch from symmetric to asymmetric modes of cell division, the impairment of microtubule networks, the disorganisation of the stem cell niche in the VZ-like area, the distribution of adherent molecules along the apical membrane of VZ-like area, and disturbance in the N/cadherin and ß-catenin signalling axis.

Observing this reverse effect, and confirming the mechanistic link between activation in the Wnt signalling pathway and N-cadherin/ß-catenin, we considered whether it would be possible to at least partially rescue the abovementioned phenotype characteristics using pharmacological manipulation of activity in the Wnt signalling pathway. The GSK3ß inhibitor CHIR99021 was selected as an agent for the pharmacological activation of ß-catenin, with the potential to partially restore alterations associated with MDS.

Exposing patient-derived organoid cultures to the GSK3ß inhibitor, we observed a prominent rescue effect on the generation and complexity (in all six defined parameters) of the cortical loops, as well as the significantly widespread of double-positive for p-Ser552-ß-catenin and p-vimentin-positive actively dividing vRGCs. Regarding the shift in the cleavage plane of dividing progenitor cells, we discovered a similar rescue effect after applying CHIR99021: the division pattern within MDS-derived organoids was reversed to the control-type situation (most of the cells began to divide symmetrically, without a significant increase in the oblique plane of cell division). Moreover, the observed rescue of the phenotypic hallmarks of MDS in patient-derived organoids appeared to be specific to MDS organoids. Conversely, exposing control-derived cultures to the same amount of CHIR99021 did not significantly alter the cortical loop parameters or the distribution of the different

modes of cell division within vRGCs. Furthermore, two phenotypic changes caused by MDS — disruption of the cytoarchitecture in the stem cell niche and the distribution of adherent molecules along the apical surface — were not affected by exposure to CHIR99021. This indicates that these MDS-associated aberrations occur upstream of ß-catenin function, regardless of the state of its activity.

5.4. Outlook

The findings summarised above provide a convincing argument in support of the application of cortical organoids to model the early stages of human cortical development *in vitro*. Nonetheless, this 3D cell culture system, as any other *in vitro* model, retains certain limitations. For instance, organoids still fail to develop the strictly defined lamination pattern present in the human embryonic cerebral cortex, arguing that radial migration of new-born cortical neurons does not occur as precisely as in the *in vivo* scenario. Consequently, organoids are the most suitable means of addressing early aspects of human corticogenesis at present. Although organoid technology is in its infancy, with improvements to the existing protocols, it demonstrates the considerable potential to enable modelling of both early and late stages of human brain development. It is assumed that the numerous differences between *in vitro* organoids and *in vivo* embryonic brains originate from the considerably diverse microenvironments in which they undergo development. Essential components of the *in vivo* microenvironment include the vascular system, the meninges (membranes that surrounds the developing brain and discharge several components that affect processes of proliferation and differentiation), and additional regions of the developing brain, such as ganglionic eminences (the source of GABAergic inhibitory neurons, the effective migration and integration of which are crucial for physiological cortical development). A recent study by Mansour et al. (2018) describes a preliminary attempt to overcome the lack of blood vessels within the cortical organoid. They suggest that human brain organoids are suitable for transplantation into a rodent host brain and provide evidence of integration, viability, survival, vascularisation, and a degree of functional neuronal activity in the grafted organoid and the studied section of the host brain.

Another research direction has focused on integrating different regions of the developing brain (e.g., the pallium and subpallium) into a potentially single functioning system by introducing 'fused organoid/spheroid cultures'. This two-step approach is based on a procedure that generates distinct cultures, each carrying region specifications that are further assembled into a single system of fused cultures using different methods. A system that resembles diverse regions of the developing brain could provide a cell-based platform to study connections and communication between them. Data obtained from fused cultures may significantly contribute towards uncovering further details about the physiological and pathophysiological

mechanisms of human brain development, potentially leading to the development of a drug-screening approach.

In its entirety, our study highlights the potential for organotypic cell-culture models to contribute towards an advanced understanding of developmental mechanisms and disease-related changes caused by a dysfunction in single genes within a complex tissue environment.

6. Abbrevations

Abbrevation	Full name
ARX	Aristaless-related homeobox
BDNF	Brain-derived neurotrophic factor
BMP	Bone morphogenetic proteins
BSA	Bovine serum albumin protein
cAMP	Cyclic adenosine monophosphate
cDNA	Complementary DNA
CP	Cortical plate
CNS	Central nervous system
CRISPR	Clustered regulatory interspaced palindromic repeats
CTCF	Corrected total cell fluorescence
Dach1	Dachshund homolog 1
DAPI	4',6-Diamidino-2-phenylindole
Dclk1	Doublecortin like kinase 1
Dclk2	Doublecortin like kinase 2
DCX	Doublecortin
DNA	Deoxyribonucleic acid
dNTPs	Nucleoside triphosphate
Dox	Doxycycline
EMX1	Empty Spiracles Homeobox 1
FCS	Fetal calf serum
FOXG1	Forkhead box G1
GABA	Gamma-Aminobutyric acid
GDNF	Glial cell-derived neurotrophic factor

Abbreviation	Full name
GFAP	Glial fibrillary acidic protein
GT	GelTrex
GW	Gestation week
hESCs	Human embryonic stem cells
hiPSCs	Human induced pluripotent stem cells
ICC	Immunocytochemistry
iPSCs	Induced pluripotent stem cells
IP	Intermediate progenitors
iSVZ	Inner subventricular zone
JNK	c-Jun N-terminal kinase
KLF4	Kruppel-like factor 4
LIS1	(official symbol PAFAH1B1) - platelet-activating factor acetylhydrolase, isoform 1b, subunit 1
lt-NES cell	long-term self-renewing neuroepithelial stem cell
MAP	Microtubuli-associated protein
MARK	Microtubule affinity regulatory kinase
MCD	Malformations in cortical development
MDS	Miller-Dieker syndrome
MRI	Magnetic resonance imaging
mRNA	Messenger RNA
MZ	Marginal zone
NDEL1	Neurodevelopment Protein 1 Like 1
NES	Nestin
OCT4	Octamer-binding protein 4
OTX2	Orthodenticle Homeobox 2

Abbreviation	Full name
oRGs	Outer radial glia cells
oSVZ	Outer subventricular zone
PAGE	Polyacrylamid gel electrophoresis
PAX6	Paired box 6
PBS	Phosphate buffered saline
PCR	Polymerase chain reaction
PFA	Paraformaldehyde
PLZF	Promyelocytic leukemia-associated zinc finger
PP	PluriPro medium
puroR	Puromycin resistance
qRT-PCR	Quantative reverse-transcriptase PCR
RELN	Relin
RNA	Ribonucleic acid
ROCK	Rho-associated, coiled-coil containing protein kinase
RT-PCR	Reverse-transcriptase PCR
SOX2	Sex determing region Y-box 2
SVZ	Subventricular zone
SNP	Single nucleotide polymorphism
TBR2	T-box brain protein 2
TGFß	Transforming growth factor β
TSC	Tuberous sclerosis complex
TUBA1A	Tubulin α1a
VLDLR	Very low-density lipoprotein receptor
VZ	Ventricular zone
WNT pathway	Wingless/Integrated

Abbreviation	Full name
YWHAE	(encodes 14.3.3ε protein) Tyrosine 3-Monooxygenase/Tryptophan 5-Monooxygenase Activation Protein Epsilon
Zo-1	Zona occludens-1

7. Abstract

The human brain is an exceptionally complex organ, both structurally and functionally, and represents the most remarkable progress in evolution. The human cortex is a highly organised and extensively folded structure consisting of radially organised layers: gyri and sulci. For many years, transgenic mouse models were used to study gene function in the developing cortex. Recently, it was suggested that human brain development could also be modelled *in vitro* using the capacity of pluripotent stem cells (PSCs) to self-organise into so-called brain organoids. They contain different cell types that organise in a spatially similar way to the developing human brain and accurately recapitulate developmental gene expression patterns. This study focuses on investigating the functional role of the LIS1 gene during human cortical development. LIS1 and its interactive partners, NDEL1 and 14.3.3ε, have been cited as crucial for neuronal migration and cortical layer formation and were recently demonstrated to have a role in the expansion of cortical progenitors. Moreover, heterozygous deletions or mutations in LIS1 constitute the most common cause of lissencephaly. We established a standardised induced PSC-derived cortical organoid model to decipher the functional role of the LIS1/NDEL1/14.3.3ε protein complex during human cortical development. To that end, we reprogrammed fibroblasts from patients suffering from haploinsufficiency of chromosome 17p13.3, which involves the genes encoding LIS1 and 14.3.3ε, and differentiate them into cortical cultures. We analysed proliferation and neurogenesis on morphological, biochemical, and molecular levels, and demonstrated that patient-derived organoids show a significant size reduction, resulting from a shift in ventricular zone radial glial cells from symmetric to asymmetric mode of cell division. This was associated with alterations in microtubule networks and the disruption of cortical niche architecture, leading to a non-cell-autonomous disturbance in the N-cadherin/ß-catenin signalling axis. Reinstallation of ß-catenin signalling resulted in a return to symmetric cell division and rescued growth deficits. We provided a novel experimental model to analyse the functional roles of LIS1 and 14.3.3ε during human cortical progenitor expansion. Significantly, our data highlights a new role for these proteins in maintaining the cortical niche and suggests that organoids may serve as a useful model for assessing aspects of early cortical development, such as progenitor cell proliferation, cell cycle dynamics, and neurogenesis.

8. Zusammenfassung

Das menschliche Gehirn ist aus struktureller und funktioneller Sicht ein hochkomplexes Organ und zeigt die deutlichste Entwicklung im Verlauf der Evolution. Der humane Kortex ist eine außerordentlich organisierte Struktur und aufwendig gefaltet. Er besteht aus radial angeordneten Schichten, den Gyri und Sulci. Jahrelang war es gängig, die Genfunktionen innerhalb des sich entwickelnden Kortex mithilfe von transgenen Mausmodellen zu untersuchen. Vor kurzer Zeit kam die Idee auf, dass die humane Hirnentwicklung auch *in vitro* untersucht werden kann. Dafür nutzt man pluripotente Stammzellen, welche die Kompetenz besitzen sich selbst zu organisieren. Diese selbst organisierte Strukturen bezeichnet man als Organoide. Ein Organoid besteht aus verschiedenen Zelltypen, die eine räumliche Anordnung besitzen, die dem menschlichen Gehirn entspricht. Dadurch ist es möglich, entwicklungsspezifische Genexpressionsmuster zu rekapitulieren.

Diese Arbeit beabsichtigt die funktionelle Rolle des LIS1 Gens während der Entwicklung des humanen Kortex zu untersuchen. Es wurde beschrieben, dass LIS1 und seine Interaktionspartner NDEL1 und 14.3.3ε ausschlaggebend für die neuronale Migration und die Formierung der kortikalen Schichten sind. Zudem wurde kürzlich gezeigt, dass sie eine Rolle bei der Expansion von kortikalen Vorläuferzellen spielen. Des Weiteren machen heterozygote Deletionen oder Mutationen des LIS1-Gens die am meisten bekannteste Ursache für Lissencephalie aus. Wir haben ein standardisiertes Organoidmodell etabliert, das von induzierten pluripotenten Stammzellen abgeleitet ist. Damit ist es möglich, die funktionale Rolle des LIS1/NDEL/14.3.3ε Proteinkomplexes im Zuge der kortikalen Entwicklung zu entschlüsseln. Dementsprechend haben wir Fibroblasten von Patienten, die an einer Haploinsuffizienz des Chromosoms 17p13.3, auf dem auch die kodierenden Gene für LIS1 und 14.3.3ε liegen, leiden, reprogrammiert. Die reprogrammierten Zellen wurden dann im weiteren Verlauf zu kortikalen Kulturen weiter differenziert. Wir haben die Proliferation und Neurogenese der Zellen morphologisch, biochemisch und auf molekularem Level analysiert. Wir konnten zeigen, dass Organoide, welche von Patientenzellen abgeleitet waren, signifikant kleiner waren. Dieser Unterschied in der Größe begründet sich auf einen Wechsel von symmetrischer zu asymmetrischer Zellteilung der radialen Gliazellen innerhalb der Ventrikularzone. Verbunden damit war eine Änderung des Mikrotubuli Netzwerks und eine Disorganisation des Aufbaus

der kortikalen Nische. Daraus resultierte eine nicht zellautonome Störung des N-cadherin/ß-catenin Signalwegs. Die Wiederherstellung des ß-catenin Signalwegs resultiert in einer Unwandlung zurück zur symmetrischen Zellteilung und hebt das Größendefizit auf. Wir bieten ein neues Experimentmodell, um die funktionale Rolle von LIS1 und 14.3.3ε während der Expansion von humanen, kortikalen Vorläuferzellen zu analysieren. Unsere Daten heben eine neue Rolle von Lis1 und 14.3.3ε bei der Erhaltung der kortikalen Nische hervor. Außerdem suggerieren sie, dass Organoide als ein nützliches Werkzeug, um Aspekte der frühen kortikalen Entwicklung zu studieren, genutzt werden können.

9. Acknowledgements

10. References

Ardhanareeswaran, K., Mariani, J., Coppola, G., Abyzov, A., and Vaccarino, F. M. (2017). Human induced pluripotent stem cells for modelling neurodevelopmental disorders. Nat. Rev. Neurology *13*, 265-278.

Ayala, R., Shu, T., Tsai, L.H. (2007). Trekking across the brain: the journey of neuronal migration. Cell *128*, 29-43.

Ban, H., Nishishita, N., Fusaki, N., Tabata, T., Saeki, K., Shikamura, M., Ta- kada, N., Inoue, M., Hasegawa, M., Kawamata, S., and Nishikawa, S. (2011). Efficient generation of transgene-free human induced pluripotent stem cells (iPSCs) by temperature-sensitive Sendai virus vectors. Proc. Natl. Acad. Sci. USA *108*, 14234–14239.

Barkovich, A.J., Kuzniecky, R.I., Dobyns, W.B., Jackson, G.D., Becker, L.E., Evrard, P. (1996). A classification scheme for malformations of cortical development. Neuropediatrics *27*, 59-63.

Barkovich, A.J. (2005). Malformations of Cortical Development. In R. I. Kuzniecky & G. D. Jackson (Ed.), Magnetic Resonance in Epilepsy, Second Edition, 226-253. New York, USA: Academic Press.

Barkovich, A.J., Guerrini, R., Kuzniecky, R.I., Jackson, G.D., Dobyns, W. B. (2012). A developmental and genetic classification for malformation of cortical development: update 2012, Brain J. Neurol. *135*, 1348-1369.

Bayatti, N., Moss, J.A., Sun, L., Ambrose, P., Ward, J.F.H., Lindsay, S., Clowry, G.J. (2008). A molecular neuroanatomical study of the developing human neocortex from 8 to 17 postconceptional weeks revealing the early differentiation of the subplate and subventricular zone. Cereb Cortex. *18*, 1536–1548.

Bershteyn, M., Nowakowski, T. J., Pollen, A. A., Di Lullo, E., Nene, A., Wynshaw-Boris, A., Kriegstein, A. R. (2017). Human iPSC-derived cerebral organoids model cellular features of lissencephaly and reveal prolonged mitosis of outer radial glia. Cell Stem Cell *20*, 435–449.

Bi, W., Sapir, T., Shchelochkov, O.A., Zhang, F., Withers, M.A., Hunter, J.V., Levy, T., Shinder, V., Peiffer, D.A., Gunderson, K.L., et al. (2009). Increased LIS1 expression affects human and mouse brain development. Nat. Genet. *41*, 168–177.

Burgess, A., Vigneron, S., Brioudes, E., Labbé, J.-C., Lorca, T. and Castro, A. (2010). Loss of human greatwall results in G2 arrest and multiple mitotic defects due to deregulation of the cyclin B-Cdc2/PP2A balance. PNAS *107*, 12564-12569.

Burges, A., Lorca, T., Castro, A. (2012). Quantitative Live Imaging of Endogenous DNA Replication in Mammalian Cells. PLoS ONE *7 (9).*

Camp, J.G., Badsha, F., Florio, M., Kanton, S., Gerber, T., Wilsch-Brauninger, M., Lewitus, E., Sykes, A., Hevers, W., Lancaster, M., et al. (2015). Human cerebral

organoids recapitulate gene expression programs of fetal neocortex development. Proc. Natl. Acad. Sci. USA *112*, 15672–15677.

Crino, P., Nathanson, K.I., Henske, E.P. (2006). The tuberous sclerosis complex. N Engl J Med *355,* 1354-1356.

Chambers, S. M., Fasano, C. A., Papapetrou, E. P., Tomishima, M., Sadelain, M. and Studer, L. (2009) Highly efficient neural conversion of human ES and iPS cells by dual inhibition of SMAD signaling. Nat. Biotechnol. *27*, 275–280.

de Vries, P.J. (2010). Targeted treatments for cognitive and neurodevelopmental disorders in tuberous sclerosis complex. Neurotherapeutics 7, 275-282.

Desir, J., Cassart, M., David, P., Van Bogaert, P., Abramowicz, M. (2008). Primary microcephaly with ASPM mutation shows simplified cortical gyrification with anterio-posterior gradient pre- and postnatally. Am. J. Med. Genet. *146A*, 1439-1443.

Dobyns, W.B., Truwit, C.L., Ross, M.E., Matsumoto, N., Pilz, D.T., Ledbetter, D.H., Gleeson, J.G., Walsh, C.A., Barkovich, A.J. (1999). Differences in the gyral pattern distinguish chromosome 17-linked and X-linked lissencephaly. Neurology *53,* 270-277.

Eiraku, M., Watanabe, K., Matsuo-Takasaki, M., Kawada, M., Yonemura, S., Matsumura, M., Wataya, T., Nishiyama, A., Muguruma, K., Sasai, Y. (2008). Self-organized formation of polarized cortical tissues from ESCs and its active manipulation by extrinsic signals. Cell Stem Cell, *3*, 519-532.

Ira Espuny-Camacho, I., Michelsen, K.A., Gall, D., Linaro, D., Hasche, A., Bonnefort, J., Bali, C., Orduz, D., ..., and Vanderhaeghen, P. (2013). Pyramidal neurons derived from human pluripotent stem cells integrate efficiently into mouse brain circuits In vivo. Neuron *77,* 440–456.

Feng, Y., Walsh, C.A. (2002). Mitotic spindle regulation by Ndel1 controls cerebral cortical size. Neuron 44, 279-293.

Fietz, S.A., Kelava, I., Vogt, J., Wilsch-Brauninger, M., Stenzel, D., Fish, J.L., Corbeil, D., Riehn, A., Distler, W., Nitsch, R., and Huttner, W.B. (2010). OSVZ progenitors of human and ferret neocortex are epithelial-like and expand by integrin signaling. Nat. Neurosci. *13*, 690–699.

Fish, J.L., Dehay, C., Kennedy, H., and Huttner, W.B. (2008). Making bigger brains-the evolution of neural progenitor cell division. J. Cell Sci. *121*, 2783–2793.

Francis, F., Meyer, G., Fallet-Bianco, C., Moreno, S., Kappeler, C., Socorro, A.C., Tuy, F.P., Beldjord, C., and Chelly, J. (2006). Human disorders of cortical development: from past to present. Eur. J. Neurosci. *23*, 877–893.

Freeman, M.R., Rowitch, D.H. (2013). Evolving concepts of gliogenesis: a look way back and ahead to the next 25 years. Neuron *80*, 613-623.

Fuerer, C. and Nusse, R. (2010). Lentiviral vectors to probe and manipulate the Wnt

signaling pathway. PLoS One, 5(2):e9370.

Ginhoux, F., Greter, M., Leboeuf, M., Nandi, S., See, P., Gokham, S., Mehler, M.F., Conway, S.J., Ng, L.G., Stanley, E.R., Samokhvalov, I.M., Merad, M. (2010). Fate mapping analysis reveals that adult microglia derive from primitive macrophages. Science *330*, 841-845.

Ginhoux, F. & Guilliams, M. (2016). Tissue-resident macrophage ontogeny and homeostasis. Immunity *44*, 439-449.

Griffith, E., Walker, S., Martin, C.A., Vagnarelli, P., Stiff,T., Vernay, B. (2008). Mutations in pericentrin cause Seckel syndrome with defective ATR-dependent DNA damage signaling. Nat. Genet. *40*, 232-236.

Hansen, D.V., Lui, J.H., Parker, P.R.L., Kriegstein, A. R. (2010). Neurogenic radial glia in the outer subventricular zone of human neocortex. Nature *464,* 554-561.

Higginbotham, H., Guo, J., Yokota, Y., Umberger, N. L., Su, C.-Y., Li, J., Verma, N., Hirt, J., Caspary, T., and Anton, E. S. (2013). Arl13b-regulated activities of primary cilia are essential for the formation of the polarized radial glial scaffold. Nat Neurosci. *16(8),* 1000–1007.

Hoeffel, G., Chen, J., Lavin, Y., Low, D., Almeida, F.F., See, P., Beaudin, A.E., Lum, J., Low, I., Forsberg, E.C., Poidinger, M., Zolezzi, F., Larbi, A., Ng, L.G., Chan, J.K.Y., Greter, M., Becher, B., Samokhvalov, I.M., Merad, M., Ginhoux, F. (2015). C-Myb+ erythro-myeloid progenitor-derived fetal monocytes give rise to adult tissue-resident macrophages. Immunity *42*, 665-678.

Iefremova, V., Manikakis G., Krefft, O., Jabali, A., Weynans K, Wilkens R, Marsoner F., Brandl, B., Muller, F.J., Koch, P. and Ladewig, J. (2017). An organoid-based model of cortical development identifies non-cell-autonomous defects in wnt signaling contributing to Miller–Dieker syndrome. Cell Rep, *19*, 50-59.

Jamuar, S.S., Walsh, C.A. (2014). Somatic mutations in cerebral cortical malformations. N. Engl. J. Med. *371*, 2038-2049.

Jo, J., Xiao, Y., Sun, A. X., Cukuroglu, E., Tran, H.-D., Göke, J., Tan, Z. Y, Saw, T., Y.,... et al. (2016). Midbrain-like Organoids from Human Pluripotent Stem Cells Contain Functional Dopaminergic and Neuromelanin-Producing Neurons. Cell Stem Cell, *19*, 248-257.

Jossin, Y., Cooper, J.A. (2011). Reelin, Rap1 and N-cadherin orient the migration of multipolar neurons in the developing neocortex. Nat. Neurosci. *14*, 697-703.

Junghaus, D., Hack, I., Frotscher, M., Taylor, V., and Kemler, R. (2005). β catenin–mediated cell adhesion is vital for embryonic forebrain development. Dev. Dynamics. *233*, 528-539.

Kadoshima, T., Sakaguchi, H., Nakano, T., Soen, M., Ando, S., Eiraku, M., Sasai, Y. (2013). Self-organization of axial polarity, inside-out layer pattern, and species-

specific progenitor dynamics in human ES cell-derived neocortex. Proc Natl Acad Sci U S A, *110*, 20284-20289.

Koch, P., Breuer, P., Peitz, M., Jungverdorben, J., Kesavan, J., Poppe, D., Doerr, J., Ladewig, J., Mertens, J., Tüting, T., et al. (2011). Excitation-induced ataxin-3 aggregation in neurons from patients with Machado-Joseph disease. Nature *480*, 543–546.

Lancaster, M., Renner, M., Martin, C. A., Wenzel, D., Bicknell, L.S., Hurles, M.E., Homfray, T., Penninger, J.M., Jackson, A.P., Knoblich, J.A. (2013). Cerebral organoids model human brain development and microcephaly. Nature, *501,* 373-379.

Lambert de Rouvroit, C., Goffinet, A.M. (2001). Neuronal migration. Mech. of Dev. *105,* 47-56.

Lee, J. (2017). Malformations of cortical development: genetic mechanisms and diagnostic approach. Korean J. Pediatr. *60*, 1-9.

Leventer, R.J., Jansen, A., Pilz, D.T., Stoodley, N., Marini, C., Dubeau, F., Malone, J., Mitchell, L.A., Mandelstam, S., Scheffer, I.E., Berkovic, S.F., Andermann, F., Andrermann, E., Guerrini, R., Dobys, W.B. (2010). Clinical and imaging heterogeneity of polymicrogyria: a study of 328 patients. Brain *133*, 1415-1427.

Li, Q., Barres, B.A. (2018). Microglia and macrophages in brain homeostasis and disease. Nat. Rev. Immunology *18,* 225-242.

Lipton, J. O. and Sahin, M. (2014). The Neurology of mTOR, Neuron *84,* 275–291,

Lui, H.J., Hansen, D.V., Kriegstein, A.R. (2011). Development and Evolution of the Human Neocortex. Cell *146*, 18-36.

Lukaszewicz A., Savatier P., Cortay V., Giroud P., Huissoud C., Berland M., Kennedy H., and Dehay C. (2005). G1 phase regulation, area-specific cell cycle control, and cytoarchitectonics in the primate cortex. Neuron *47*, 353-364.

Mansour, A. A., Goncalves, J. Tiago, Bloyd, C. W., Li, H., Fernandes, S., Quang, D., Johnston, S., Parylak, S. L., Jin, X., and Gage, F. H. (2018). An in vivo model of functional and vascularized human brain organoids. Nat. Biotech. *36*, 432-441.

Marín, O., Rubenstein, J.L.R. (2003). Cell migration in the forebrain. Annu. Rev. Neurosci. *26*, 441-483.

Marín, O. (2012). Interneuron dysfunction in psychiatric disorder. Nat. Rev. Neurosci. *13*, 107-120.

Marthiens, V., Kazanis, I., Moss, L., Long, K., and Ffrench-Constant, C. (2010). Adhesion molecules in the stem cell niche–more than just staying in shape? J. Cell Sci. *123*, 1613–1622.

Maroof, A.M., Keros, S., A. Tyson, J. A., Ying, S.-W., M. Ganat, Y.M., Merkle, F.T., ..., and Studer, L. (2013). Directed Differentiation and Functional Maturation of Cortical Interneurons from Human Embryonic Stem Cells. Cell Stem Cell 5, 559-572.

McCloy, R.A., Rogers, S., Caldon, C.E., Lorca, T., Castro, A., and Burges, A. (2014). Partial inhibition of Cdk1 in G2 phase overrides the SAC and decouples mitotic events. Cell Cycle. *13*, 1-12.

Method of the year 2017: organoids. Nature Methods 2018, *15,* 1- 1.

Mo, Z., Zecevic, N. (2008). Is Pax6 critical for neurogenesis in the human fetal brain? Cereb Cortex.*18*, 1455–1465.

Moon, H.M., and Wynshaw-Boris, A. (2013). Cytoskeleton in action: Lissencephaly, a neuronal migration disorder. Wiley Interdiscip. Rev. Dev. Biol. *2*, 229–245.

Moon, H.M., Youn, Y.H., Pemble, H., Yingling, J., Wittmann, T., and Wynshaw- Boris, A. (2014). LIS1 controls mitosis and mitotic spindle organization via the LIS1-NDEL1-dynein complex. Hum. Mol. Genet. *23*, 449–466.

Molyneaux, B.J., Arlotta, P., Menezes, J.R.L., Macklis, J.D. (2007). Neuronal subtype specification in the cerebral cortex. Nat. Rev. Neurosci. *8*, 427-437.

Nadarajah, B., Brunstrom, J.E., Grutzendler, J., Wong, R.O., Pearlman, A.L. (2001). Two modes of radial migration in early development of the cerebral cortex. Nat. Neurosci. *4*, 143-150.

Nadarajah, B., Alifragis, P., Wong, R.O., Parnavelas, J.G. (2002). Ventricle-directed migration in the developing cerebral cortex. Nat Neurosci. *5*, 218–224.

Otani, T., Marchetto, M.C., Gage, F.H., Simons, B.D., Livesey, F. J. (2016). 2D and 3D stem cell models of primate cortical development identify species-specific differences in progenitor behavior contributing to brain size. Cell Stem Cel, *18*, 467-480.

Pang, T., Atefy, R., Sheen, V. (2008). Malformations of cortical development. Neurologist *14*, 181-91.

Pasca, S. (2018). The rise of three-dimensional human brain cultures. Nature, *553,* 437-445.

Pawlisz, A.S., Mutch, C., Wynshaw-Boris, A., Chenn, A., Walsh, C.A., and Feng, Y. (2008). Lis1-Nde1-dependent neuronal fate control determines cerebral cortical size and lamination. Hum. Mol. Genet. *17*, 2441–2455.

Poduri, A., Evrony, G.D., Walsh, C.A. (2013). Somatic mutation, genomic variation, and neurological disease. Science *341*, 25-37.

Qian, X., Jacob, F., Song, M.M., Nguyen, H.N., Song, H., Ming, G. I. (2018). Generation of human brain region-specific organoids using a miniaturized spinning bioreactor. Nature Protoc, *13,* 565-572.

Quadrato, G., Nguyen, T., Macosko, E.Z., Sherwood, J.L., Min Yang, S., Berger, D.R., Maria, N., Scholvin, J., Goldman, M., Kinney, J.P. et al. (2017). Cell diversity and network dynamics in photosensitive human brain organoids. Nature, *545*, 48-53.

Rakic, P., Stensas, L. J., Sayre, E. & Sidman, R. L. (1974). Computeraided three-dimensional reconstruction and quantitative analysis of cells from serial electron microscopic montages of foetal monkey brain. Nature *250*, 31–34.

Romero, D.M., Bahl-Buisson, N., Francis, F. (2018). Genetics and mechanisms leading to human cortical malformations. Seminars in cell & develpmental biology *76,* 33-75.

Ropers, H.H. (2010). Genetics of early onset cognitive impairment. Annu. Rev. Genom. Hum. Genet. *11*, 161-187.

Shen, J., Gilmore, E.C., Marshall, C.A., Haddadin, M., Reynolds, J.J., Eyaid, W. (2010). Mutations in PNKP cause microcephaly, seizures and defects in DNA repair. Nat. Genet. *42*, 245-249.

Sheen, V.L., Ferland, R.J., Neal, J., Harney, M., Hill, R.S., Banham, A., Brown, P., Chenn, A., Corbo, J., Hecht, J., et al. (2006). Neocortical neuronal arrange- ment in Miller Dieker syndrome. Acta Neuropathol. *111*, 489–496.

Sheridan, E., Wright, J., Small, N., Corry, P.C., Oddie, S., Whibley, C., Petherick, E.S., Malik, T., Pawson, N., McKinney, P.A., Parslow, R.C. (2013). Risk factors for congenital anomaly in a multiethnic birth cohort: an analysis of the born in Bradford study. Lancet Lond. Engl. *382*, 1350-1359.

Shi, Y., Kirwan, P., Smith, J., Robinson, H.P., and Livesey, F.J. (2012). Human cerebral cortex development from pluripotent stem cells to functional excit- atory synapses. Nat. Neurosci. *15*, 477–486.

Smart, I.H., Dehay, C., Giroud, P., Berland, M., and Kennedy, H. (2002). Unique morphological features of the proliferative zones and postmitotic compartments of the neural epithelium giving rise to striate and extrastriate cortex inthe monkey. Cereb. Cortex *12*, 37–53.

Stouffer, M.A., Golden, J.A., Francis, F. (2016). Neuronal migration disorders: focus on the cytoskeleton and epilepsy. Neurobiol. Dis. *92*, 18-45.

Tabata, H., Nakajima, K. (2003). Multipolar migration: the third mode of radial neuronal migration in the developing cerebral cortex. J. Neurosci. Off. J. Soc. Neurosci. *23*, 9996-10001.

Takahashi, K., Tanabe, K., Ohnuki, M., Narita, M., Ichisaka, T., Tomoda, T., Yamanaka, S. (2007). Induction of pluripotent stem cells from adult human fibroblasts by defined factors. Cell, *131*, 861-872.

Thornton, G.K., Woods, C.G. (2009). Primary microcephaly: do all roads lead to Rome? Trends Genet. *25*, 501-510.

Toyo-oka, K., Shionoya, A., Gambello, M.J., Cardoso, C., Leventer, R., Ward, H.L., Ayala, R., Tsai, L.H., Dobyns, W., Ledbetter, D., et al. (2003). 14-3-3epsilon is important for neuronal migration by binding to NUDEL: a mo- lecular explanation for Miller-Dieker syndrome. Nat. Genet. *34*, 274–285.

Wynshaw-Boris, A. (2007). Lissencephaly and LIS1: Insights into the molecular mechanisms of neuronal migration and development. Clin. Genet. *72*, 296–304.

Yingling, J., Youn, Y.H., Darling, D., Toyo-Oka, K., Pramparo, T., Hirotsune, S., and Wynshaw-Boris, A. (2008). Neuroepithelial stem cell proliferation requires LIS1 for precise spindle orientation and symmetric division. Cell 1*32*, 474–486.

Zechner, D., Fujita, Y., Hülsken, J., Müller, T., Walther, I., Taketo, M.M., Cren-shaw, E.B., 3rd, Birchmeier, W., and Birchmeier, C. (2003). beta-Catenin signals regulate cell growth and the balance between progenitor cell expan- sion and differentiation in the nervous system. Dev. Biol. *258*, 406–418.

Zhang, J., Woodhead, G.J., Swaminathan, S.K., Noles, S.R., McQuinn, E.R., Pisarek, A.J., Stocker, A.M., Mutch, C.A., Funatsu, N., and Chenn, A. (2010). Cortical neural precursors inhibit their own differentiation via N-cadherin main- tenance of beta-catenin signaling. Dev. Cell *18*, 472–479.

Zhang, J., Shemezis, J.R., McQuinn, E.R., Wang, J., Sverdlov, M., and Chenn, A. (2013). AKT activation by N-cadherin regulates beta-catenin signaling and neuronal differentiation during cortical development. Neural Dev. *8*, 7.

11. Erklärung

Hiermit versichere ich, dass diese Dissertation von mir persönlich, selbständig und ohne jede unerlaubte Hilfe angefertigt wurde. Die Daten, die im Rahmen einer Kooperation gewonnen wurden sind ausnahmslos gekennzeichnet. Die aus anderen Quellen übernommenen Daten, Abbildungen und Konzepte sind unter Angabe der jeweiligen Quelle gekennzeichnet.

Ergebnisse dieser Arbeit trugen in Teilen zu folgenden Veröffentlichungen bei:

Vira Iefremova, George Manikakis, Olivia Krefft, Ammar Jabali, Kevin Weynans, Ruven Wilkens, Fabio Marsoner, Björn Brändl, Franz-Josef Müller, Philipp Koch, and Julia Ladewig
An organoid-based model of cortical development identifies non-cell autonomous defects in ß-catenin signaling contributing to Miller-Dieker-Syndrome
Cell Reports, 2017, April 4, 19, 50–59

Olivia Krefft, Ammar Jabali, **Vira Iefremova**, Philipp Koch, Julia Ladewig
Generation of standardized and reproducible forebrain-type cerebral organoids from human induced pluripotent stem cells
J. Vis. Exp., 2018, (131), e56768

Die vorliegende Arbeit wurde an keiner anderen Hochschule als Dissertation eingereicht. Ich habe früher noch keinen Promotionsversuch unternommen.

Vira Iefremova,
Bonn, den 15.04.21

12. Publications

'An organoid-based model of cortical development identifies non-cell autonomous defects in ß-catenin signaling contributing to Miller-Dieker-Syndrome'. **Iefremova et al**., 2017, Cell Reports 19, 50–59 April 4, 2017. doi: 10.1016/j.celrep.2017.03.047

Using Miller-Dieker-syndrome-specific iPSC-derived forebrain-type organoid cultures, we were able to show that an impairment of cortical niche signaling leads to alterations in N-cadherin/ß-catenin signaling that result in a non-cell autonomous expansion defect of ventricular zone radial glia cells.

'Generation of standardized and reproducible forebrain-type cerebral organoids from human induced pluripotent stem cells'. Krefft, O., Jabali, A., **Iefremova, V**., Koch, P., Ladewig, J., January 2018, J. Vis. Exp. (131), e56768, doi: 10.3791/56768

The method we described for the generation of homogeneous and reproducible forebrain-type organoids from iPSC combines the intrinsic ability of PSC to self-organize with guided differentiation towards the anterior neuroectodermal lineage and matrix embedding to support the formation of a continuous neuroepithelium. As such, this protocol provides an easily applicable system for the generation of standardized and reproducible iPSC-derived cortical tissue structures in vitro.

'Human stem cell-based models for studying autism spectrum disorder-related neuronal dysfunction'. Cheffer, A., Flitsch, L. J., Krutenko, T., Röderer, P., Liubov Sokhranyaeva, L., **Iefremova, V.**, Hajo, M., Michael Peitz, M., Schwarz, M., and Brüstle, O. *Molecular Autism* 11, 99 (2020). doi:10.1186/s13229-020-00383-w

'Dissecting Alzheimer's disease pathogenesis in human 2D and 3D models'. Cenini, G., Hebish, M., **Iefremova, V.**, Flitsch, L. J., Breitkreuz, Y., Tanzi, R. E., Kim, D. Y., Peitz, M., and Brüstle, O. Molecular and Cellular Neuroscience *110* (2021). doi: 10.1016/j.mcn.2020.103568